Applied Catalysis B: Environmental 176–177 (2015) 396–428

Contents lists available at ScienceDirect

Applied Catalysis B: Environmental

journal homepage: www.elsevier.com/locate/apcatb

Review

Self-cleaning applications of TiO_2 by photo-induced hydrophilicity and photocatalysis

Swagata Banerjee[a], Dionysios D. Dionysiou[b], Suresh C. Pillai[c,d,*]

[a] Centre for Research in Engineering Surface Technology (CREST), FOCAS Institute, Dublin Institute of Technology, Kevin St, Dublin 8, Ireland
[b] Environmental Engineering and Science Program, Department of Biomedical, Chemical and Environmental Engineering (DBCEE), 705 Engineering Research Center, University of Cincinnati, Cincinnati, OH 45221-001, USA
[c] Nanotechnology Research Group, Department of Environmental Science, Institute of Technology Sligo, Sligo, Ireland
[d] Centre for Precision Engineering, Materials and Manufacturing Research (PEM), Institute of Technology Sligo, Sligo, Ireland

ARTICLE INFO

Article history:
Received 30 December 2014
Received in revised form 24 March 2015
Accepted 31 March 2015
Available online 2 April 2015

Keywords:
Anti-microbial
Synthesis
Energy and environmental
Tunable wettability
Water contact angle (WCA)
Hydrophobic
Graphene heterojunctions
Reduced graphene oxide (rGO)
Fluoroalkylsilane
Doped titania

ABSTRACT

Self-cleaning materials have gained considerable attention for both their unique properties and practical applications in energy and environmental areas. Recent examples of many TiO_2-derived materials have been illustrated to understand the fundamental principles of self-cleaning hydrophilic and hydrophobic surfaces. Various models including those proposed by Wenzel, Cassie-Baxter and Miwa-Hashimoto are discussed to explain the mechanism of self-cleaning. Examples of semiconductor surfaces exhibiting the simultaneous occurrence of superhydrophilic and superhydrophobic domains on the same surface are illustrated, which can have various advanced applications in microfluidics, printing, photovoltaic, biomedical devices, anti-bacterial surfaces and water purification.

Several strategies to improve the efficiency of photocatalytic self-cleaning property have been discussed including doping with metals and non-metals, formation of hetero-junctions between TiO_2 and other low bandgap semiconductors, and fabrication of graphene based semiconductor nano-composites. Different mechanisms such as band-gap narrowing, formation of localized energy levels within the bandgap and formation of intrinsic defects such as oxygen vacancies have been suggested to account for the improved activity of doped TiO_2 photocatalysts. Various preparation routes for developing efficient superhydrophilic–superhydrophobic patterns have been reviewed. In addition, reversible photo-controlled surfaces with tuneable hydrophilic/hydrophobic properties and its technological applications are discussed. Examples of antireflective surfaces exhibiting self-cleaning properties for the applications in solar cells and flat panel displays have also been provided. Discussion is provided on TiO_2 based self-cleaning materials exhibiting hydrophilic and underwater superoleophobic properties and their utilities in water management, antifouling applications and separation of oil in water emulsions are discussed. In addition, ISO testing methods (ISO 27448: 2009, ISO 10678: 2010 and ISO 27447: 2009) for analysing self-cleaning activity and antibacterial action have also been discussed. Rapid photocatalytic self-cleaning testing methods using various photocatalytic activity indicator inks such as resazurin (Rz), basic blue 66 (BB66) and acid violet 7(AV7) for a broad range of materials such as commercial paints, tiles and glasses are also described. Various commercial products such as glass, tiles, fabrics, cement and paint materials developed based on the principle of photo-induced hydrophilic conversion of TiO_2 surfaces have also been provided. The wide ranges of practical applications of self-cleaning photocatalytic materials suggest further development to improve their efficiency and utilities. It was concluded that a rational fabrication of multifunctional photocatalytic materials by integrating biological inspired structures with tunable wettability would be favorable to address a number of existing environmental concerns.

Contents

* Corresponding author at: Center for Precision Engineering, Materials and Manufacturing Research (PEM), Institute of Technology Sligo, Sligo, Ireland. Tel.: +353 719305816.
E-mail address: Pillai.suresh@itsligo.ie (S.C. Pillai).

http://dx.doi.org/10.1016/j.apcatb.2015.03.058
0926-3373/

1. Introduction

Development of self-cleaning materials, understanding their structure-function relationship, and engineering artificial surfaces with variable wettability suitable for various commercial applications constitute an active research domain in material science [1]. These materials have received substantial interest in recent years due to their wide applications in various fields ranging from indoor applications in fabrics [2–4], furnishing materials [5,6], window glasses [7–9], to exterior construction materials, roof tiles [10,11], car mirrors [5,6], and solar panels [12–14]. These materials can easily be cleaned by a stream of natural water such as rainfall, which in turn significantly reduces the routine maintenance cost. Self-cleaning activity is predominant in nature, for example, in the cases of leaves of lotus plant [15,16], rice plant [17], butterfly wings [18], fish scales [19] etc. The waxy surface of lotus leaves combined with the presence of microscopic structures result in an extremely hydrophobic surface [20]. Consequently, when water droplets roll off the leaves, the dust/dirt particles are also removed. This mechanism is widely known as "Lotus effect" [16]. Broadly, self-cleaning surfaces can be divided into two categories: (i) hydrophilic surfaces and (ii) hydrophobic surfaces [21,22]. In the case of hydrophilic surfaces water drops spread over the surface and form a film of water. During the process of spreading, the contaminants on the surface are washed away (Fig. 1a). In the case of hydrophobic surfaces, the water drops roll off the surface quickly due to the water repellent and low adhesive properties of hydrophobic surfaces, and thereby remove the contaminants on the surface (Fig. 1b). A great amount of work has been devoted in recent years to design self-cleaning biomimetic surfaces displaying anti-fouling, anti-reflective properties [23–27]. Several reviews have been published on self-cleaning action of TiO_2 over the past years that mainly discuss photocatalytic activity of TiO_2 [8,28–30]; however, there are not many articles that deal with photocalytic self-cleaning activity of TiO_2 with particular emphasis on fundamental mechanism of photoinduced hydrophilicity and its commercial applications [21]. In the current review, a number of TiO_2 based photocatalytic materials are illustrated to understand the fundamental principles of self-cleaning hydrophilic and hydrophobic surfaces. In addition, composite materials containing self-cleaning materials exhibiting hydrophilic and underwater superoleophobic properties and photocatalytic antibacterial activity are discussed in detail and recent advances in the self-cleaning action by photocatalytic action are comprehensively reviewed. In addition, detailed information on a number of self-cleaning commercial products such as glass, tiles, fabrics, cement and paint materials are discussed.

2. Contact angle and wettability

The wettability of a surface can be determined by measuring the contact angle (θ) of the liquid drop over the solid surface, which is defined as the angle formed between the solid surface and the tangent drawn at the liquid drop as shown in Fig. 2 and is a measure of the angle between solid–liquid and liquid–vapor interfaces. At thermodynamic equilibrium condition between the solid, liquid and vapor phases, the relation between the interfacial energies per unit area is given by Young's relation (Eq. (1)).

$$\gamma_{sv} = \gamma_{SL} - \gamma_{LV}\cos\theta \quad (1)$$

where γ_{SV}, γ_{SL} and γ_{LV} represent the interfacial energy per unit area of the solid–vapor, solid–liquid and liquid–vapor interfaces and θ is the contact angle. For partial or totally wettable surfaces the contact angle is usually low ($0^\circ < \theta < 90^\circ$). For superhydrophilic surfaces θ approaches to zero value ($\theta < 5^\circ$) and the liquid drop tends to evenly spread on the surface (Table 1) [31,32].

Eq. (1) relate parameters such as θ, γ_{SV}, γ_{SL} and γ_{LV} which cannot usually be obtained experimentally [33,34]. In addition, it was previously showed that the contact angle (θ) measurement is not always highly reproducible. The real contact angle θ, can take any value within $\theta_R \leq \theta \leq \theta_A$, (where θ_A and θ_R are defined

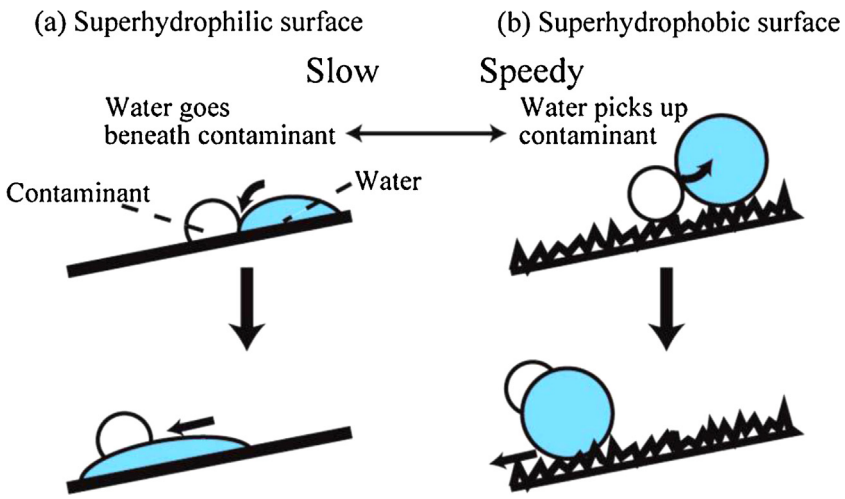

Fig. 1. Schematic representation of self-cleaning processes on (a) a superhydrophilic and (b) a superhydrophobic surface. (Reproduced from RSC Adv. 3 (2013) 671–690, with permissions from Royal Society of Chemistry).

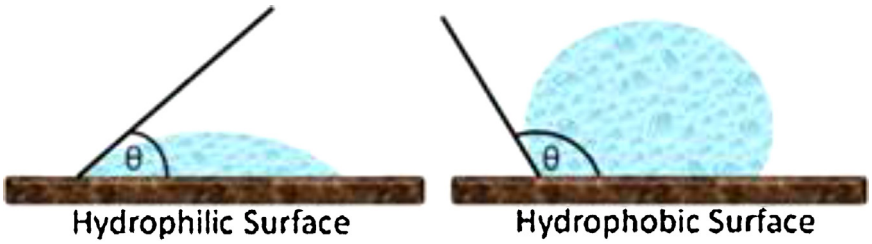

Fig. 2. Schematic representation of a liquid drop in equilibrium on a hydrophilic and a hydrophobic surface.

Table 1
Relationship of contact angle values and wettability behavior.

Contact angle	Wettability
$\theta > 90^\circ$	Hydrophobic
$\theta > 150^\circ$	Superhydophobic
$0^\circ < \theta < 90^\circ$	Hydrophilic
$\theta < 10^\circ$	Superhydrophilic

as the advancing and receding angles, respectively) and the difference between θ_A and θ_R is termed as hysteresis. Both θ_R and θ_A are characteristic of the surface chemistry, texture and topography.

It should be noted here that Eq. (1) is valid only for ideal solid surfaces, characterised by chemically homogeneous, inert, rigid and smooth surfaces. The wettability properties of rough surfaces are commonly described by the model proposed by Wenzel [35] and the model by Cassie-Baxter (Fig. 3) [36].

According to the Wenzel model, for a rough surface, which has higher surface area than a smooth surface, the liquid droplet forms contact with the entire surface and completely penetrates into the cavities on the surface. For such a rough surface the "apparent" contact angle θ_{app} for a liquid droplet is related to the "true" contact angle θ_s of the droplet on a smooth surface by the roughness factor r of the surface as described in Eq. (2).

$$\cos\theta_{app} = r\cos\theta_s \tag{2}$$

where the surface roughness factor r is defined as the ratio of geometric surface area to the actual surface area (Eq. (3)).

$$r = \frac{\text{Geometric Surface Area}}{\text{Actual Surface Area}} \tag{3}$$

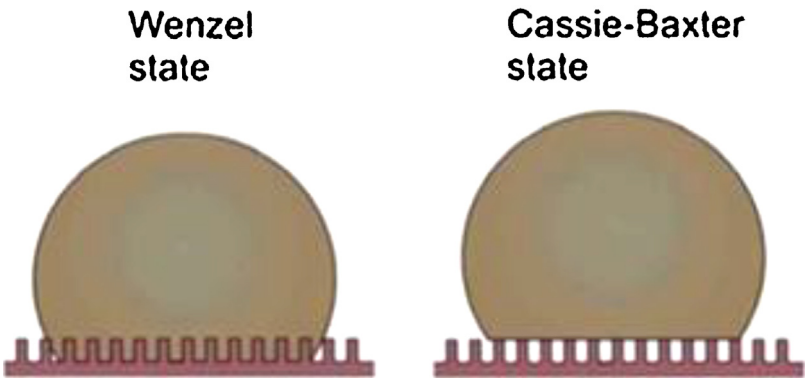

Fig. 3. Effect of the surface structure on the wetting property of a solid surface. (Reproduced from Adv. Colloid Interface Sci. 210 (2014) 47–57 with permissions from Elsevier).

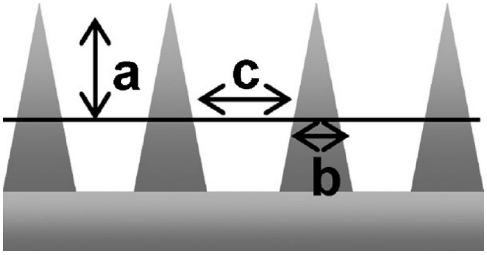

Fig. 4. Effect of surface structure on the wetting behavior according to Miwa-Hashimoto surface model.
(Reproduced from Langmuir 26 (2010) 15875–15882 with permission from American Chemical Society).

The Wenzel equation predicts that hydrophilicity and hydrophobicity of a surface depends on the nature of the corresponding surface. For a hydrophilic surface ($\theta < 90^\circ$ and $r > 1$), with an increase in surface roughness, hydrophilicity also increases. Conversely for a hydrophobic surface, ($\theta > 90^\circ$ and $r > 1$), surface hydrophobicity increases with increasing surface roughness. Although these trends are observed in most cases, Wenzel model cannot satisfactorily deal with all heterogeneous surfaces.

The Cassie-Baxter model does not postulate complete penetration of a liquid droplet into the surface cavities. This model suggests that the spreading of a liquid droplet on a rough surface destroys the solid–vapor interface and forms solid–liquid and liquid–vapor interfaces as shown in Fig. 3b. According to Cassie-Baxter model, the "apparent" contact angle θ_{app} for a liquid droplet on a rough surface is related to the true contact angle by Eq. (4),

$$\cos\theta_{app} = f_s \cos\theta_s + f_v \cos\theta_v \quad (4)$$

where f_s and f_v represent the area fraction of the liquid droplet in contact with the solid surface and area fraction of the liquid droplet in contact with the vapor trapped in the cavities on the rough surface, respectively, and θ_v is the contact angle of the liquid in air. For $\theta_v = 180^\circ$, and $f_s + f_v = 1$, Eq. (4) can be written as,

$$\cos\theta_{app} = -1 + f_s(\cos\theta_s + 1) \quad (5)$$

Effects of the surface roughness on water contact angle of superhydrophobic surfaces were investigated by Miwa et al. [37]. Various superhydrophobic surfaces with various roughness parameters were compared. It has been observed that in superhydrophobic region, the sliding angles decrease with increasing contact angle depending on the surface roughness. This model combines the Wenzel and the Cassie-Baxter models through the Eq. (6) and is usually referred as Miwa-Hashimoto model [38].

$$\cos\theta' = r_{MH} f_{MH} \cos\theta + f_{MH} - 1 \quad (6)$$

where θ' and θ represent the equilibrium contact angles on a rough surface and on a flat surface, respectively; r_{MH} is the ratio of the side area to the bottom area of the needle (Fig. 4) and f_{MH} is the fraction of surface area of the material in contact with the liquid.

Various types of hydrophilic, superhydrophilic and superhydrophobic surfaces can be found in nature (Fig. 5). For example, the contact angle of lotus leaf and butterfly wings are measured as about 164° and 152°, respectively [22]. Functional materials and surfaces created by understanding the mechanism of self-cleaning surfaces found in the living nature are called bio-inspired process [22].

The presence of superhydrophilic and superhydrophobic domains on the same surface can have various applications in microfluidics, printing, biomedical devices and water collection [39–43]. Superhydrophobic–superhydrophilic micro patterned films have been fabricated based on a three layered structure consisting of a Al_2O_3 gel film, a very thin TiO_2 gel layer, and a

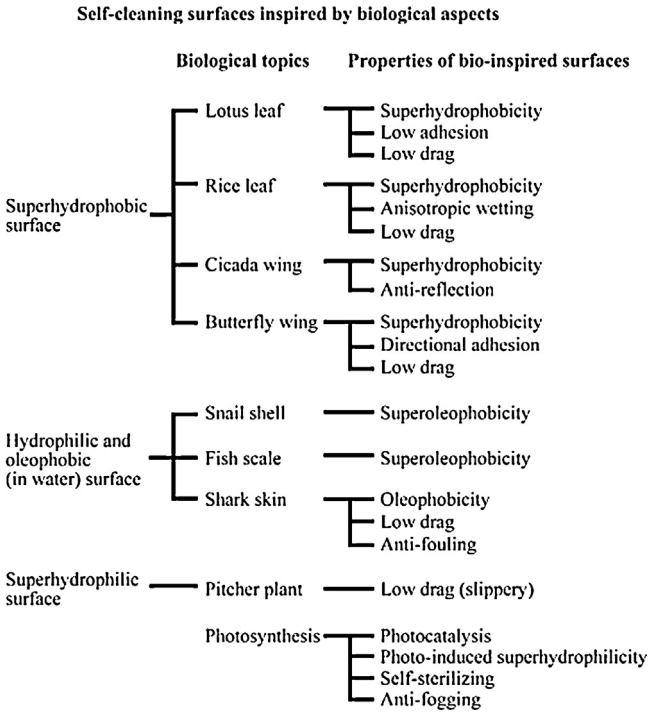

Fig. 5. Different types of hydrophilic, superhydrophilic and superhydrophobic surfaces found in nature and corresponding properties of bio-inspired surfaces.
(Reproduced from RSC Adv. 3 (2013) 671–690, with permissions from Royal Society of Chemistry).

fluoroalkylsilane (FAS) layer [44]. The surface showed a WCA of 150° and the contact angle decreased sharply to 5° upon UV illumination. Irradiation with UV light initiates photocatalytic processes in TiO_2, which in turn result in the cleavage of fluoroalkyl chain and the FAS layer consequently convert to a silica layer. The hydrophilic property of the surface is further enhanced due to the rough structure of Al_2O_3 layer. Superhydrophobic TiO_2 surfaces have been developed by roughening the surface using radio-frequency plasma with CF_4 as an etchant [45]. The rough wedge-like TiO_2 surface was subsequently modified with a hydrophobic monolayer of octadecylphosphonic acid (ODP). TiO_2 surfaces plasma etched for 10 s and subsequent surface modification with ODP showed a WCA greater than 150°. The surface was converted into a superhydrophilic surface (WCA = 0°) upon UV illumination, due to rapid decomposition of ODP coating resulting from TiO_2 photocatalysis. The superhydrophobicity was recovered by dipping the TiO_2 surface in a solution of ODP and the superhydrophilic/superhydrophobic conversion was repeated for more than five cycles without any significant loss in hydrophobicity, which suggests possibility of designing superhydrophilic/superhydrophobic micro patterns based on such structures, with sharp contrast in light induced wettability behavior. Superhydrophilic–superhydrophobic patterns with tunable wettability have been developed using nanostructured TiO_2 films modified with fluoroalkylsilanes (FAS) using photocatalytic lithography technique [46,47]. The WCA on the modified surface was found to be 156° attributed to the rough morphology of the surface and the wettability was found to change drastically (WCA < 5°) upon UV-exposure due to selective photocleavage of the fluoroalkyl chain assembled on TiO_2 surface. The generation of superhydrophilic–superhydrophobic micropatterns can be used to fabricate various devices. For example, the fabrication of superhydrophilic–superhydrophobic patterns with a resolution of 133 and 150 lines per inch on titanium substrates for offset printing is reported [48]. The micropattern formation was further used as a template to develop coating of nano octacalcium

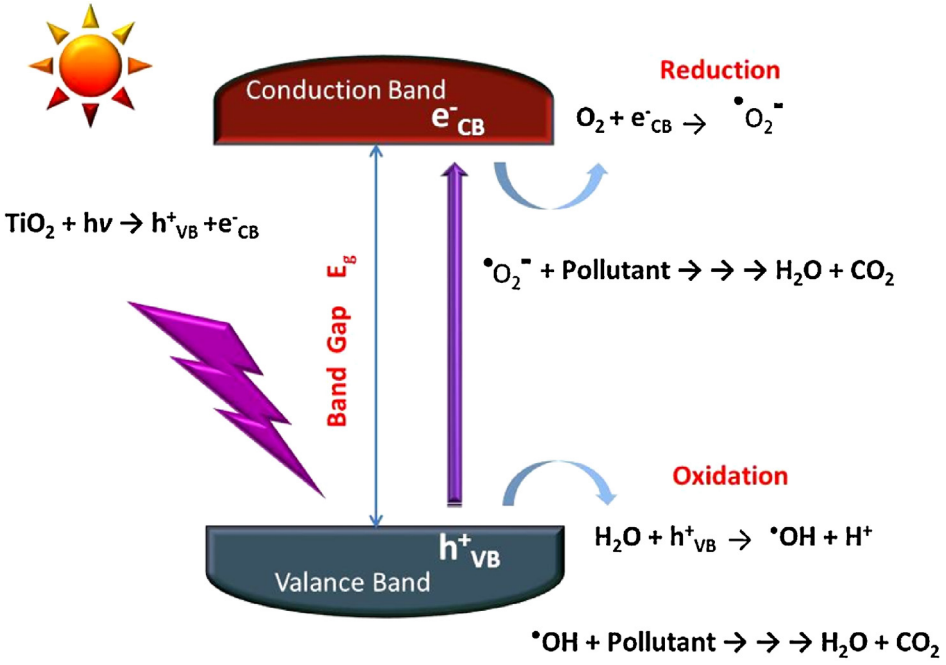

Fig. 6. Schematic illustration of various processes occurring after photoexcitation of pure TiO_2 with UV light.

phosphate by electrochemical deposition [46]. Such micropatterns with sharp contrast in wettability have been used to construct three dimensional functional patterns for applications in biomedical devices for high throughput molecular sensing, drug delivery, etc [49].

3. Photocatalytic hydrophilic surfaces

The photocatalytic hydrophilic surfaces utilize sunlight/indoor light to decompose the dirt and other impurities [50–54]. TiO_2 based photocatalysts have gained considerable attention as TiO_2 exhibits significantly high physical and chemical stability, low cost, easy availability, low toxicity and excellent photo-activity [50,55–60]. In the presence of light of suitable energy (where, the energy of the excitation source is higher than the band-gap energy of the material), an electron (e^-_{CB}) is excited from valence band of TiO_2 to the conduction band, generating a positive electron hole (h^+_{VB}) in the valence band (Fig. 6). The photoexcited electron (e^-_{CB}) can in turn recombine with the electron hole (h^+_{VB}) and reduce the overall efficiency of the photoprocess. The charge carriers, which can escape the charge-annihilation reaction, migrate to the surface, where the photoexcited electrons can reduce atmospheric oxygen to generate superoxide radicals ($^{\bullet}O_2^-$) or hydroperoxyl radicals ($HO_2^{\bullet}$). The valence band hole can also oxidize surface adsorbed water or OH^- and produce $^{\bullet}OH$. These reactive oxygen species (ROS) can convert organic pollutants into CO_2 and water resulting in the cleaning of the surface. A major limitation in developing self-cleaning materials based on TiO_2 is the wide band gap of the semiconductor, limiting its absorption to the UV region of sunlight, which comprises only 3–5% of the solar spectrum [57]. Due to this wide band gap, utility of pure TiO_2 is restricted in fabrication of self-cleaning materials (e.g., glass and tiles) for outdoor application. In order to efficiently utilize the visible region of solar spectrum, several strategies have been developed [57], which will be discussed in a later section.

$$\text{Semiconductor} + h\nu \rightarrow h^+_{VB} + e^-_{CB} \quad (7)$$

$$e^-_{CB} + h^+_{VB} \rightarrow \text{Energy} \quad (8)$$

$$h^+_{VB} + H_2O \rightarrow {}^{\bullet}OH + H^+ \quad (9)$$

$$e^-_{CB} + O_2 \rightarrow {}^{\bullet}O_2^- \quad (10)$$

The superhydrophilic and oleophilic character of TiO_2 was first reported by Wang et al. [7]. A thin polycrystalline film of TiO_2 (anatase) displayed a contact angle of $72 \pm 1^\circ$ for water in the absence of light. Wang et al. reported that if the TiO_2 film is irradiated with ultraviolet light, the contact angle reduced to 0° resulting in a spreading of water droplets on the surface (Fig. 7). Similar trend was also observed for oily liquids such as glycerol trioreate and hexadecane [7]. The changes in wettability were observed for both anatase and rutile TiO_2 irrespective of their photocatalytic properties. In recent years, thin films of anatase TiO_2 nanowire arrays with exposed highly reactive (0 0 1) facet have been synthesized through a fluorine free hydrothermal technique [61]. The oriented anatase TiO_2 thin films exhibited high transparency, photocatalytic activity and superhydrophilicity upon UV-irradiation, which are advantageous for applications in self-cleaning coatings. Self-cleaning materials have been developed from mono and self-assembled multilayer TiO_2 nanosheets deposited on quartz glass slides by layer by layer deposition technique [62]. The photocatalytic activities of the nanosheets were examined in terms of their ability to degrade methylene blue dye. The photocatalytic efficiency of TiO_2 nanosheets was lower than the anatase TiO_2 films and the photobleaching rate decreased with increasing number of layers. A cost-effective electrospinning technique has been recently developed to fabricate photocatalytic, superhydrophilic and optically transparent TiO_2 films suitable for applications in window coatings and photovoltaic cells [63]. Several mechanisms have been proposed to account for the photoinduced hydrophilicity exhibited by TiO_2 including (i) generation of light-induced surface vacancies [7], (ii) photoinduced reconstruction of surface hydroxyl groups [64,65] and (iii) photoinduced removal of the carbonaceous layer present on TiO_2 surfaces exposed to air [66].

3.1. Generation of light-induced surface vacancies

The initial and widely accepted mechanism for photoinduced hydrophilicity was proposed by Wang et al. which relies on the

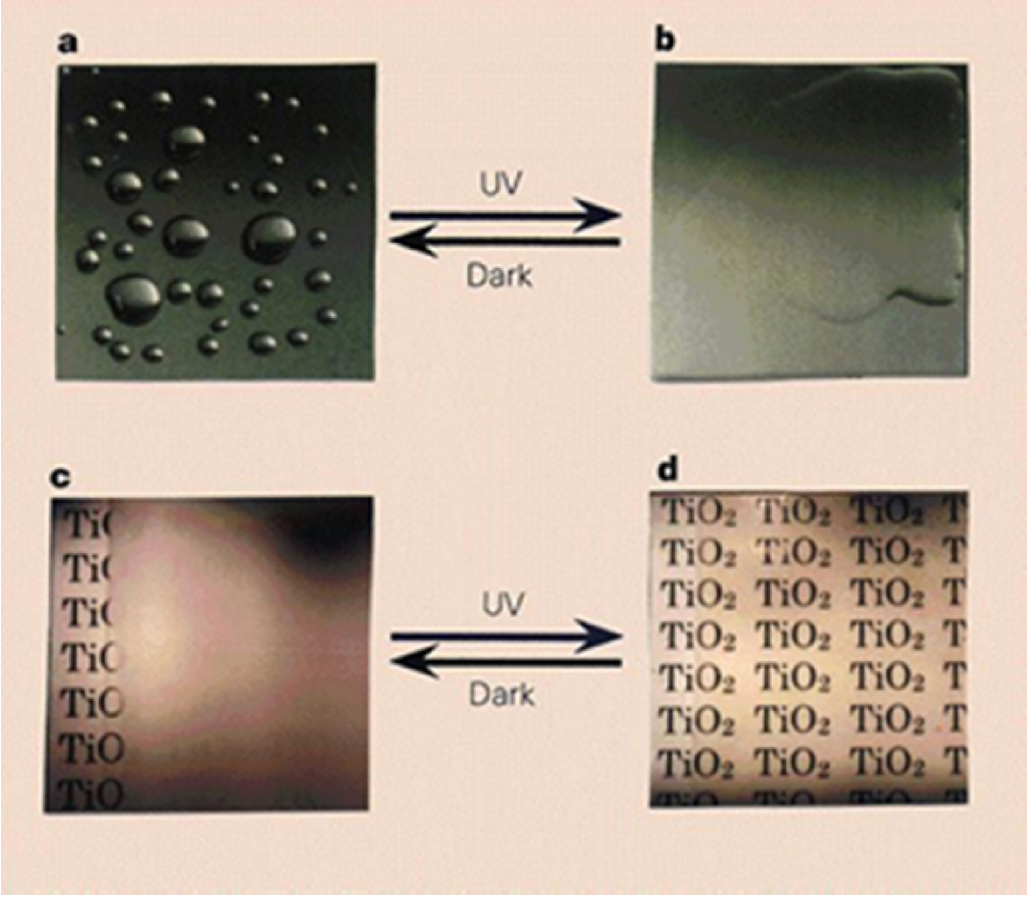

Fig. 7. Photoinduced wettability switching, where a hydrophobic TiO_2 surface (a) is converted into a superhydrophilic surface (b) upon UV-irradiation, (c) exposure of a hydrophobic TiO_2-coated glass to water vapor results in the formation of fog (small water droplet), (d) antifogging effect induced by UV-illumination. (Rreproduced from Nature 388 (1997) 431–432 with permission from Nature Publishing Group).

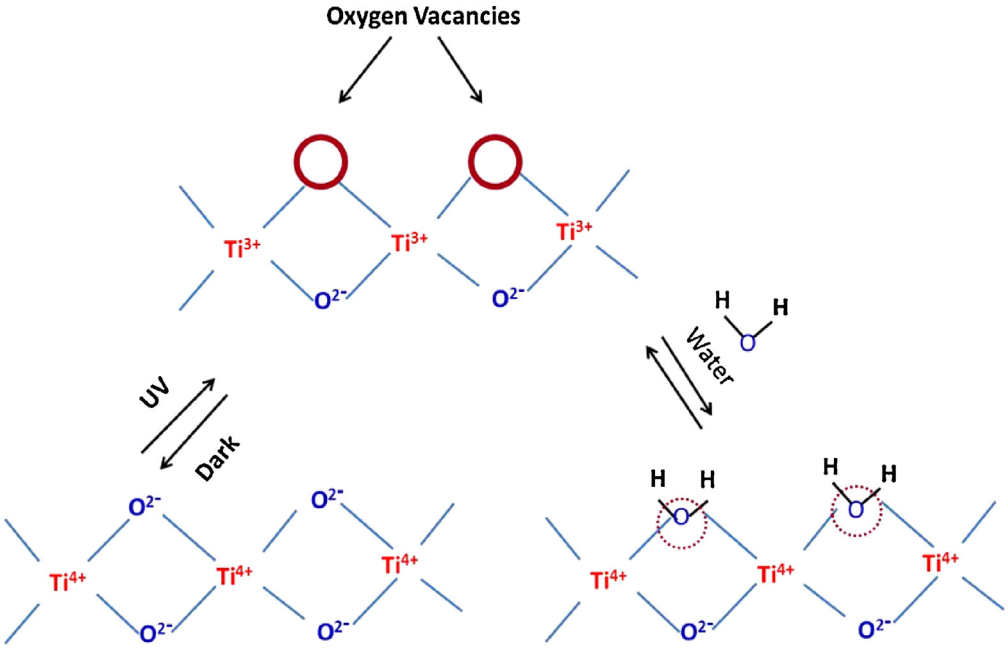

Fig. 8. Schematic representation of photo-induced hydrophilicity. Electrons reduce the Ti(IV)–Ti(III) state and thereby the oxygen atoms will be ejected (creation of oxygen vacancies). Oxygen vacancies will increase the affinity for water molecules and thereby transforming the surface hydrophilic.

formation of surface defects upon UV light illumination [7]. Friction force microscopic studies suggested that UV irradiation resulted in a structural change at the TiO_2 surface thereby influencing the interfacial force along the solid–liquid boundary and consequently changing the contact angle [67]. The surface of TiO_2 consists of five coordinated Ti atoms with the sixth position occupied by H_2O or OH^-. It is believed that UV irradiation creates oxygen vacancies at the two coordinated oxygen bridging sites at the surface, thereby converting Ti^{4+} ions to Ti^{3+} [67]. These defects can in turn increase the affinity for hydroxyl ions formed by dissociation of chemisorbed water molecules and thereby forming hydrophilic domains (Fig. 8). Moreover, crystal planes (1 1 0) and (1 0 0) of rutile TiO_2 with bridging oxygen sites showed higher efficiency for hydrophilic conversion compared to the planes such as (0 0 1) without bridging oxygen sites [68,69]. Atomic force microscopic study of UV-illuminated rutile TiO_2 single crystal showed that TiO_2 surface consists of microscopic hydrophilic and oleopholic domains, which are believed to generate capillary flow channels for oil and water [67]. It was found that if the hydrophilic TiO_2 material is stored in dark for a couple of days, the hydrophilic character gradually decrease due to slow replacement of the chemisorbed hydroxyl and water molecules by oxygen molecules from air. However, the hydrophilic nature of the surface can be retrieved by further UV illumination. Nakajima et al. demonstrated the photoinduced amphiphilic surface formation for polycrystalline anatase TiO_2 thin films [70]. However, prolonged UV irradiation was shown to convert the surface into a hydrophilic–oleophobic one, which is considered to be due to variation in the rate of hydrophilic conversion of TiO_2 grains. Rutile TiO_2 exhibited photoinduced surface hardness correlated with the conversion of hydrophilic surface [71]. This photo-induced change in surface hardness has been attributed to surface volume expansion resulting from the increase in distance between the adjacent Ti atoms arising from the dissociative adsorption of water molecules upon UV exposure.

3.2. Photoinduced reconstruction of Ti—OH bonds

Sakai et al. demonstrated that the rate of hydrophilic conversion of TiO_2 film electrode upon UV light irradiation was increased at high positive electrode potentials and decreased in the presence of hole scavenging agents [65]. Based on these observations, it was suggested that the diffusion of photogenerated holes play an important role in the hydrophilic conversion. Subsequently to account for photoinduced hydrophilic conversion of TiO_2 surfaces, Sakai et al. proposed that UV illumination results in the reconstruction of hydroxyl groups at the surface [64]. The extent of hydrophilic conversion was linked to the density of surface hydroxyl group, which in turn was correlated to the reciprocal of the contact angle. According to this model, the positive hole generated upon illumination of TiO_2 can diffuse to the surface and gets trapped at lattice oxygen. Consequently, the binding energy between the Ti and lattice oxygen becomes weak and water molecules can rupture this bond resulting in the formation of new hydroxyl bonds. In the absence of light, the hydroxyl groups gradually desorb from the surface in the form of H_2O_2 or $H_2O + O_2$ and the surface reverts back to the original less hydrophilic state. Mechanical treatments such as ultrasonication [72] and wet rubbing [73] can cause desorption of thermodynamically less stable hydroxyl groups induced by UV illumination and make the surface less hydrophilic.

3.3. Photo-oxidation of adsorbed hydrocarbon

In contrast to the widely accepted mechanism of surface-hydroxylation explaining the gradual hydrophilic conversion of TiO_2 induced by UV illumination, Zubkov et al. reported the sudden onset of UV light induced surface wetting under highly controlled atmospheric conditions [66]. According to their mechanism, the organic pollutant is photocatalytically degraded upon UV-irradiation on a water droplet. With an increasing irradiation time, photocatalytic degradation continues leading to a decrease in the surface coverage by the contaminant. At the critical point, where the surface coverage approaches zero (i.e., beyond the perimeter of the water droplet), rapid spreading of water droplet occurs.

Takeuchi et al. proposed that thermal energy of the irradiating light can cause desorption of the weakly attached water molecules from the surface of TiO_2 [74]. As shown in Fig. 9, heating TiO_2 thin film causes desorption of water molecules from the surface and results in a decrease in H-bonded network on the surface and decrease in surface tension of the water cluster, which is considered to be crucial for the surface wetting. In the presence of UV irradiation, water desorption due to heating effect occurs simultaneously with the photocatalytic degradation of organic contaminants leading to hydrophilic conversion. It should also be noted that the free energy of cohesion of water does not significantly decrease with temperature. The change in contact angle due to heating can also be explained in such a way that, during water evaporation there will be a reduction in size of the water droplet. Therefore, the receding contact angle (θ_R) will be smaller than the advancing contact angle (θ_A) due to wide contact angle hysteresis.

Sakai et al. described the enhancement of hydrophilic conversion rate of TiO_2 in the presence of UV illumination and high electrode potential [65], which demonstrated the importance of electronic photoexcitation rather than thermal action of the illuminating light. Yan et al. also demonstrated that photoinduced hydrophilic conversion of TiO_2 thin films occurs in two stages, where in the first phase WCA decreases only when the surface is illuminated with a monochromatic light of wavelength shorter than the absorption edge, emphasizing the importance of photoinduced electron–hole generation [75].

3.4. A combination of various mechanisms

Guan explained the relationship of adsorption of water molecules and hydrophilicity (Fig. 10). The water molecules will initially be chemisorbed on the TiO_2 surface and these water molecules will further 'adsorb' water by physisorption (van der Waals forces or hydrogen bounds) [76]. These physisorbed water molecules will act as a barrier to prevent the close contact between the surface and pollutants. Therefore, the pollutants which come in contact with the surface will easily be removed by these loose water molecules [76]. The synergistic effect of photocatalysis and hydrophilicity will result in long-term self-cleaning activity. The contact angle of the pure TiO_2 coatings was about 10° and it reduces below 5° when 40 mol% SiO_2 was added. The high surface acidity due to the presence of Si cations and its ability to adsorb more hydroxyl group was the main reason for the reduced contact angle.

Several treatments such as alkaline wash and vacuum UV treatments, which remove organic contaminants from the surface, can improve surface wettability; however, superhydrophilic surface could not be obtained by these treatments. Moreover, the water contact angle for several metal oxides such as tungsten oxide and vanadium oxide, was found to decrease in response to UV-irradiation. However, no significant photocatalytic activity was detected, which suggests photocatalytic decomposition of surface adsorbed pollutants cannot be solely responsible for the surface wetting phenomenon [77]. The photoinduced hydrophilic surface of TiO_2 gradually reverts back to the hydrophobic state in the absence of UV-illumination and the rate of this conversion was found to increase in pure oxygen atmosphere. If photocatalytic removal of hydrocarbon was the principal mechanism for hydrophilicity, then hydrophilic–hydrophobic conversion should

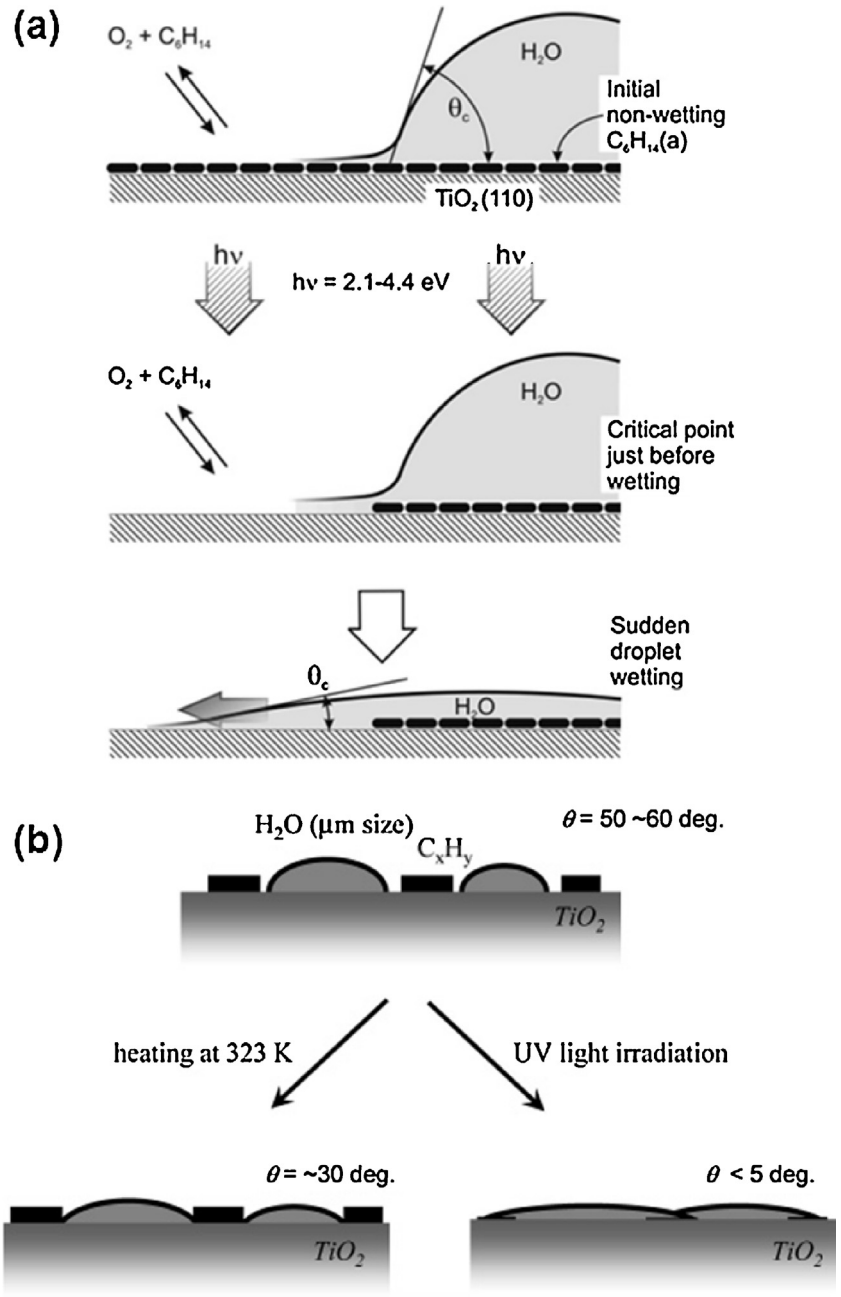

Fig. 9. (a) Schematic illustration of hydrophilicity arising from the photocatalyzed decomposition of hydrocarbons (reproduced from J. Phys. Chem. B 109 (2005) 15454–15462 with permission from American Chemical Society) and (b) suggested mechanism to improve surface wettability of TiO_2 surface upon solar illumination (reproduced from J. Phys. Chem. B 109 (2005) 15422–15428 with permission from American Chemical Society).

have been higher under ambient condition compared to oxygen atmosphere due to higher concentration of hydrocarbon contaminants [77].

As evident from the above discussion, various hypotheses have been proposed to account for the observed hydrophilic conversion of TiO_2 surfaces; however, no consensus mechanism has been elucidated so far to clarify the photoinduced superhydrophilicity. Recently, Emeline et al. described that the efficiency of photoinduced superhydrophilic conversion depends strongly on the intensity and wavelength of the actinic light, which suggests the initial step involves photoexcitation of electrons and generation of charge carriers [78]. Moreover, hydrophilic conversion was shown to depend strongly on temperature and surface acidity indicating the involvement of external hydrate layers in the hydrophilic conversion. Alteration of surface acidity was found to change the efficiency of charge carrier trapping, which in turn changes the interaction between the surface hydroxyl groups and outer hydrate layers and vary the efficiency of the photoinduced hydrophilic conversion due to change in surface energy and entropy of the hydrate layers [78].

4. Improving photocatalytic and self-cleaning activities of TiO_2

Due to the wide band gap of TiO_2 (3.2 eV for anatase and 3.0 eV for rutile), light absorption by the semiconductor material and consequently superhydrophilic conversion of undoped TiO_2 are limited to only ultraviolet region (wavelength <390 nm) and thereby restricting the practical uses of self-cleaning phenomenon

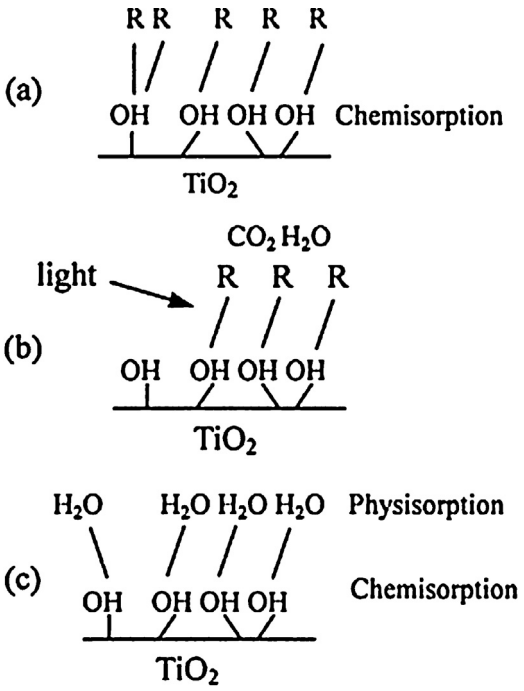

Fig. 10. Self-cleaning mechanism by the adsorption of water. (Reproduced from Surf. Coat. Technol. 191 (2005) 155–160 with permissions from Elsevier).

to outdoor applications only. Additionally, rapid electron–hole recombination also limits utility of pure TiO_2 based materials.

4.1. Impact of surface roughness and porosity on photocatalytic self-cleaning properties

It has been noted by a number of authors that the contact angle of a surface is highly depended on the texture of the surface [79]. Lee et al. investigated the relationship of surface roughness and hydrophilicity and showed that the contact angle of rough titania surface was 15°, while the smooth titania surfaces showed a contact angle of 70°. It has also been shown that the recovery rate to hydrophilicity under UV irradiation had a reverse dependence on the surface roughness. The rough titania surface can have a high concentration of Ti^{3+} produced by UV irradiation and these non-stoichiometric species on the surface play the pivotal role as adsorption sites of ^{-}OH from water molecules [72,79]. Formation of highly porous structure to increase the surface roughness appeared as an alternative approach to achieve superhydrophilic surfaces. Superhydrophilic TiO_2/SiO_2 composite film containing 0.5 wt% polyethylene glycol (PEG), showed excellent antifogging properties due to increased surface roughness, where the WCA changed from 15° to 3° within 0.16 s [80]. The super-hydrophilic titania films synthesized from alkoxide with PEG were studied to understand the impact of porosity and contact angle [80]. As the quantity and molecular weight of PEG increased, the porosity of the resultant coating also increased after the heat treatment. The OH groups adsorbed on the porous surface were found to increase due to the larger surface area of these coatings. The water contact angle measurement on the porous TiO_2 coating showed correlation between superhydrophilic nature and number of surface OH groups as well as surface roughness [81]. Porous titania coatings with super-hydrophilic properties were synthesized by the carbonatation of amorphous Li–Ti–O. Porous TiO_2 meso-channels were created by a chemical etching process (Fig. 11) [82]. After UV irradiation for 10 min, the contact angle on these highly porous meso-channels was reduced below 5° [82].

4.2. Non-metal doping

In order to utilize the sunlight/interior light effectively and to overcome the rapid charge carrier recombination, various research groups have developed metal and non-metal doped TiO_2. Doping with non-metallic elements such as N [83–86], C [87–93], and S [94,95] has shown to enhance the visible light absorption of TiO_2. Several mechanisms have been proposed to account for the shift in absorption band, including band gap narrowing resulting from the mixing of orbitals of TiO_2 and impurity [96], generation of oxygen vacancies [97], and formation of localized energy levels in the band gap (Fig. 12) [98–101].

Asahi et al. demonstrated that N-doped TiO_2 exhibited efficient degradation of organic pollutants upon visible light irradiation [96]. The $TiO_{2-x}N_x$ film with a 5 nm thick SiO_2 coating to hold the adsorbed water showed conversion to hydrophilic surface with a contact angle of 6° upon interior light exposure [96]. The hydrophilic nature of the surface was maintained even after 30 days. Irie et al. subsequently reported the correlation between the hydrophilic conversions to the extent of dopant nitrogen concentrations under irradiation with visible light [102]. The visible light activity of the N doped TiO_2 thin film was thought to be arising from localized N centred 2p orbitals. The rate for the hydrophilic conversion increased and the critical contact angle decreased with increasing the concentrations of doped nitrogen for various $TiO_{2-x}N_x$ films. The enhanced hydrophilicity obtained with increasing the extent of N substitution was ascribed to an increase in absorbed photons. Visible light active N-doped TiO_2 thin films were also prepared using magnetron sputtering [103].

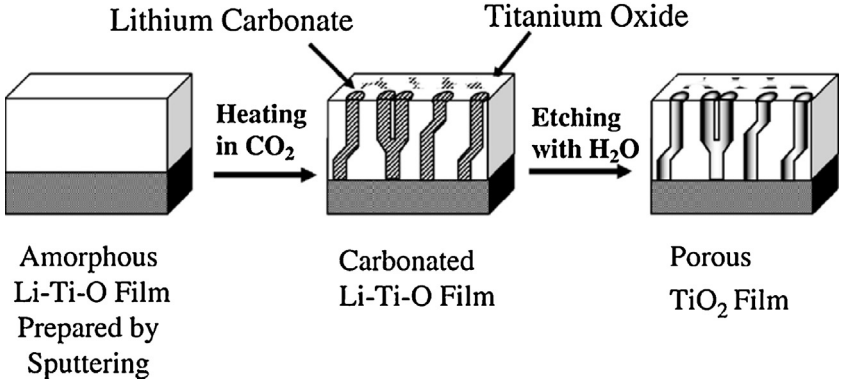

Fig. 11. Formation of porous TiO_2 channels. (Reproduced from Thin Solid Films 516 (2008) 3888–3892 with permission from Elsevier).

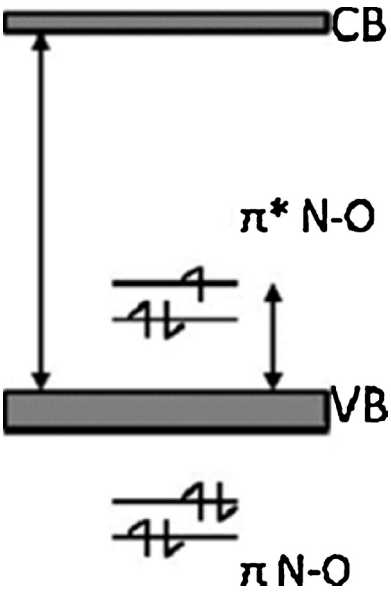

Fig. 12. Formation of localized energy levels in the band gap due to nitrogen doping into titanium dioxide photocatalyst [85].
(Reproduced from J. Hazard. Mater. 211–212 (2012) 88–94 with permission from Elsevier).

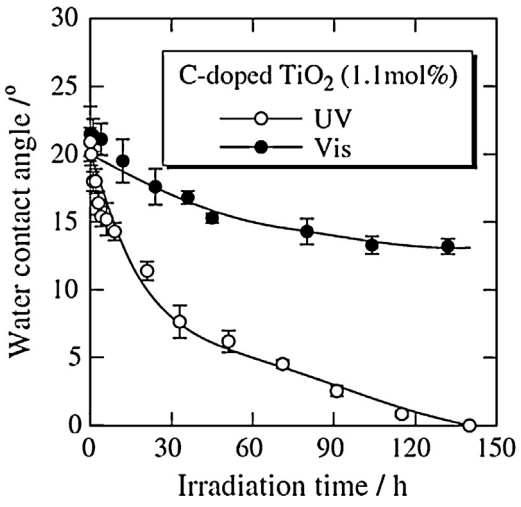

Fig. 13. Changes in contact angle of C-doped TiO_2 under UV and vis irradiation conditions.
(Reproduced from Thin Solid Films 510 (2006) 21–25 with permission from Elsevier).

The visible light activity of $TiO_{2-x}N_x$ films has been assigned to the band gap narrowing resulting from the shift of the top edge of the valence band toward negative direction due to mixing of 2p orbitals of N and O as well as anodic shifting of the bottom edge of the conduction band due to the formation of oxygen vacancies. $TiO_{2-x}N_x$ thin film electrode was converted to a hydrophilic one under visible light illumination and application of anodic oxidation potential. The extent of hydrophilic conversion was found to increase with increasing anodic potential possibly due to efficient separation of the charge carriers. N-doped visible light active TiO_2 thin films demonstrated photocatalytic degradation of organic pollutants and antimicrobial activity [104]. The N-doped films also exhibited superhydrophilicity (water contact angle or WCA <5°) under white light illumination. Surface wetting was also observed in the absence of light. The superhydrophilicity presumably results from the combined effect of improved photocatalytic activity and the porous structure of the material. The activity of the N-doped TiO_2 films were further enhanced in the presence of Ag nanoparticles formed in situ on the surface of TiO_2 films [104].

TiO_2 thin films doped with various concentrations of carbon (1.1, 0.9, 0.7 mol%) have been prepared that undergo hydrophilic conversion (WCA <5°) under UV and visible light irradiation (Fig. 13) [105]. It has been suggested that at lower concentration of the dopant (0.7 mol%), isolated energy states corresponding to C 2p orbital in the band gap account for the visible light activity. However, at the higher concentration of the dopant (1.1 mol%), band gap narrowing occurs due to mixing of 2p orbitals of carbon and oxygen in addition to the presence of localized dopant based energy levels.

Surface fluorination of TiO_2 has resulted in improved hydrophilicity upon UV irradiation, due to increased adsorption of water and other polar molecules, which is attributable to the enhanced acidity [106]. Additionally, fluorination is also thought to favor formation of Ti^{3+} through charge compensation between Ti^{4+} and F^-, which promotes charge carrier separation resulting in an efficient photocatalytic conversion [107].

Co-doping TiO_2 with two or more elements such as S–N [108], C–N [109,110], N–F [111–113] has been found to be an effective strategy to enhance the visible light induced photocatalytic activity and inhibit charge carrier recombination. N, S-co-doped TiO_2 thin film synthesized through radio-frequency (RF) sputtering method demonstrated higher visible light induced photocatalytic activity than the N and S-doped TiO_2 [114]. The N, S-co-doped TiO_2 film also exhibited better photoinduced hydrophilic conversion compared to undoped TiO_2 under fluorescent light bulb irradiation. Ab initio calculations suggested that the improved activity of N,S-co-doped TiO_2 presumably results from bandgap narrowing due to mixing of N 2*p*, S 3*p* and O 2*p* orbitals [114].

N–F co-doped TiO_2 synthesized by a fluorosurfactant based modified sol–gel technique, showed improved visible light response and slow hydrophilic conversion with a WCA 8° upon illumination with visible light for 14 days [115]. Two separate wetting stages were observed for the N,F–TiO_2 films, where in the first phase the contact angle decreased up to 40°, while the second phase representing the transition to hydrophilic state (contact angle below 20°). The photocatalytic activity of the N,F–TiO_2 films were found to be correlated with their hydrophilic conversion properties. The improved wettability and photocatalytic activity of the N,F-co-doped TiO_2 films compared to undoped TiO_2 have been assigned to the rough and porous structure of the co-doped TiO_2, which suggests promising use of these materials in self-cleaning applications.

C–N–F-co-doped TiO_2 films possessing self-cleaning property have been fabricated by a layer-by-layer dip-coating method using TiO_2 sol and NH_4F as precursors [116]. The C–N–F-co-doped TiO_2 film exhibited enhanced photocatalytic degradation of stearic acid under visible light irradiation, which has been assigned to the synergistic effect of the doped C, N and F atoms and the high surface area of the photocatalyst.

N,F-co-doped TiO_2 nanotube arrays with dispersed PdO nanoparticles have been developed that showed higher visible light absorption compared to N,F-co-doped TiO_2 [117]. The enhanced visible light absorption possibly results from the synergistic effect of N,F co-doping combined with higher crystal lattice distortion of the nanotube structure. It has also been suggested that metallic Pd° nanoparticles are generated by visible light induced reduction of PdO nanoparticles and the surface plasmon resonance of Pd° nanoparticles also accounts for the visible light activity of these nanocomposites. The N,F-co-doped TiO_2/PdO nanotube arrays exhibited enhanced photocatalytic activity and rapid conversion to superhydrophilic surface upon visible light illumination [117]. The improved visible light induced response has been explained in terms of optoelectronic coupling between N,F-

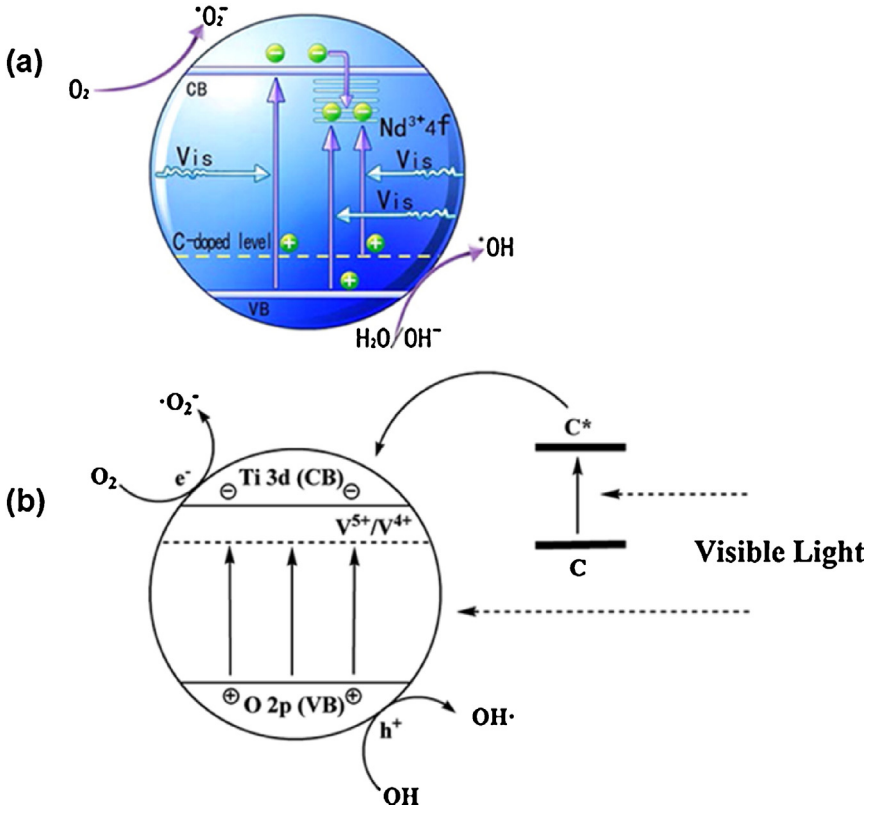

Fig. 14. (a) Schematic illustration of the visible light induced electronic transitions for a C–Nd co-doped TiO_2 sample, showing transitions from unoccupied Nd–4f energy levels to the TiO_2 conduction band, C-centred energy levels to the Nd-energy states as well as to the conduction band of TiO_2 (reprinted from J. Phys. Chem. C 117 (2013) 8345–8352 with permission from American Chemical Society, (b) schematic representation of photoprocesses in a C–V co-doped TiO_2, where C on the surface of TiO_2 acts as a sensitiser, absorbs visible light and transfers electron to the conduction band or impurity energy levels, while V-doping into TiO_2 lattice results in a band gap narrowing (reprinted from ACS Appl. Mater. Interfaces 3 (2011) 1757–1764 with permission from American Chemical Society).

co-doped TiO_2 and PdO nanoparticles, which favors trapping of photogenerated electrons by PdO nanoparticles thereby inhibiting electron–hole recombination.

4.3. Metal doping

Photocatalytic activity and visible light response of TiO_2 can be enhanced by doping with various metal ions, including 3d transition metal ions [118–122], lanthanides [123–125], and noble metals [126–130]. Various mechanisms such as bandgap narrowing, formation of impurity based energy levels within the bandgap and formation of intrinsic defects such as oxygen vacancies and interstitial Ti have been suggested to account for the improved activity of metal ion doped TiO_2. Y_2O_3 doped TiO_2 nanocomposite film deposited on indium tin oxide (ITO) glass substrate has been fabricated using sol–gel–dip coating technique [131]. The Y_2O_3 doped TiO_2 film was converted into a hydrophilic surface (WCA 8°) upon illumination with a daylight lamp for 1 h [131]. A significantly high number of oxygen vacancies can be created by the addition of Y_2O_3 into TiO_2 during the UV irradiation [131,132]. These oxygen vacancies are responsible for the hydrophilicity of the Y_2O_3–TiO_2 nanocomposite film.V_2O_5–TiO_2 nanoporous layers (pore size of 50–400 nm) were synthesized using micro-arc oxidation method that exhibited higher hydrophilicity upon visible light illumination due to their rough surface [133]. Visible light absorption arises from the doping of V_2O_5 in the TiO_2 lattice resulting in a narrow band gap. Zang et al. reported the visible-light photo-degradation of 4-chlorophenol in aqueous solution using amorphous microporous metal oxides of titanium (AMM-Ti) loaded with chlorides of Pt^{IV}, Ir^{IV}, Rh^{III}, Au^{III}, Pd^{II}, Co^{II}, and Ni^{II} [134]. It was proposed that the metal salts perform as chromophores, transferring the charges generated during the photo-reactions to the amorphous region.

Modification of TiO_2 lattice with varying amount of Zn^{2+} ion was found to enhance the photocatalytic activity and visible light absorption of TiO_2, which has been assigned to the formation of surface oxygen vacancies, resulting in various sub energy levels situated near the bottom edge of the conduction band of TiO_2, which are responsible for the visible light absorption of Zn-doped TiO_2 [135]. Moreover, Zn^{2+} doped anatase TiO_2 films deposited on ITO glasses showed improved hydrophilicity compared to the undoped TiO_2 films due to formation of surface oxygen vacancies [136]. Co-addition of Zn^{2+} and an anionic surfactant sodium dodecylbenzenesulfonate (DBS) in the precursor sol increased the surface roughness of TiO_2 films and resulted in a superhydrophilic surface (WCA 3°), which was found to be maintained for two weeks in dark [136].

4.4. Metal-non-metal co-doping

Co-doping TiO_2 using both metal and non-metal elements have gained considerable attention. The co-doped systems such as N–Cu [39], N–Fe [137], N–W [138], V–N [139], C–Mo [140], C–Nd [141], S–Fe [142], etc showed higher photocatalytic activity due to the synergistic effects of metal and non-metal dopants. The doped metal and non-metal elements can create additional energy levels in the band gap (Fig. 14a). Upon visible light the electronic transition can occur from the valence band of TiO_2 to the metal centred energy levels as well as from doped non-metal based energy levels to the metal energy levels and TiO_2 conduction band (Fig. 14a) thereby increasing the overall visible light absorption [137–139]. Alternatively, the metal element can substitute at the Ti site in the

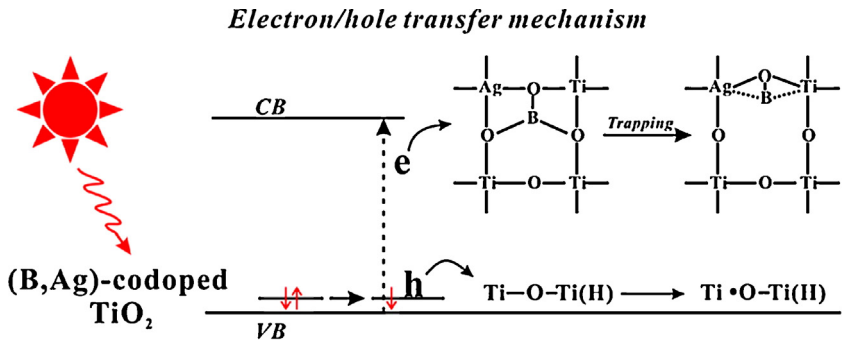

Fig. 15. Schematic representation of the electron/hole transfer mechanism for the B–Ag codoped TiO_2 under solar irradiation. (Reprinted from J. Am. Chem. Soc. 135 (2013) 1607–1616, with permission from American Chemical Society).

lattice while the non-metal can exist as a surface species (Fig. 14b). The visible light activity of the co-doped TiO_2 increases due to the synergistic effects of metal and non-metal dopants, resulting from the narrow band gap and separation of electron–hole pair [143,144]. Recently, Feng et al. demonstrated the extraordinarily high photocatalytic activity of B-Ag-co-doped TiO_2 under solar irradiation [145]. It has been suggested that doped B species can weave into the interstitial sites of the TiO_2 lattice. Incorporation of Ag in the close proximity of the tri-coordinated interstitial B (B_{int}) sites favors the formation of B_{int}–O–Ag structural units, which can trap the photoinduced electron and facilitate electron–hole separation (Fig. 15).

4.5. Dye sensitization

Sensitization of TiO_2 by a visible light absorbing dye has been widely used in semiconductor photocatalysis, for the degradation of organic pollutants as well as in dye sensitized solar cells [146–149]. The sensitization process involves photoexcitation of a sensitizer molecule (usually a transition metal complex or an organic dye) to the appropriate singlet or triplet electronic excited state, followed by an electron injection from the excited sensitizer molecule into the conduction band of semiconductor material. The resulting electron–hole pair can in turn generate various reactive oxygen species that lead to degradation of organic pollutants. Metalloporphyrins, and ruthenium complexes are considered as efficient sensitizers due to the presence of delocalized π electron systems and strong absorption in the visible region and high thermal and chemical stability [150–154]. In addition to Ru(II) complexes and metalloporphyrins, other metal complexes based on Os(II) [155], Pt(II)[156] and Re(I) [157] have also been extensively used as sensitizers.

Visible light active self-cleaning cotton fibers functionalized with TiO_2 have been developed using meso-tetra(4-carboxyphenyl) porphyrin (TCPP) and meso-tetra(4-carboxyphenyl)-porphyrinato M(II) (MTCPP: M = Fe, Co, Cu, Zn) sensitizers (Fig. 16) [151,158]. The photocatalytic self-cleaning properties of the functionalized cotton fibers have been assessed by their ability to remove coffee/wine stain under visible light irradiation. Free base TCPP/cotton fibers exhibited lower photostability compared to the M-TCPP/cotton, thereby limiting the use of TCPP as a sensitizer in practical self-cleaning applications. Among

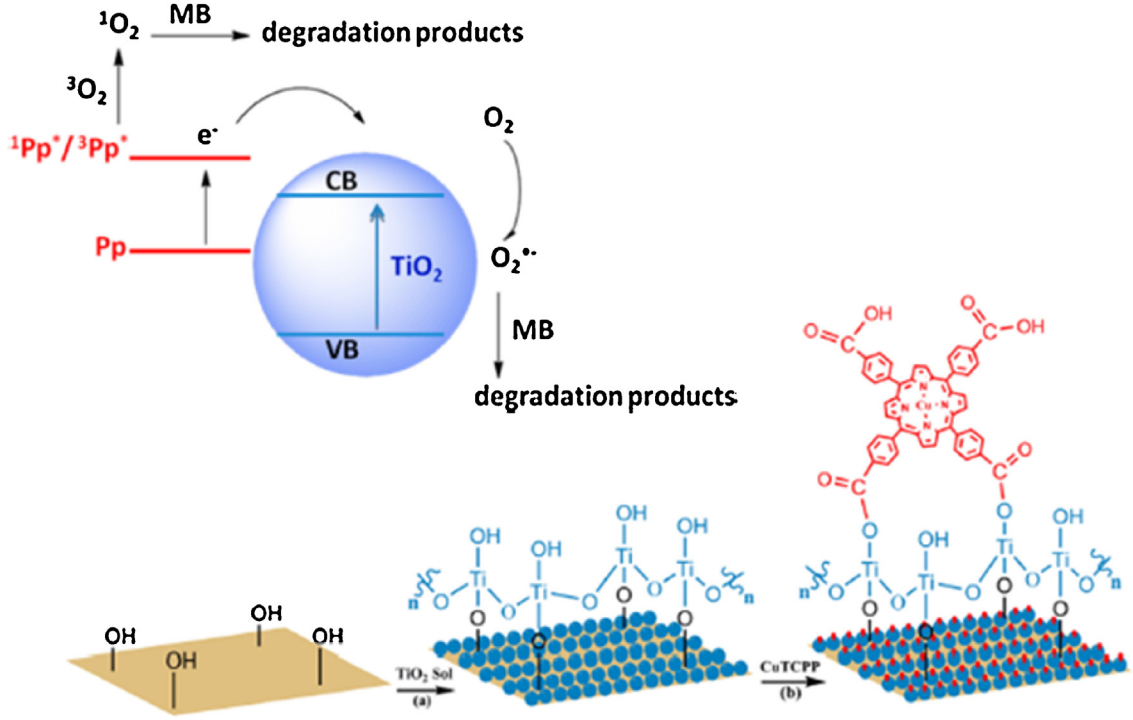

Fig. 16. Schematic illustration showing the mechanism of dye sensitization in cotton functionalized with TiO_2 and Cu–TCPP. (Reprinted from ACS. Appl. Mater. Interfaces 5 (2013) 4753–4759 with permission from American Chemical Society).

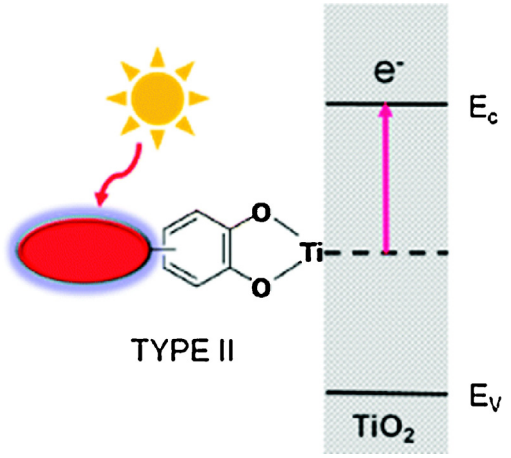

Fig. 17. Catechol–thiophene light harvesting molecules for dye-sensitization.
(Reproduced from J. Phys. Chem. C (114) 2010 17964–17974 with permission from the American Chemical Society).

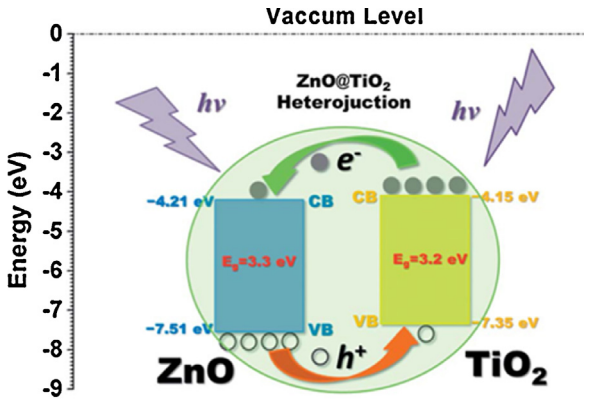

Fig. 19. Schematic diagram demonstrating the charge transfer between ZnO and TiO_2 nanotube arrays.
(Reproduced from J. Mater. Chem. A 2 (2014) 7313–7318 with permission from Royal Society of Chemistry).

the metalloporphyrins, CuTCPP showed higher photocatalytic activity.

A new type of dye-sensitized TiO_2 system is reported using a simple thiophene-catechol system (Fig. 17) [159]. In this case, the charge transfer follows through a type II injection system, where the charge injection occurs directly from the HOMO (highest occupied molecular orbital) of the organic system to the conduction band of titania. (Fig. 17) [159]. The device performances were optimized in relation to the dye loading, open circuit voltage and current density. The light harvesting efficiency was consistent with the level of conjugation (e.g., with 1, 2 or 3 thiophene units).

4.6. Heterojunction/heterostructure formation

Formation of heterojunction structures incorporating TiO_2 and other narrow bandgap semiconductor material is an attractive strategy to improve the photostability and efficiency of photocatalytic processes by increasing the separation between charge carriers. Various heterojunction structures such as ZnO/TiO_2 nanocomposites [160], anatase–rutile or anatase-brookite TiO_2 heterojunctions [161–164], have been developed for improving photocatalytic reactions.

The hybrid film of TiO_2/WO_3 (Fig. 18) was developed by depositing WO_3 particles on a TiO_2 film that exhibited an enhanced rate for photocatalytic oxidation of methylene blue and transformed to a highly hydrophilic surface upon illumination with a 10 W fluorescent lamp [165,166]. The smaller band gap of WO_3 (2.8 eV), allows excitation by visible light, where photogenerated holes can be transferred to TiO_2, which take part in subsequent photocatalytic oxidation reactions and hydrophilic conversion. Presence of an intermediate SiO_2 later between TiO_2 and WO_3 was found to inhibit the charge migration and photoinduced processes. Pt or other multielectron cocatalysts can accept electron from the conduction band of WO_3 and thus facilitates the charge separation and photocatalytic process [167]. TiO_2/WO_3 bilayer films having low W(VI)/Ti(IV) molar ratio were generated by layer-by-layer technique [168]. A high photonic efficiency (1.5%) was reported for 30 TiO_2/WO_3 bilayers for the degradation of acetaldehyde (1 ppm) upon UV-illumination.

Hierarchical flake like Bi_2MoO_6/TiO_2 bilayer films have been developed, which showed significantly enhanced photocatalytic activity and self-cleaning properties under visible light irradiation [169]. The porous and flake like structure of the hybrid material provide higher surface area for efficient visible light harvesting coupled with efficient separation of electron and holes at the interface of two semiconductors. In order to obtain low band gap material, anatase TiO_2/Cr-doped TiO_2 composite thin film deposited on glass slide was developed using DC magnetron sputtering [170]. The composite film showed significantly improved hydrophilicity than the TiO_2 thin film with the WCA reaching a value of 10° upon 5 h of UV illumination. The enhanced hydrophilicity of the composite film has been assigned to the effective charge separation at the interface. The anatase TiO_2/4.8% Cr-doped TiO_2 exhibited the slowest conversion into a hydrophobic surface and retained hydrophilicity for 48 h after the UV-illumination was discontinued.

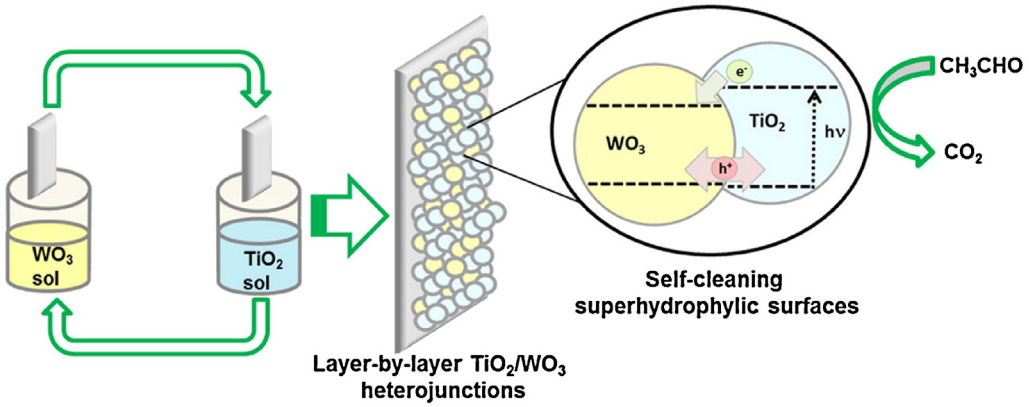

Fig. 18. Schematic illustration of photoinduced electron transfer in TiO_2/WO_3 heterojunction in bilayer films.
(Reproduced from ACS Appl. Mater. Interfaces 6 (2014) 16859–16866, with permission from American Chemical Society).

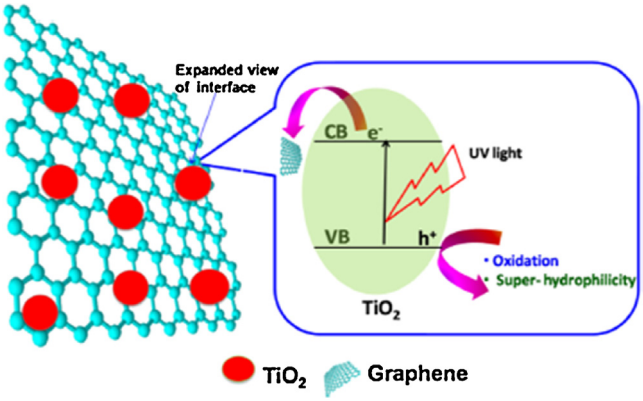

Fig. 20. Schematic illustration showing charge transfer in graphene/TiO_2 composite. (Reprinted from ACS Appl. Mater. Interfaces 5 (2012) 207–212 with permission from American Chemical Society).

ZnO/TiO_2 core–shell nanorod arrays (Fig. 19) have been further developed by coating ZnO nanorods with a thin TiO_2 nanosheet with exposed (0 0 1) facets through a hydrothermal method [171]. Presence of the TiO_2 coating provided chemical stability and imparted enhanced photocatalytic activity and hydrophilicity. The improved photocatalytic activity results from the combination of enhanced surface area of the heterojunction photocatalyst and increased charge separation resulting from the injection of photoexcited electron from the conduction band of TiO_2 to the conduction band of ZnO and the transfer of photogenerated holes of ZnO to the valence band of TiO_2. The heterojunction coating displayed high transmittance and hydrophilicity (WCA 10°) upon UV irradiation owing to the highly porous structure of the nanorod arrays. Transparent thin films of TiO_2–ZnO were deposited on polycarbonate sheets using interlayers of SiO_2 [172]. The self-cleaning coating with a TiO_2:ZnO molar ratio of 1:0.05 showed the most efficient photocatalytic activity and superhydrophilicity under prolonged UV irradiation. Visible light active TiO_2/multiwalled carbon nanotube (CNT) heterostructures have been fabricated by atmospheric pressure chemical vapor deposition technique [173]. The TiO_2/CNT showed superhydrophilicity upon exposure to UV/vis light due to slow recombination of electron and hole at the interface. Application of electric bias, also converted the TiO_2/CNT surface into a superhydrophilic one due to formation of *p*–*n* junction at the interface.

4.6.1. Graphene based heterostructures

In recent years, nanocomposites of graphene with semiconductor materials have been found to exhibit improved optoelectronic and photocatalytic properties [174–176]. Highly conductive and optically transparent thin films comprising of graphene loaded TiO_2 showed significantly enhanced photocatalytic properties and superhydrophilicity compared to pure TiO_2 under illumination from a white fluorescent lamp [177]. The enhanced photocatalytic activity of graphene/TiO_2 can be attributed to the efficient electron injection from the conduction band of TiO_2 to graphene (Fig. 20). The water contact angle for the graphene loaded TiO_2 film decreased with increasing irradiation time. However, the film did not show hydrophilic conversion under visible light, indicating that only the UV portion of the white fluorescent light was effective for photoinduced hydrophilic conversion. Electroconductive cotton fibers coated with TiO_2/graphene nanocomposite exhibited improved self-cleaning and antimicrobial properties under UV and solar irradiation [178].

TiO_2/reduced graphene oxide (RGO) hybrid films have been developed by a combination of surface sol–gel process and layer-by-layer assembly method [179]. The hybrid film showed improved photocurrent generation under broadband light illumination, where RGO can be photoexcited under both UV and visible-NIR irradiation, while TiO_2 is photoactive under UV radiation, resulting in the overall broadband response of the hybrid film. Additionally, photoexcited electrons from the conduction band of TiO_2 can be injected into RGO, which supresses charge carrier recombination through rapid charge transport and charge separation. The hybrid TiO_2/RGO film was converted into a superhydrophilic one with a WCA 4.2° after broadband light illumination and exhibited excellent antifogging properties, which suggest potential utility of these films in designing self-cleaning optoelectronic devices.

4.6.2. TiO_2/SiO_2 heterostructures for superhydrophilic and antireflective surfaces

Self-cleaning TiO_2 coatings with low surface reflection/antireflection property and high light transmission ability is beneficial for their applications such as in flat panel displays, solar energy collectors, and greenhouses [180–187]. Additionally, for practical applications, it is desirable that the hydrophilic character of self-cleaning coatings is maintained for a long period even in the absence of light. However, photoinduced superhydrophilic character of pure TiO_2 film generally reverts back gradually in the absence of light illumination. TiO_2/SiO_2 composite films were found to exhibit enhanced superhydrophilicity and improved maintenance of hydrophilicity in dark [188–192]. The TiO_2/SiO_2 composite films showed increased Lewis acidity resulting from the excess positive charge generated due to the doping of silicon atoms into the TiO_2 lattice [193]. Increased acidity of the composite films also accounts for the increase in the hydroxyl groups at the surface, resulting in an enhanced hydrophilicity. Additionally, presence of SiO_2 can also decrease the refractive index of the TiO_2/SiO_2 composite film and increase the extent of light absorption by the composite film and hence increase the photocatalytic activity [194,195]. Photocatalytic activity of TiO_2/SiO_2 composite films was found to be closely related to their hydrophilic property (Fig. 21) [76,196].

Macroporous superhydrophilic TiO_2/SiO_2 composite was also developed using a template free sol–gel method that involved mixing the precursors of TiO_2 sol and SiO_2 sol in the presence of two complexing agents, acetyl acetone and diethanolamine, to control the rate of hydrolysis and precipitation of metal alkoxide [197]. Presence of SiO_2 layer has also been reported to enhance the photocatalytic antibacterial property of TiO_2 films [198]. TiO_2/SiO_2 composite films doped with 3d metals have been prepared by sol–gel dip coating technique, which showed red shifted absorption compared to TiO_2/SiO_2 composite and photoinduced superhydrophilicity [199,200]. Doped metal ions act as hole trapping sites, which enhance the charge carrier separation and account for the enhanced photocatalytic and self-cleaning properties. In recent years, several groups have reported fabrication of superhydrophilic wool and cotton fibers using TiO_2/SiO_2 composites, which displayed photocatalytic self-cleaning activity against bacterial adhesion [198] and for removal of food, coffee and wine strains [201–204].

Antireflective, self-cleaning coatings have been developed using layer-by-layer assembly of SiO_2–TiO_2 core–shell nanoparticles on glass support, that exhibit superhydrophilicity both in the presence and absence of UV illumination [185,205]. The antireflection property arises from the presence of submicrometer sized SiO_2 particle layer, which also provided a porous structure. The superhydrophilic property of the coatings results from enhanced surface area of the nanoparticles and higher surface roughness of the particle coating. In order to produce antireflective self-cleaning coatings, TiO_2 particles were used to coat poly(ethylene terephthalate) [206] and poly(methyl methacrylate) [207] films having moth-eye-like surfaces. The antireflection and

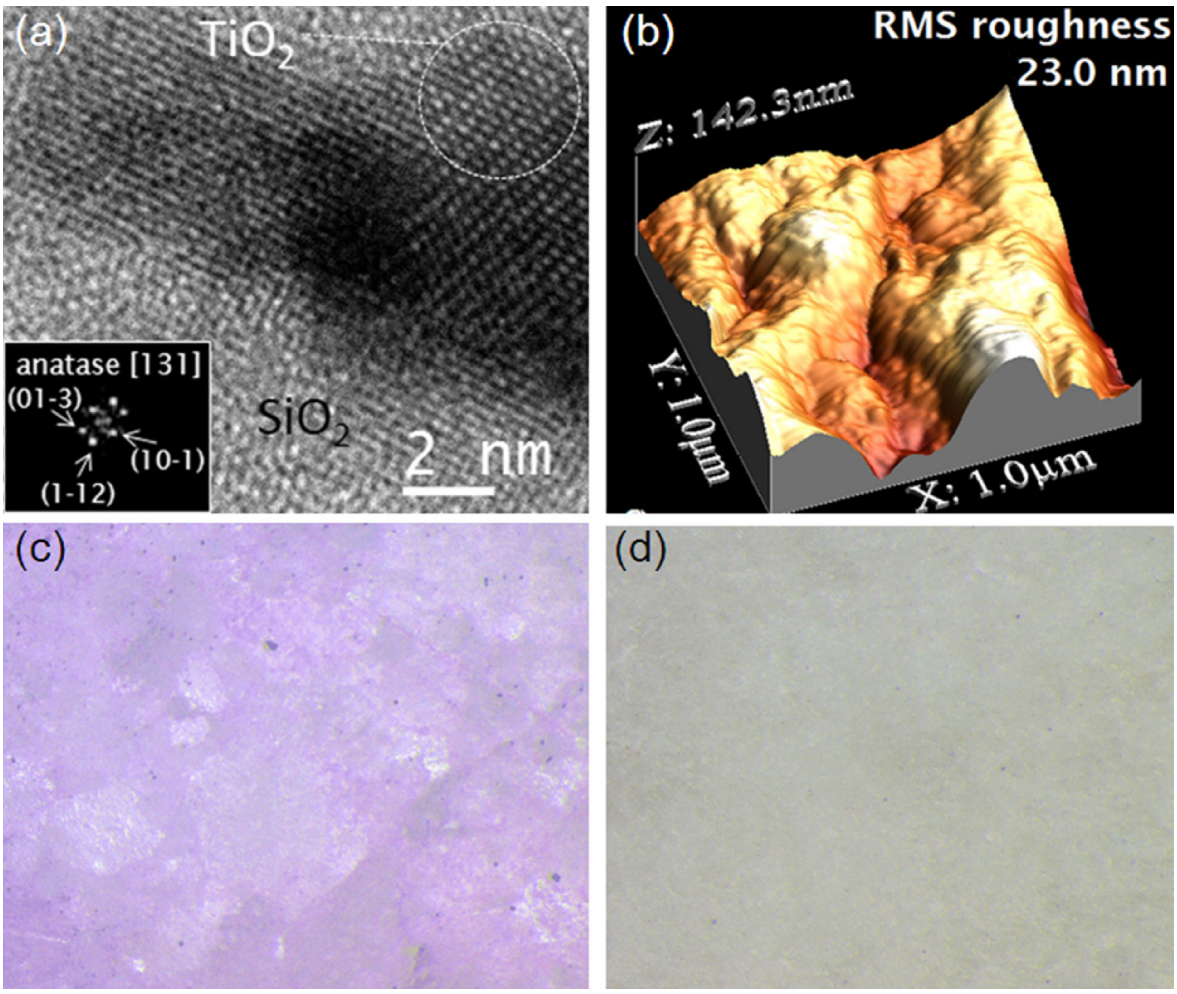

Fig. 21. (a) High resolution electron micrograph of TiO_2/SiO_2 nanocomposite containing anatase TiO_2 synthesized in the presence of oxalic acid and polydimethyl siloxane, (b) 3D AFM image of the nanocomposite, (c) optical microscopic image of an uncoated marble surface treated with methylene blue after UV irradiation, (d) microscopic image of the methylene blue treated marble surface coated with TiO_2/SiO_2 nanocomposite following UV illumination.
(Reproduced from Appl. Catal. B 156–157 (2014) 416–427, with permission from Elsevier).

self-cleaning properties of the coatings can be applied in solar cells and flat panel displays. Dust and other organic pollutants can typically reduce the conversion efficiency up to 30% and therefore the application of a self-cleaning coating can significantly improve the efficiency of solar cells [208]. On the other hand, the light-absorbing materials coated solar cells could decrease the overall light to electricity conversion efficiency. No significant studies have been found so far on the impact of hydrophilic self-cleaning coatings on the light conversion efficiency [209]. Low cost antireflection coatings possessing self-cleaning properties have been designed employing a self-assembled block copolymer in combination with silica sol–gel chemistry and anatase TiO_2 nanocrystals [210]. In order to overcome the problem associated with polymer instability during outdoor applications of antireflective coatings, hydrophobic surfaces were fabricated from vertically oriented rutile nanorods grown on glass surface [211]. The resulting glass substrates demonstrated high transmittance in the visible light region (520–800 nm) and enhanced photocatalytic self-cleaning activity toward hydrophilic and oily contaminants. The nature of the solvent present in the precursor solution showed significant effects on the nucleation and growth of the nanorods and played crucial roles in determining the microstructure and morphology of the surface (Fig. 22).

4.7. Summary of contact angles of various TiO_2 composites

As discussed in previous sections, several strategies have been developed by various groups to improve the photocatalytic activ-

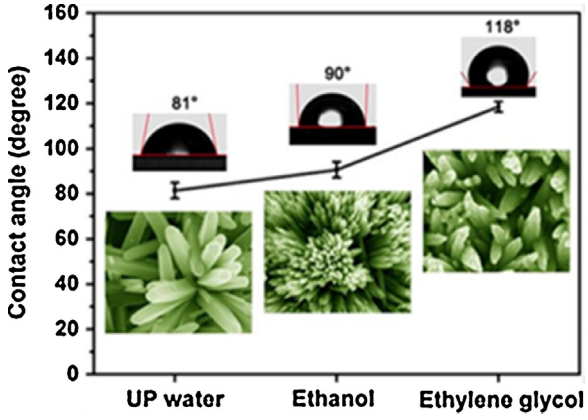

Fig. 22. Field emission scanning electronic microscopic images showing the effect of solvent composition present in the precursor solution on the morphology and water contact angle of TiO_2 nanorods deposited on glass substrate.
(Reproduced from J. Colloid Interface Sci. 365 (2012) 308–313, with permission from Elsevier).

Table 2
Summary of contact angles of various TiO_2 composites discussed.

System	Contact angle	Illuminating source	Intensity of illumination	Reference
PdO–N,F–TiO_2	0°	Visible light <4 min	1.0 mW/cm^2	[117]
WO_3/TiO_2	0°	UV > 10 h	5–10 μW/cm^2	[166]
Bi_2MoO_6/TiO_2	0–12° (depending on reactime time)	UV	Not specified	[169]
CNT/TiO_2	0°	Visible light 10 min	Not specified	[173]
SiO_2/TiO_2	3°	UV	Not specified	[80]
DBS–Zn–TiO_2	3°	Visible light	Not specified	[136]
C,N,F–TiO_2	3–4°	Measured in dark	–	[212]
RGO/TiO2	4.2°	Broadband illumination	Not specified	[179]
V_2O_5–TiO_2	<5°	UV (25 W lamp) for 45 min	Not specified	[133]
Graphene/TiO_2	<5°	While fluorescence light	20 μW/cm^2	[177]
Ag–N–TiO_2	<5°	White light for 2 h	Not specified	[104]
N–TiO_2	<5°	White light for 2 h	Not specified	[104]
C–TiO_2	<5°	UV > 1.5 h	0.2 mW/cm^2	[105]
SiO_2/N–TiO_2	6°	Visible light for 30 days	159.4 μW/cm^2	[96]
Y_2O_3–TiO_2	8°	Daylight lamp (60 W) irradiation for 60 min	Not specified	[131]
N,F–TiO_2	8°	Visible > 5 h	3 mW/cm^2	[115]
TiO_2/Cr–TiO_2	<10°	UV for 5 h	0.5 mW/cm^2	[170]
ZnO/TiO_2	10°	UV illumination	Not specified	[171]
C–TiO_2	>10°	Visible > 1.5 h	0.2 mW/cm^2	[105]
N,S–TiO_2	>10°	Visible > 1 h	0.5 mW/cm^2	[114]
Zn–TiO_2	27°	Visible light	Not specified	[136]

ity and hydrophilicity of TiO_2 based materials. Although there is no straight forward way to compare the activity of various materials due to variation in the nature of illuminating light, intensity of light, irradiation time, contact angle values, the systems were compared to obtain a general idea about the efficiency of self-cleaning of different types TiO_2 reported and are summarized in Table 2.

In general, modifications that increased surface roughness, for example C,N,F co-doping [212], co-addition of Zn and DBS [136] etc., appeared a promising way to increase the self-cleaning activity of the materials and also useful for maintaining hydrophilicity upon storage in dark. Formation of heterostructure of TiO_2 with other materials to increase the charge separation appeared another effective approach to increase the photocatalytic activity and self-cleaning efficiency. Introduction of rough surface morphology in combination to heterostructure formation was found to be more effective for fabrication of photocatalytic self-cleaning materials. This was illustrated by the examples of Bi_2MoO_6/TiO_2 [169] and ZnO/TiO_2 [171] systems. Doping with non-metals, especially nitrogen, was found to increase the hydrophilicity and visible light induced photocatalytic activity [96].

5. Photocatalytic antibacterial composites

In recent years TiO_2 based photocatalysts have gained significant attention for developing self-cleaning antibacterial materials [213,214]. Kikuchi et al. initially demonstrated the UV-light induced photocatalytic antibacterial activity of TiO_2 thin films [215]. TiO_2 microspheres with reactive (1 1 1) facets exposed on the external surface produced higher amount of •OH compared to Evonik Degussa P25 upon UV illumination and demonstrated higher rate of bacterial inactivation, which results from the suppressed electron–hole recombination in crystallized faceted TiO_2 microsphere structures [216]. Visible light absorbing Cu_xO/TiO_2 nanocomposites have been developed for indoor applications, where the Cu_xO clusters composed of a mixture of Cu(II) and Cu(I) species [217]. Presence of Cu(II) favored induced visible light absorption of TiO_2 and photocatalytic oxidation of volatile organic compounds, while Cu(I) imparted antimicrobial activity in the absence of light [217].

Visible light active C-doped anatase-brookite nanoheterojunction displayed significantly higher photocatalytic activity and higher rate of inactivation against *Staphylococcus aureus* compared to commercially available photocatalyst Evonik-Degussa P-25 [162]. *S. aureus* inactivation rate constants of 0.0023 and −0.0081 min^{-1} were found for TiO_2 hetero-junctions and Evonik Degussa P-25, respectively. The efficient electron–hole separation at the TiO_2 hetero-junctions interface is accountable for greater antibacterial activity of the carbon doped TiO_2 nano-heterojunctions. Photocatalytic disinfection of *Escherichia coli*, *S. aureus*, *Enterococcus faecalis*, *Candida albicans* and *Aspergillus niger* using C-doped visible light photocatalysts was also reported and the inactivation was found in the following order *E. coli* > *S. aureus* ≈ *E. faecalis* » *C. albicans* ≈ *A. niger* [218]. Anatase TiO_2 nanotubes fabricated on Ti surface and loaded with Ag nanoparticles demonstrated high antibacterial activity against *E. coli* [219]. To achieve long-term antibacterial activity, Ag nanoparticles were generated in situ within TiO_2 nanotubes, coated with a quaternary ammonium salt. The resulting nanocomposites exhibited high biocompatibility and long-term antibacterial activity. Presence of the quaternary ammonium salt coating resulted in a reduced release of Ag from the nanocomposites [220]. Anti-bacterial properties of undoped titania nano-tubes prepared by electrochemical anodization method have also been analysed using *E. coli* and *S. aureus*. These nanotube materials were found to be very effective in disinfecting both *E. coli* (97.5%) and *S. aureus* (99.9%) using UV irradiation. Surface morphology and physico-chemical characteristics of titania nanotube materials play a significant role in the anti-bacterial activity [221]. Nanostructured AgI/TiO_2 photocatalysts have been developed that showed efficient visible light active photocatalytic degradation of organic pollutants and photoinduced antibacterial activity [222]. Visible light active self-cleaning cotton has been fabricated by loading AgI particles on TiO_2 functionalized cotton fibers, which exhibited efficient degradation of methyl orange under visible light irradiation compared to TiO_2-cotton fibers [223]. The improved visible light activity has been assigned to photoexcitation of the narrow band AgI, where photogenerated electrons from the conduction band of AgI can be transferred to the conduction band of TiO_2, thereby increasing the charge separation along the heterojunction interface. Silver nanoparticles were deposited on the surface of TiO_2 nanoarrays to construct photocatalytic self-cleaning substrate combined with surface enhanced Raman active detection platform [224,225].

Several mechanisms have been proposed to account for the antibacterial activity of TiO_2. Upon illumination of TiO_2 with suitable light, several ROS such as hydroxyl radical, hydrogen peroxide, and superoxides are generated, which can be potentially fatal for

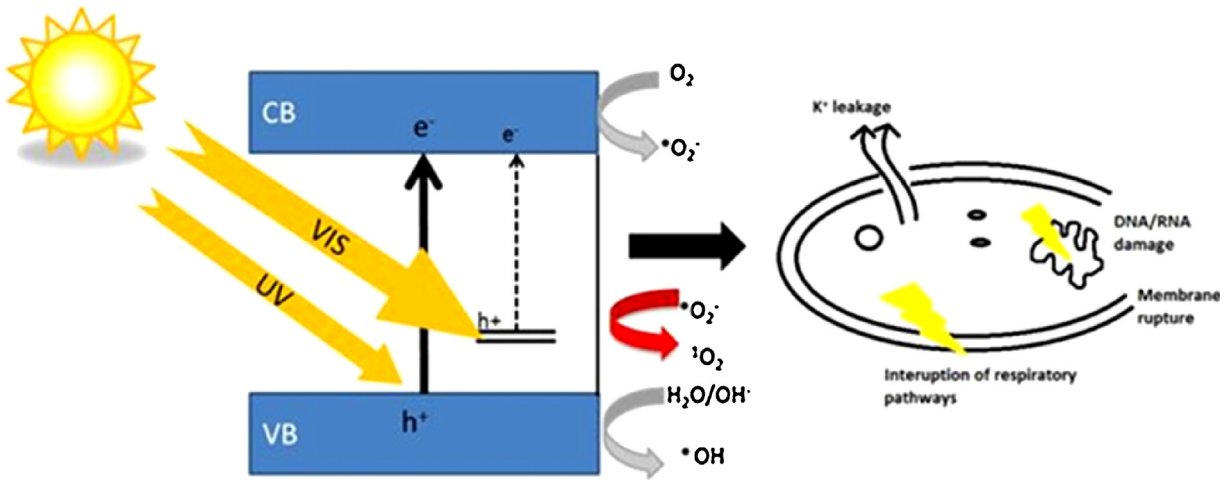

Fig. 23. Proposed mechanism of photocatalytic self-cleaning antimicrobial action.
(Reprinted from Appl. Catal. B: Environ. 130–131 (2013) 8–13 copyright (2013) permission from Elsevier Science).

microorganisms (Fig. 23). Irradiation of TiO_2 can destroy the cell wall and cell membrane of bacterial cell [226,227]. Rengifo-Herrera et al. reported that for N, S co-doped TiO_2, photogenerated holes generated upon visible light irradiation do not possess suitable reduction potential to produce •OH radical by the oxidation of H_2O [228,229]. Under visible light irradiation, less oxidative $O_2^{\bullet-}$, and $^1O_2$ are thought to be responsible for the photocatalytic decomposition of bacterial cells. However, UV light excitation can produce highly oxidizing •OH radicals, which can cause photocatalytic bacterial inactivation [228,229].

6. Photocatalytic hydrophobic surfaces

Superhydrophobic surfaces are characterised by low free energy surfaces possessing a WCA greater than 150°. The hydrophobic surfaces can be fabricated by controlling the chemical compositions and geometric structures of solid surfaces. In contrast to superhydrophilic photocatalytic materials, there are very limited examples of superhydrophobic photocatalytic surfaces [70,230–233]. However, these surfaces offer several advantages as self-cleaning materials over superhydrophilic surfaces, including reduction in bacterial adhesion [234], superior cleaning action due to "lotus effect" [235] and anti-misting property [236]. The examples provided in this section summarize various strategies such as functionalization of TiO_2 surfaces with PTFE, PDMS, fluorinated alkyl moieties and modification of surface morphology, which can increase surface roughness and lower the surface free energy. The presence of the hydrophobic coatings, in most of the cases, prevents complete hydrophilic conversion of TiO_2 upon irradiation while the TiO_2 surfaces display photocatalytic and hydrophobic properties simultaneously.

Nakajima et al. developed transparent superhydrophobic films by calcination of a mixture of aluminium acetylacetonate and titanium acetylacetonate, followed by coating with a fluoroalkylsilane [237]. The films were characterized by rough, porous surface and the roughness was correlated to the concentration of TiO_2 in the film. The film containing 2 wt% TiO_2 showed a WCA 140° after illumination with UV light (1.7 mW/cm^2) for 800 h. The film maintained its hydrophobicity and exhibited photocatalytic degradation of stains upon exposure to outdoor light for 1800 h. The self-cleaning action of the superhydrophobic film has been explained in terms of photocatalytic activity of TiO_2 combined with its photoinduced amphiphilic property (i.e., possessing both hydrophilic (*water-loving*) and lipophilic (*fat-loving*) properties, simultaneously). Calcium hydroxyapatite (HAP) based photocatalyst has been developed, where Ti(IV) ions partially substitute Ca^{2+} ions [238]. Ti(IV)-doped HAP particles showed decomposition of acetaldehyde under UV irradiation. Further coating of Ti(IV)-doped HAP particles with a fluoroalkyl silane (FAS) and a methacrylate based hydrophobic organic polymer resulted in a superhydrophobic film with a WCA 155° and an oil repellent property [232]. However, the FAS treated Ti(IV)-HAP polymer composite displayed low photocatalytic efficiency for the degradation of isopropanol, which presumably resulted from the low surface exposure of Ti(IV)-HAP photocatalytic particles and the presence of FAS coating that prevented diffusion of gaseous contaminants. The FAS treated Ti(IV)-HAP-polymer composite films maintained their hydrophobic character for a long period of time (>600 h) upon exposure to exterior light. This probably arises from the presence of FAS coating, which inhibits direct contact with Ti(IV)-HAP and polymer.

Superhydrophobic nanocomposite coating of TiO_2 and polytetrafluoroethylene (PTFE) has been developed using a radio frequency-magnetron sputtering (RF–MS) deposition method [239]. The film exhibited UV-light induced photocatalytic degradation of oleic acid and the superhydrophobicity was retained after five cycles of oleic acid adhesion and UV-illumination (Fig. 24).

Thin film of TiO_2 nanoparticles dispersed in polydimethylsiloxane (PDMS) has been synthesized using aerosol assisted chemical vapor deposition technique [240]. The resultant thin film exhibited superhydrophobic nature (WCA 162°) due to high surface roughness and low surface energy of the polymer. Additionally, the film also retained its superhydrophobic character and did not undergo any significant degradation after prolonged irradiation with UV light (λ = 365 nm). The high surface area of the polymer surface also allows incorporation of a higher concentration of titania nanoparticles and thus a high rate of photocatalysis. Superhydrophobic coatings were also developed using TiO_2 nanowires and PDMS though simple dipping process [241]. Scanning electron microscopy images showed that the TiO_2 nanowires aggregate in the coating to form dendrite structures, which increase surface roughness, with WCA 158 ± 2° (see Fig. 25a); however, the surface was found to convert into a hydrophilic one (WCA 25°) after UV illumination for 6 h (8 W Hg lamp, λ = 254 nm) and also displayed anti-fouling property for low boiling solvents. Following UV illumination, the increased value of oxygen/Ti ratio suggested an increase in the concentration of hydroxyl group [241]. The self-cleaning action of the surface was examined in terms of its ability to remove graphite powder sprinkled on the surface, which adsorbs

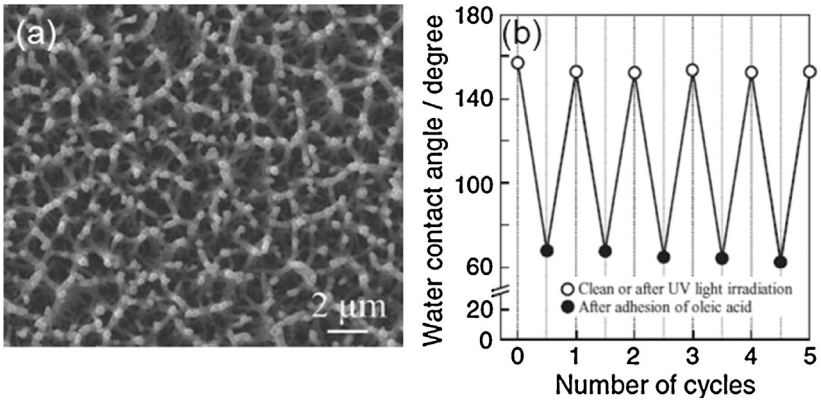

Fig. 24. (a) Field emission scanning microscopic image of TiO_2/PTFE. (b) Changes in water contact angle on TiO_2/PTFE on Ti substrate on oleic acid and UV illumination. (Reproduced from Adv. Mater. 24 (2012) 3697–3700, with permission from Wiley).

readily on the surface of a water droplet placed on the hydrophobic surface and can be readily slided off the surface (see Fig. 25b). The easy fabrication method also allows easy repairability and regeneration of the superhydrophobic surface, which is beneficial to reduce mechanical damage and useful for applications in self-cleaning materials.

Multifunctional TiO_2–high-density polyethylene (HDPE) nanocomposite surface has been fabricated through a template lamination method [242]. The nanocomposite surface possessed hierarchical roughness ranging from micro to nanoscale (Fig. 26). The surface exhibited superhydrophobicity (WCA 158°), low slip-off angle and self-cleaning properties, which were also maintained in the absence of UV light. Illumination of the photocatalytic hydrophobic surface with UV light resulted in a hydrophilic surface due to the oxygen vacancies and the hydrophobicity was eventually restored by heating, which presumably changes the surface composition by reversing the UV induced Ti—O—H bonds to more hydrophobic Ti—O bonds. Superhydrophobic films with WCA as high as 155.5° have been developed using hybrid layers of TiO_2 and dodecylamine [243]. The film retained hydrophobicity for 4 weeks in outdoor applications in the presence of high relative humidity (>90%). The enhanced hydrophobicity of the inorganic–organic hybrid films was attributed to the outward orientation of hydrocarbon chains in the hybrid film.

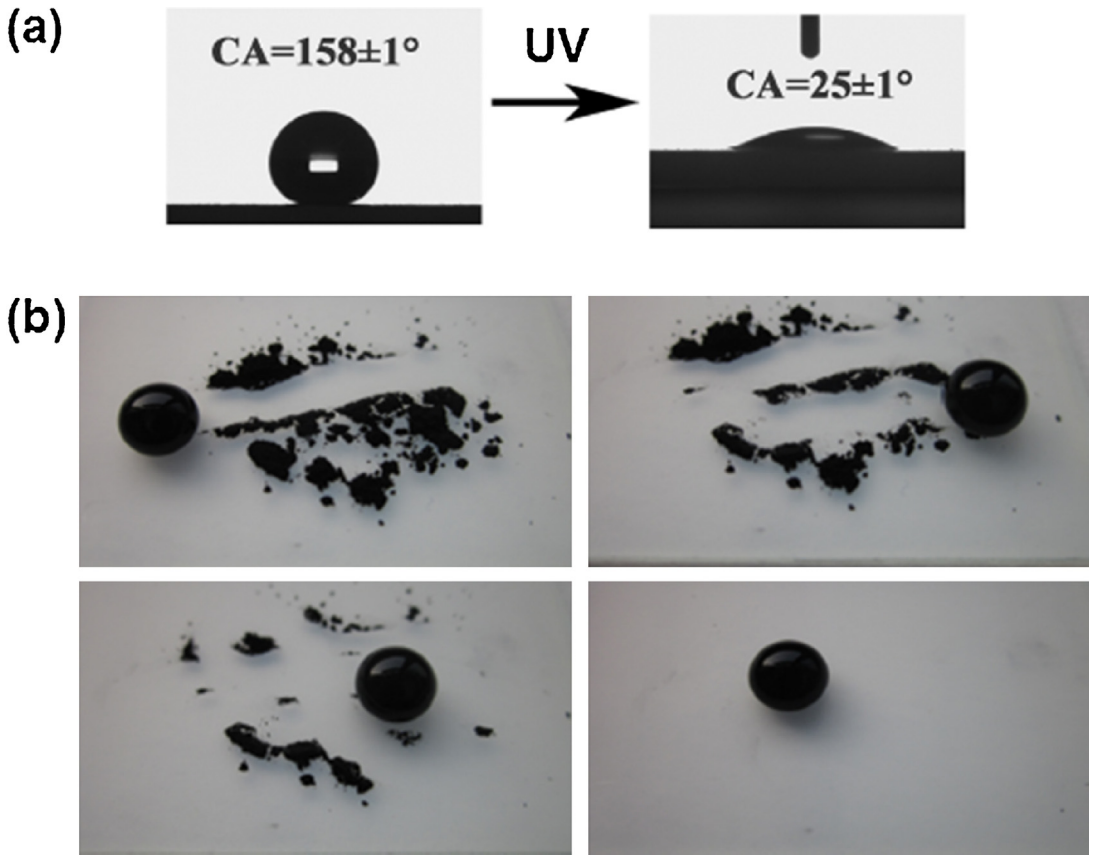

Fig. 25. (a) Changes in WCA of superhydrophobic TiO_2 upon UV-illumination, (b) self-cleaning process on a superhydrophobic TiO_2 surface. (Reprinted from Appl. Surf. Sci. 284 (2013) 319–323 with permission from Elsevier).

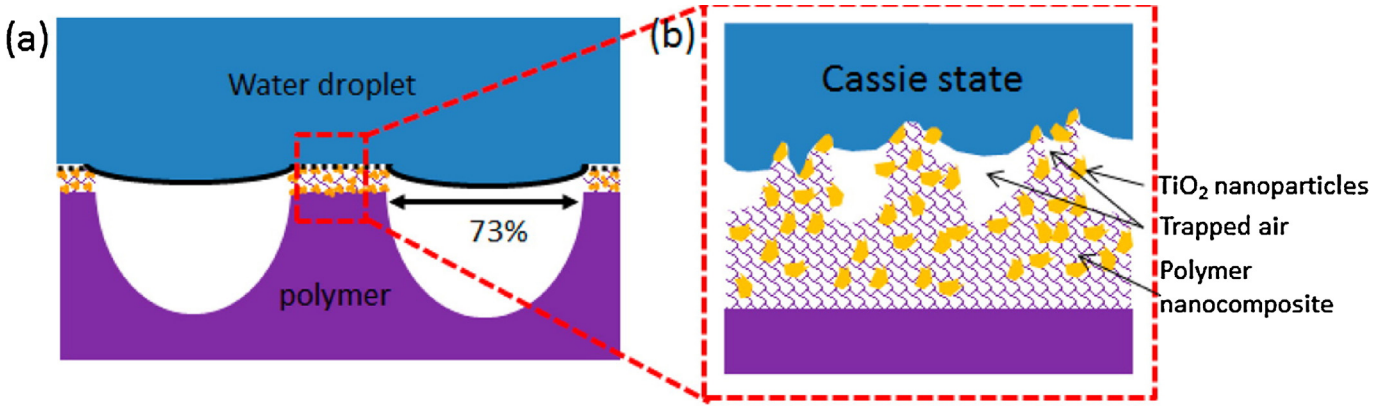

Fig. 26. Schematic illustration of water–air interface on TiO_2–HDPE nanocomposite surface possessing hierarchical structural roughness. (Reprinted from ACS Appl. Mater. Interfaces 5 (2013) 8915–8924 with permission from American Chemical Society).

7. Reversible photo-controlled wetting

Reversible photo-response surfaces with controlled wetting properties have attracted significant attention due to its application in surface engineering of ceramic and bio-materials [244–248]. These tuneable 'smart coatings' can switch reversibly between hydrophilic and hydrophobic surfaces by irradiating with light of appropriate wavelength [248]. The unique properties of these materials have applications in a number of technological areas such as sensors, controlled drug delivery and smart membranes or coatings [248–251]. Most important factors in controlling the reversible nature of wetting are surface roughness, morphology, and the polarity of the surface [244,247,252,253]. Li et al. reported the preparation of a novel micro-nano hierarchical titania/silica composite thin-film by modifying the microspheres of SiO_2 with nano-spheres of TiO_2 and a commercial water-resistant agent

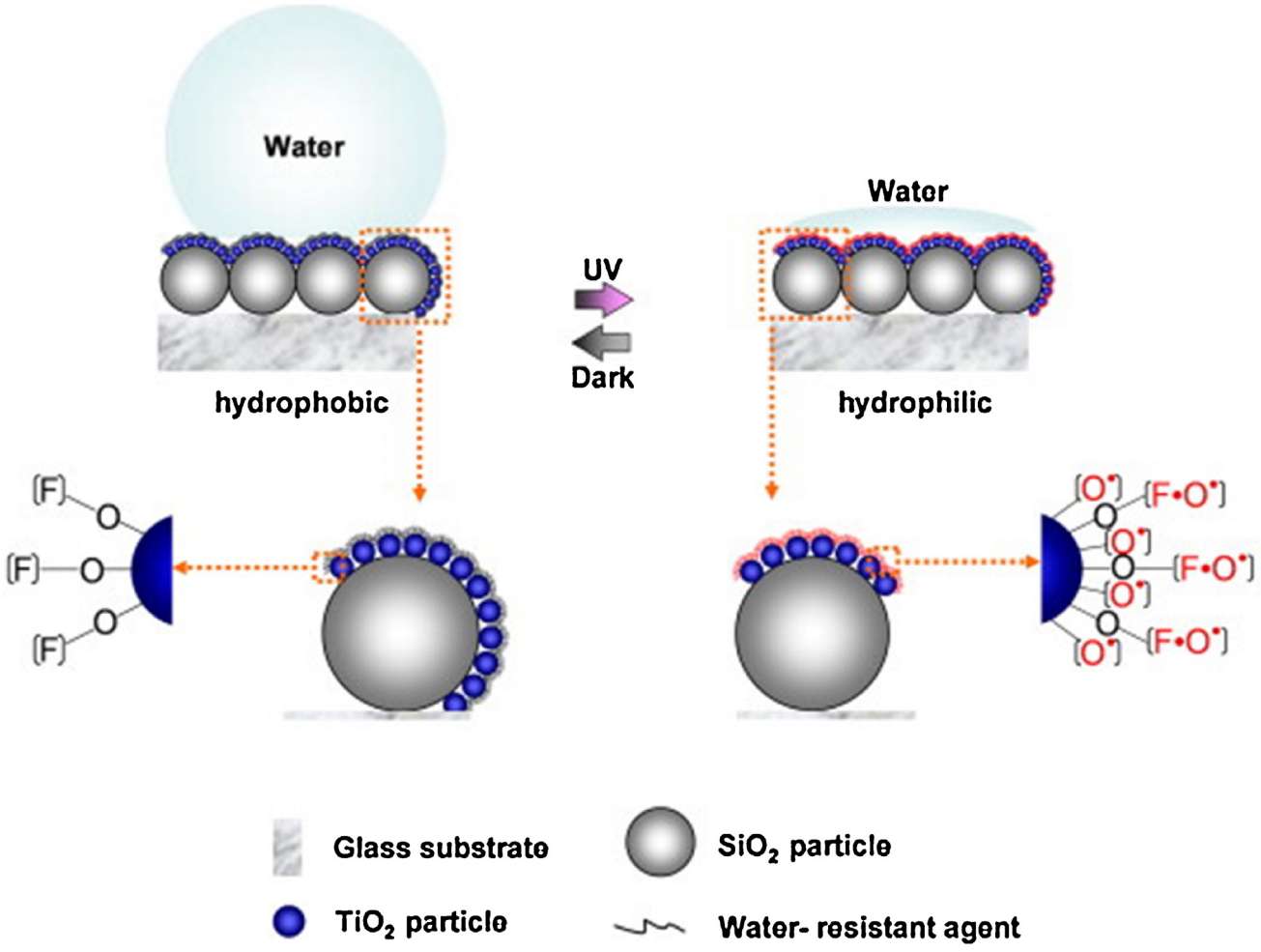

Fig. 27. Schematic representation of the reversible photo-controlled wetting of TiO_2–SiO_2 composites under UV irradiation. (Reproduced from Appl. Surf. Sci. 283 (2013) 12–18 with permission from Elsevier).

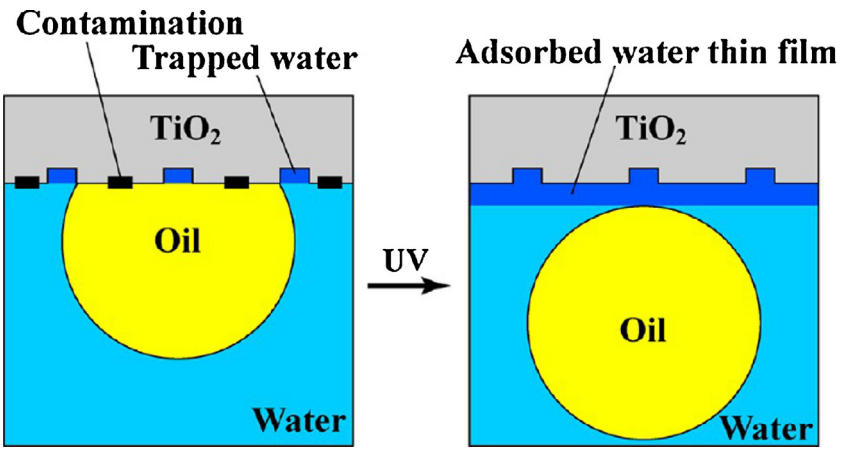

Fig. 28. Origin of underwater superoleophobicity due to formation of thin film of water between an oil drop and TiO_2 surface. (Reprinted from Langmuir 29 (2013) 6784–6789, with permission from American Chemical Society).

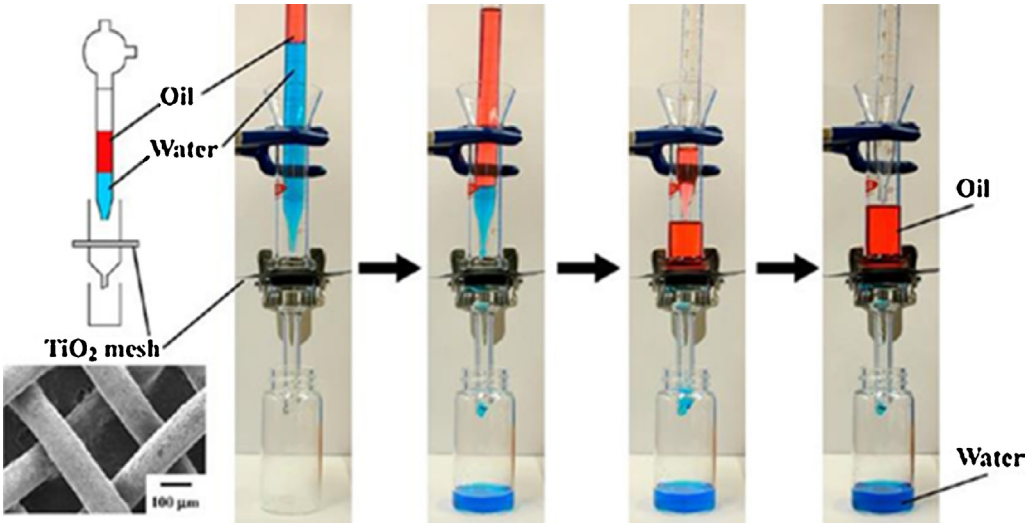

Fig. 29. Oil–water separating device based on titanium mesh, *n*-hexadecane dyed with Sudan IV (red) and water dyed with methylene blue (blue) were used as oil and water phases, respectively. (For interpretation of the references to color in this figure legend, the reader is referred to the web version of this article.) (Reprinted from Langmuir 29 (2013) 6784–6789 with permission from American Chemical Society).

(Aquapel), as shown in Fig. 27. These ordered TiO_2–SiO_2 composites exhibited diverse degrees of amplified wettability [248]. It was also showed that the water contact angle is significantly reliant on the microscopic surface roughness [248]. The effect of TiO_2–SiO_2 size ratio on the wetting properties of these composites were described using the Cassie-Baxter equation [248]. It should also be noted that Mills et al. have indicated that photo-induced superhydrophilicity may be due to the surface restructuring of an intrinsically hydrophobic titania surface during the irradiation process [254].

8. Underwater-superoleophobicity

In recent years, materials that exhibit underwater superoleophobicity have received significant attention due to their applications in marine antifouling, oil spill clean-up, water management etc. [26,255]. Photoinduced underwater superhydrophobicity of TiO_2 surfaces has been reported for TiO_2 thin films prepared by sol–gel process, coated on a glass slide or synthesized by calcination of a Ti plate at 500 °C [256]. UV irradiation resulted in a highly amphiphilic TiO_2 surface demonstrating underwater superoleophobicity with an oil contact angle (OCA) higher than 160°. The photoinduced underwater superoleophobicity results from the presence of a thin water film formed from the trapped water molecules on the surface (Fig. 28), which in turn inhibits the contact between oil droplets and TiO_2 surface. TiO_2 surface was found to lose its superwetting property upon contamination treatment, which was recovered after UV-irradiation and the wettability conversion was reversible for at least three cycles. An oil/water-separating device (Fig. 29) has been designed containing TiO_2 surface on a titanium mesh with a pore size of approximately 150 μm, which exhibited an efficient separation of oil (treated with a red dye Sudan IV) and water (dyed using methylene blue as the blue dye).

An underwater superoleophobic coating derived from flower like rutile TiO_2 grown on fluorine doped tin-oxide (FTO) substrate has been reported recently [257]. The coatings exhibited superamphiphilicity in an air–solid–liquid three-phase system, with both WCA and OCA values of 0°, which results from the hydrophilicity of TiO_2 combined with the hierarchical flower like structure of the coatings. The coatings showed an oil-repellent property similar to fish scales with an underwater OCA 155°, which presumably results from the presence of water molecules trapped in the cavities of rough TiO_2 surface thus resulting in a repulsive

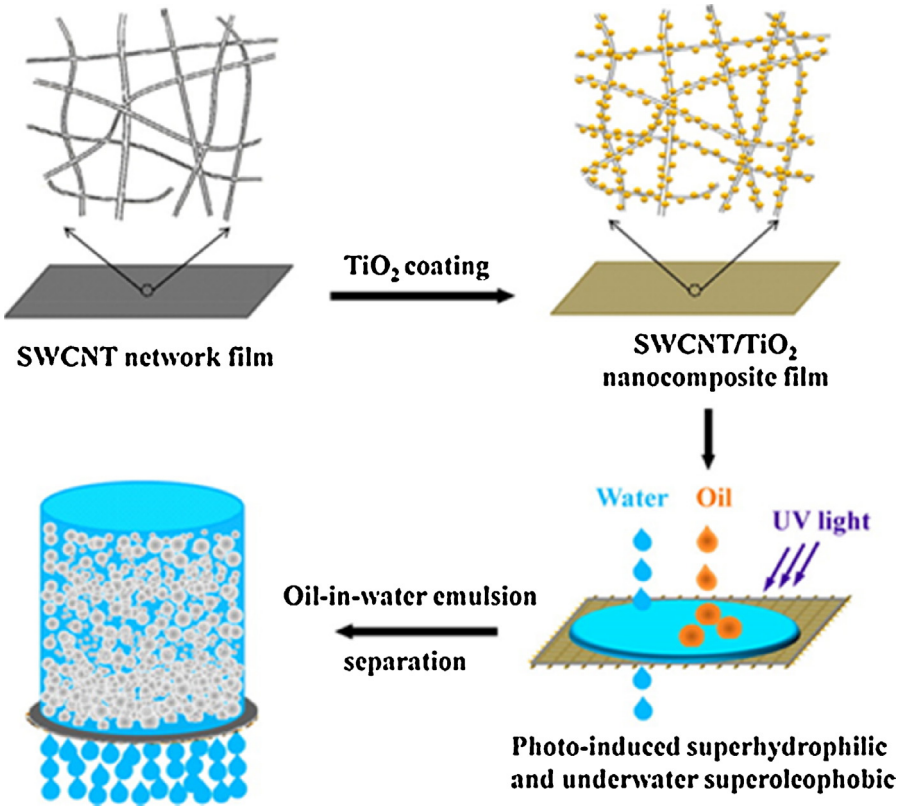

Fig. 30. Schematic illustration showing the fabrication of SWCNT/TiO_2 nanocomposite and its application in separation of oil in water emulsion. (Reproduced from ACS Nano 8 (2014) 6344–6352, with permission from American Chemical Society).

interaction between water and oil molecules. In the presence of contaminants, superwetting state of the coating decreased, resulting in an increase in WCA from 0° to 137° and decrease in OCA from 155° to 64°. However, the superamphiphilicity and underwater superoleophobic property of the film recovered upon irradiation with UV light for 2 h and the reversible transition between underwater oleophilicity and underwater superoleophobicity could be performed for several cycles without any loss in response by changing between contaminant treatment and UV exposure [257]. An ultrathin film made of single-walled carbon nanotubes (SWCNTs) and TiO_2 nanocomposites has been fabricated that demonstrated superhydrophlicity, superoleophilicity, and underwater superoleophobicity upon UV-illumination (Fig. 30) [258]. The UV-illuminated film exhibited underwater contact angles higher than 150° for different oils, which result from the extremely low oil-adhesion force of the UV-irradiated film. The SWCNT network provides nanoscale thick and porous (20–60 nm pore size) structure that enables efficient and ultrafast separation of both surfactant free and surfactant-stabilized oil-in-water emulsions compared to commercial filtration membranes. Moreover, the UV-induced photocatalytic activity of TiO_2 imparts additional antifouling property to the SWCNT/TiO_2 thin films, which is beneficial for the repeated and long-term use of the filtration membranes. Superhydrophobic and underwater superoleophilic membranes composed of sulfonated graphene oxide (SGO) nanosheets and nanostructured TiO_2 spheres have been fabricated for efficient separation of surfactant stabilized oil in water emulsion [259]. The crosslinked nanostructured networks of SGO/TiO_2 membrane provide mechanical flexibility and allow high oil rejection rate combined with very low membrane fouling.

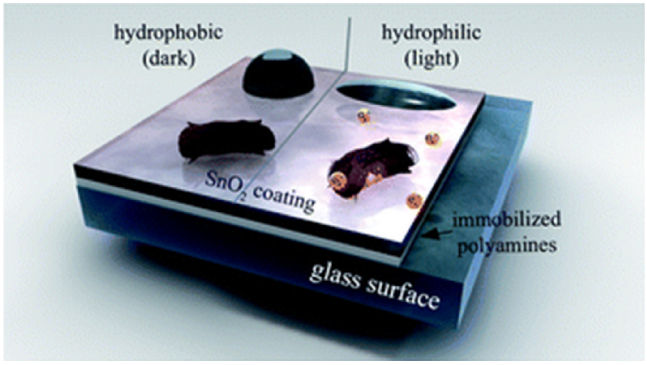

Fig. 31. Schematic diagram showing the bio-inspired SnO_2 films causing degradation of organic dyes and pathogen. (Reproduced from Nanoscale 5 (2013) 3447–3456 with permission from Royal Society of Chemistry).

9. Other material displaying self-cleaning activity

Though TiO_2 based photocatalytic materials have received most attention for developing self-cleaning materials, other *n*-type metal oxides such as ZnO and SnO_2, also exhibit both photocatalytic activity and photoinduced hydrophilic conversion [77]. SnO_2 nanorods displayed switchable superhydrophobicity (WCA 154.1°) before UV exposure and superhydrophilicity (WCA 0°) upon UV irradiation [260]. The hydrophilic conversion has been attributed to surface roughness, formation of oxygen vacancies and surface hydroxyl groups upon UV illumination. Deposition of bio-inspired SnO_2 films on glass surface has been achieved by functionalization with spermine [261]. The bio-inspired SnO_2 films generated superoxide radicals ($^{\bullet}O_2^-$) upon exposure to sunlight and caused degradation of organic dyes and pathogens (Fig. 31).

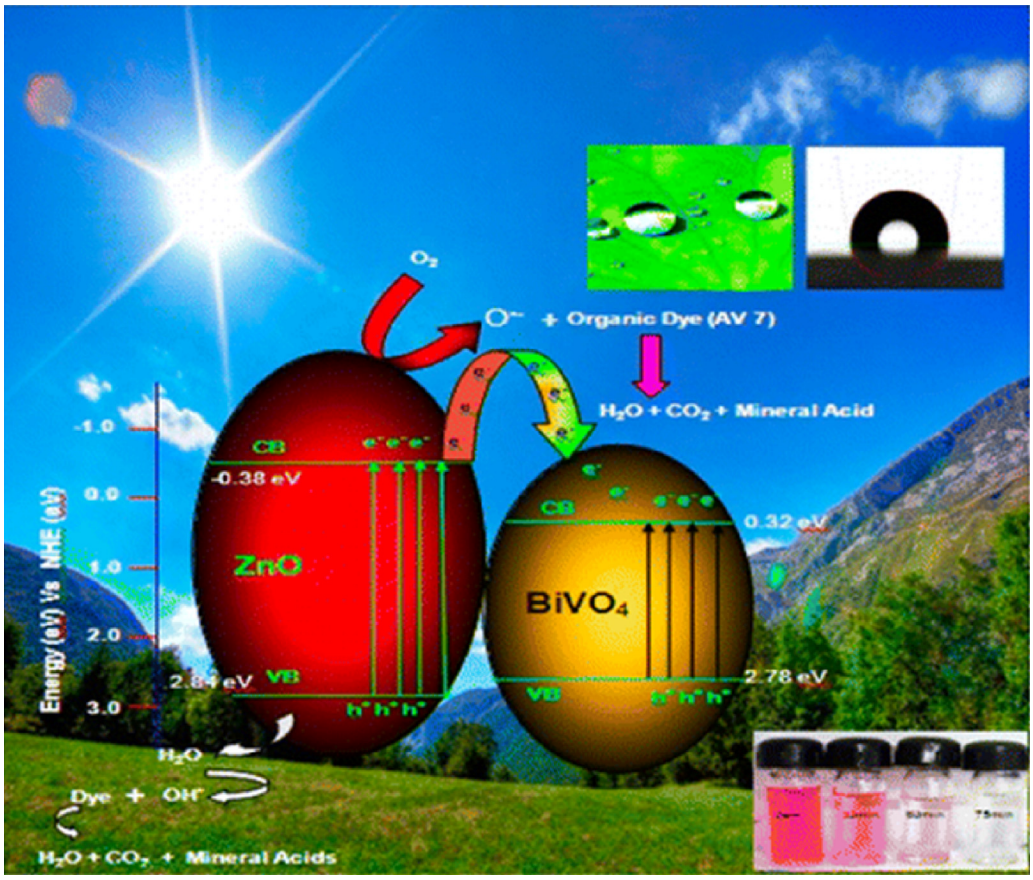

Fig. 32. Heterojunction formation of ZnO with $BiVO_4$.
(Reproduced from Ind. Eng. Chem. Res. 53 (2014) 8346–8356 with permission from American Chemical Society).

The photocatalytic activity combined with the photoinduced hydrophilicity of SnO_2 films can be applied to develop coatings with antifouling properties. Pan et al. reported the fabrication of SnO_2 nanowire based heterostructures that exhibit hydrophobicity due to rough morphology of the surface [262]. The grooves present in the surface microstructure allow trapping of air and prevent penetration of water molecules. These heterostructures demonstrated switchable wettability changes upon alternating exposure to UV illumination, storage in dark and O_2 annealing, which can be beneficial to develop industrial coatings for self-cleaning applications.

Sun et al. demonstrated that thin films of ZnO show a WCA of 109° before UV irradiation and their surfaces are converted to highly hydrophilic upon UV exposure [263]. The photoinduced hydrophilic conversion has been attributed to the formation of surface defects similar to TiO_2 upon UV exposure and subsequent adsorption of water molecules to the defect sites. Plasmon assisted visible light absorbing Ag–ZnO hybrids have been fabricated that exhibit surface enhanced Raman scattering (SERS) and enhanced photocatalytic activity due to efficient separation of charge carriers along the hybrid structure [264]. These UV–visible light induced photocatalytic and uniform SERS active nanoarrays can potentially be used for self-cleaning applications. Guo et al. reported the fabrication of superhydrophobic self-cleaning ZnO/CuO heterohierarchical nanotrees after silinazation [265]. The superhydrophobicity was attributed to the surface roughness and presence of trapped air in the rough surface cavities. Heterojunction formed using ZnO and $BiVO_4$ showed enhanced visible light absorption and superior photocatalytic degradation of organic dyes compared to pure ZnO [266]. The improved activity of the heterojunction results from reduced rate of electron–hole recombination and enhanced visible light absorption (Fig. 32). The heterojunction showed hydrophobic surface (WCA 112.5°) after treatment with tetraorthosilicate (TEOS), which can be useful to design self-cleaning materials.

Kako et al. demonstrated the photoinduced hydrophilic and lipophilic property of $InNbO_4$ thin films [267]. The number of polar groups (e.g., hydroxyl group) was found to increase in the presence of UV irradiation and the mechanism of photoinduced amphiphilicity was thought to be similar to that of TiO_2. Unilamellar nanosheets of $TiNbO_5$, Ti_2NbO_7, Ti_5NbO_{14}, and Nb_3O_8 were evaluated for their photocatalytic activity and photoinduced hydrophilicity [268]. Nanosheets of Nb_3O_8 exhibited higher thermal stability and efficient photoinduced hydrophilicity compared to polycrystalline anatase TiO_2. The high stability of Nb_3O_8 photocatalysts at elevated temperature is advantageous for applications in building materials, which require high processing temperatures.

10. Testing methods for photocatalytic self cleaning surfaces

Measurement of contact angle and photocatalytic degradation of organic dyes are commonly used to evaluate the self-cleaning activity of photocatalytic surfaces [254]. International standard methods have been developed to determine the efficiency of self-cleaning, which can be used by manufactures to characterize their products and ensure quality and reliability.

10.1. ISO 27448: 2009: Standard testing method for photocatalytic self-cleaning surfaces by measuring the contact angle

An international standard organization (ISO) testing method (ISO 27448: 2009) has been published to determine the efficiency

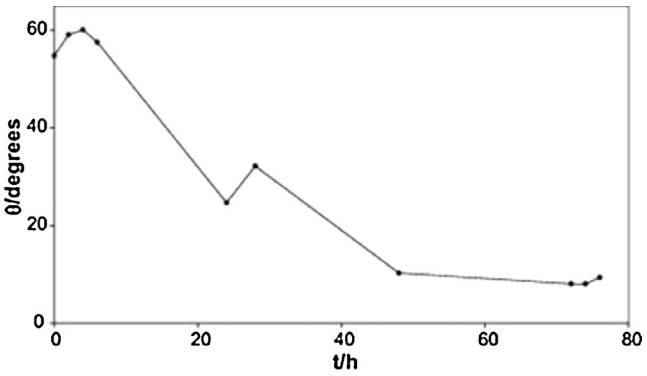

Fig. 33. Typical data generated for contact angle, θ, vs. irradiation time, in the standard ISO 27448: 2009.
(Reproduced from J. Photochem. Photobiol. A 237 (2012) 7–23, with permission from Elsevier).

of self-cleaning of photocatalytic surfaces, which relies on the measurement of WCA upon UV illumination [269]. The method involves application of an organic compound (usually oleic acid, $C_{18}H_{34}O_2$) on the photocatalytic surface and the wettability of the surface is subsequently monitored by measuring the WCA as a function of UV-irradiation time. The oleic acid can be applied either manually or by employing a dipping process. In the manual coating process, 200 μl $C_{18}H_{34}O_2$ is dropped onto the middle of an initially weighed sample. The dropped $C_{18}H_{34}O_2$ should be evenly spread by employing a non-woven cloth. Excess $C_{18}H_{34}O_2$ should be wiped off so that the total weight of the $C_{18}H_{34}O_2$ becomes 20 μg cm^{-2}, as measured by weighing the coated sample. For the dipping process, the sample is placed in a 0.5% v/v solution of $C_{18}H_{34}O_2$ in *n*-hexane. These coated samples should then be dried in an oven set at 70 °C for 15 min. The measurement is continued until the WCA reaches a value less than 5° (Fig. 33). Carbon dioxide and water will be formed after the photocatalytic mineralization of oleic acid in the presence of oxygen and light irradiation (Eq. (11)).

$$C_{18}H_{34}O_2 + 25.5\,O_2 \xrightarrow[h\vartheta \geq 3.2eV]{\text{Photocatalyst}} 18CO_2 + 17H_2O \quad (11)$$

Before carrying out the measurements, the surface should be irradiated for at least 24 h under UV irradiation (for manual coating recommended irradiance dose is 2 mW/cm^2 while the dipped samples should be irradiated with 1 mW cm^{-2} of UVA) to remove organic contaminants and should be handled with proper care to avoid any further contamination. It is also recommended that the initial contact angle should be higher that 20° to observe the change upon UV irradiation and measurements should be performed at five different points in order to obtain an accurate average contact angle. The method provides an easy and effective measure to determine the self-cleaning efficiency of photocatalytic materials; however, it does not incorporate extremely hydrophobic surfaces, granular and water permeable substrates and visible light active photocatalysts. The advantage of this test is that it provides a quick and easy method to identify the photocatalytic self-cleaning action. The major disadvantage of this method is that the conditions for carrying out the testing procedures (e.g., operating temperature and humidity) are not well defined [254] and the contact angle measurements can vary significantly with different experimental conditions. It is also not reported why two different coating procedures are suggested and why two different UVA irradiance dose should be employed for the two differently coated samples [254].

10.2. ISO 10678; 2010, 'Determination of photocatalytic activity of surfaces in an aqueous medium by degradation of methylene blue'

A UV/visible spectrophotometric method (ISO 10678; 2010) has been developed utilizing the photo-induced bleaching of methylene blue (MB) dye to assess the activity of photocatalytic self-cleaning materials [270]. The high molar extinction coefficient of MB ($C_{16}H_{18}N_3SCl$) allows monitoring the photocatalytic process conveniently through a striking color change of the dye from blue to colorless due to photo-mineralization (Eq. (12)). $C_{16}H_{18}N_3SCl$ can completely be mineralized into simple molecules such as HCl, H_2SO_4, HNO_3, CO_2 and H_2O through a series of photocatalytic degradation process [271]. However, these photo-assisted degradation reactions take place on a much larger timescale than the oxidative photo-bleaching of $C_{16}H_{18}N_3SCl$. It should therefore be noted that the rate of photo-bleaching of $C_{16}H_{18}N_3SCl$ is not equal to that of the mineralization of the dye.

$$C_{16}H_{18}SCl + 25.5O_2 + \xrightarrow[h\vartheta \geq 3.2eV]{\text{Photocatalyst}} HCl + H_2SO_4 + 3HNO_3 + 16CO_2 + 6H_2O \quad (12)$$

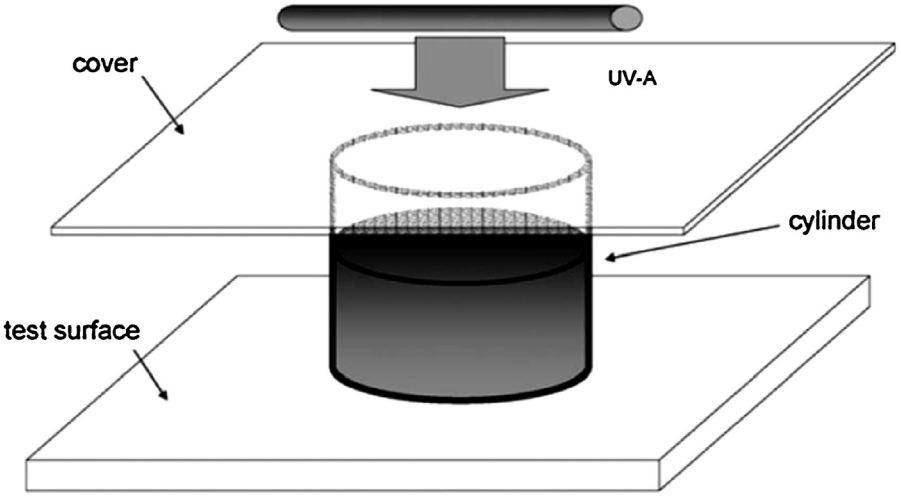

Fig. 34. Set up for the photocatalytic degradation studies of methylene blue.
(Reproduced from Energy Environ. Sci. 5 (2012) 7491–7507 with permission from Royal Society of Chemistry).

The experimental setup (Fig. 34) involves fixing a glass cylinder on a sample plate (typically 10 cm^2) containing the photocatalytic coating. During the preconditioning step, ca. 35 mL MB (20 μM) is added to the cylinder and covered with a UV-A transparent glass plate for 12 h in dark to ensure adsorption of dye on the surface. This is followed by irradiation with UV-A light (recommended dose 1.0 mW/cm^2) with occasional agitation of the solution at every 20 min. The photocatalytic process is monitored through decomposition of MB by measuring absorbance of the solution at 665 nm spectrophotometrically. From the known values of rate of photocatalytic bleaching of MB (r), the UV-A irradiance, photonic efficiency (ξ) for a photocatalytic sample can be calculated according to the following equation.

$$\xi = \frac{100 \times r}{I_{UV}} \quad (13)$$

Photocatalyzed decomposition of MB provides a simple and convenient measure of the activity of photocatalytic self-cleaning materials; however, varying purity of commercially available MB often affect the molar extinction coefficient and therefore results in errors in preparing dye solution of a specific concentration. It should be mentioned that in addition to photocatalytic decomposition, photobleaching of MB can also occur through a dye sensitization mechanism, during which an electronically excited dye molecule (D^*) injects an electron to the conduction band of the semiconductor and gets converted to radical cation ($D^{\bullet+}$). The dye radical cation can in turn undergo decomposition resulting in photobleaching. This dye sensitization mechanism can be avoided by choosing proper excitation source, ($\lambda_{excitation}$ = 365 nm), where MB does not absorbs significantly. The non-catalytic dye-sensitized reaction can be minimized by controlling the pH of the solution at 5.5 (lower than the point of zero charge of the semiconductor ca 6.6 for TiO_2), which ensures minimal dye adsorption and thus lowers the extent of dye sensitized photobleaching reaction. MB decomposition test provides reliable results for moderately active materials such as commercial self-cleaning glass; however, the low diffusion coefficient of the dye limits its use in evaluating the highly active materials [254,272]. Additionally, due to lower photostability of MB, this method is not very effective in assessing low activity materials such as commercial photocatalytic tiles [272].

The advantage of ISO 10678; 2010 is the simplicity of the experimental set up. The major disadvantage is that the purity of the $C_{16}H_{18}N_3SCl$ is not defined in the standard and as noted by Mills et al. the high variation in the purity of commercially supplied $C_{16}H_{18}N_3SCl$ means that it may not be possible to prepare a 10^{-5} M concentration of methylene blue with confidence [254]. It was previously noted that the methylene blue test is more appropriate as a water-purification test than a self-cleaning test [254].

10.3. ISO 27447: 2009, 'Fine ceramics, advanced technical ceramics – test method for antibacterial activity of semiconducting photocatalytic materials'

ISO 27447: 2009 defines a testing process for the antibacterial activity of photocatalytic materials or films on the surface (Fig. 35), by evaluating the enumeration of bacteria under UV irradiation [273]. This protocol is usually used for photocatalytic materials coated on construction supplies (such as boards, flat sheets or plates) or antimicrobial fabrics. ISO 27447: 2009 method does not include powder, granules or porous ceramics. There are two major procedures employed in this analysis: (i) film adhesion, and (ii) glass adhesion. The former method is recommended for the analysis of flat surfaces while the latter method is designed for the assessment of fabric materials. For the film adhesion method bacteria such as *S. aureus* and *E. coli* are the recommended bacteria employed in the test while the glass adhesion method recommends the use

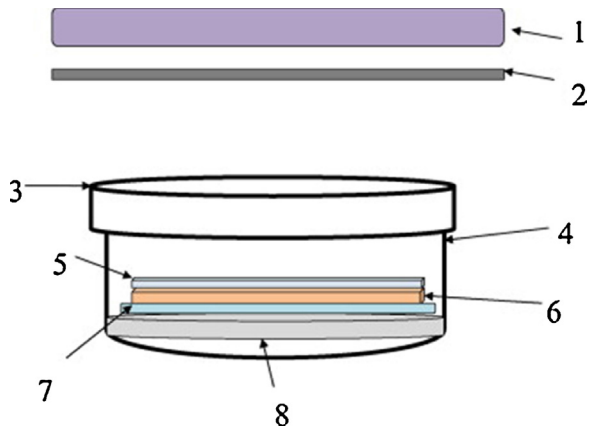

Fig. 35. Experimental set up for sample irradiation (1) UV light source, (2) metal plate (for irradiation level adjustments), (3) lid, (4) petri dish, (5) adhesive film, (6) test samples with inoculated bacteria (7) U-shaped glass rod or tube and (8) moist filter paper.
(Reproduced from J. Photochem. Photobiol. A 237 (2012) 7–23 with permission from Elsevier).

of *S. aureus* and *Klebsiella pneumoniae* [55,254]. It should be noted that ISO 27447: 2009 is specifically designed for testing surfaces and does not deal with the photocatalytic disinfection of water or air.

In the film adhesion method, the bacterial strains (e.g., *S. aureus* and *E. coli*) are inoculated into the nutrient agar and then subjected to incubation at a temperature of 37 °C up to 24 h. The bacteria are then moved to a new agar medium and incubated for another 24 h. A portion of these bacteria is then transferred to a diluted form of the nutrient broth (1/500 NB) and then bacteria are counted using an optical microscope. The bacterial suspension is then diluted with 1/500 NB to get a concentration of 6.7×10^5–2.6×10^6 cells ml^{-1} [273]. This sample will then be inoculated on the surface of the material to be tested [254]. The photocatalytic anti-microbial action (R_L) after 8 h of UV treatment with light irradiance L mW cm^{-2}, can be written as:

$$R_L = \log(B_L/C_L) \quad (14)$$

where C_L and B_L are the number of live bacteria after the illumination period for photocatalytic samples and non-photocatalytic specimens, respectively. Dark control materials with and without the photocatalyst coating should also be developed and kept under the dark condition for 8 h. Live bacteria counts on the specimens with and without the photocatalyst coating after 8 h under the dark conditions are then analysed as: B_D and C_D. The overall photocatalytic antibacterial action ΔR, can be calculated as:

$$\Delta R = \log(B_L/C_L) - \log(B_D/C_D) \quad (15)$$

This is a well-defined and the best available standard to date for benchmarking the commercial photocatalyst based anti-bacterial products. However, the main disadvantage is the recommendation to use two different methods for flat surfaces and fabrics. It is also not fully clear why different strains of bacteria are recommended for these two methods [254,274].

10.4. Photocatalytic activity indicator inks

Most of the ISO standard methods developed until today require expensive analytical instrumentation, skilled personnel, and long analysing time. Recently photocatalytic activity indicator inks have been developed that utilize various redox dyes such as resazurin (Rz), basic blue 66 (BB66) and acid violet 7(AV7) to evaluate the photocatalytic activities of a broad range of materials such as

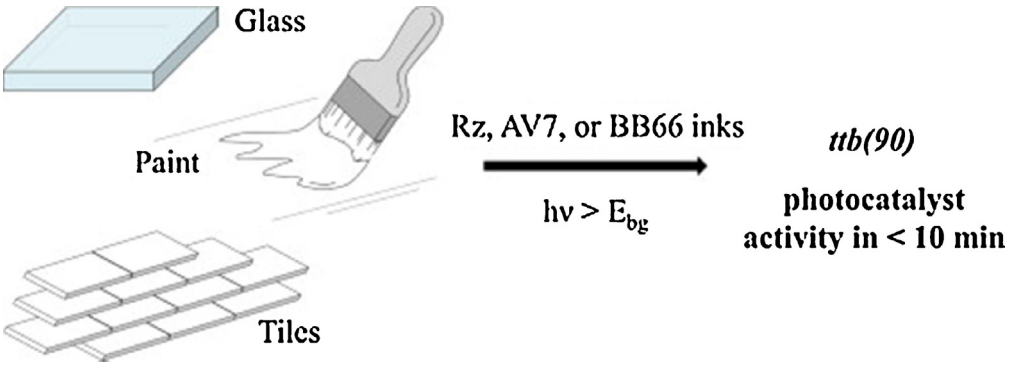

Fig. 36. Photocatalytic activity indicator tests for probing glass, paint and tile surfaces. (Reproduced from J. Photochem. Photobiol. A 290 (2014) 63–71 with permission from Elsevier).

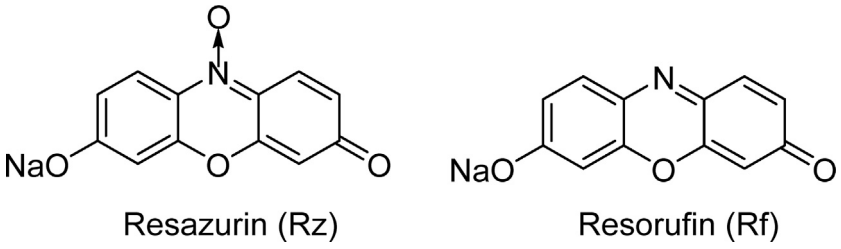

Fig. 37. Structures of resazurin (Rz) and resorufin (Rf).

commercial paints, tiles and glasses (Fig. 36) with varying activities [275–278].

The photocatalytic activity indicator ink consists of a redox dye (D) and a sacrificial electron donor (SED) such as glycerol. Both the dye and the SED are incorporated in a suitable polymer such as hydroxyl ethyl cellulose and applied onto the semiconductor (SC) surface. The working mechanism of the ink involves a photo-reduction reaction, where the photocatalytic surface upon illumination generates an electron and hole pair. The photogenerated electrons reduce the dye resulting in a color change of the indicator ink [279]. For example, the reaction mechanism of testing using dye molecules such as resazurin (Rz) can be described as follows in Eqs. (16)–(18). The system consists of a dye (in this case it is Rz), a sacrificial electron donor or SED (e.g., glycerol) and a polymer material (for example, hydroxyl ethyl cellulose (HEC)), to perform as an encapsulating agent for Rz and SED.

The reaction follows through a photo-reduction pathway as described by reactions 16–18.

$$TiO_2 \overset{h\nu\ E_g}{\rightarrow} TiO_2 * \left(h^+_{vb}, e^-_{CB}\right) \quad (16)$$

$$SED + TiO_2 * \left(h^+_{vb}, e^-_{CB}\right) \rightarrow SED_{ox} + TiO_2 * \left(e^-_{CB}\right) \quad (17)$$

$$Rz + e^-_{CB} + 2H^+ \rightarrow Rf + H_2O \quad (18)$$

Illumination of the surface coated with a semiconductor such as TiO_2 with a light having energy of excitation higher than the band-gap energy (E_g) of the semiconductor, facilitates photoexcitation of valence band electron to the conduction band resulting a positive electron hole (h^+_{VB}) in the valence band. Rz, which is blue coloured, can accept the conduction band electron (e^-_{CB}) and gets reduced to a pink coloured resorufin (Rf) during this reaction (Fig. 37).

The time required for the change from blue to pink or the overall rate of color change gives a measure of the self-cleaning photocatalysis. The details and conditions required for this test are comprehensively explained in previous publications [275–277].

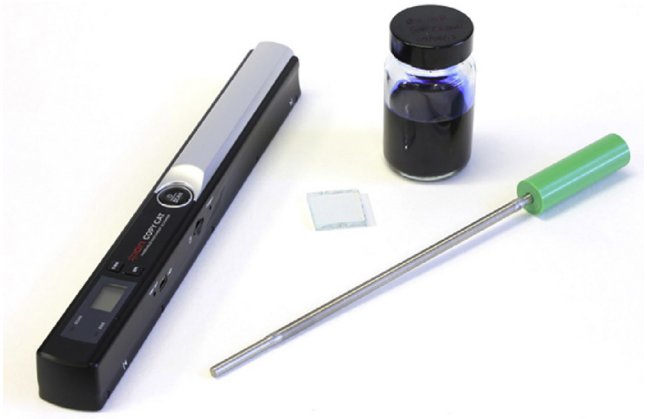

Fig. 38. The tools employed to carry out the photocatalytic activity indicator ink. (J. Photochem. Photobiol. A 272 (2013) 18–20. Reproduced with permission from Elsevier).

The tools employed to carry out this ink test include Rz dye, a wire wound rod (K-bar) and a scanner (Fig. 38)

The photocatalytic activity of a material can be evaluated by monitoring the color change of the indicator ink as a function of irradiation time. Semi-quantitative information can be obtained by recording the digital images of the color changes using a hand-held scanner and analyzing the changes in red–blue–green components as a function of time using an image analysis software (Fig. 39). This testing method provides an inexpensive and quick measure to probe photocatalytic materials with varying activities and is therefore highly beneficial for both researchers and manufacturers to rapidly screen activities of new materials.

Unlike the previously discussed ISO test protocols, these dye based characterization are inexpensive, simple and quick (typically <10 min) [276]. These dye testing results correlate well with tests such as the self-cleaning activity measurements using stearic acid.

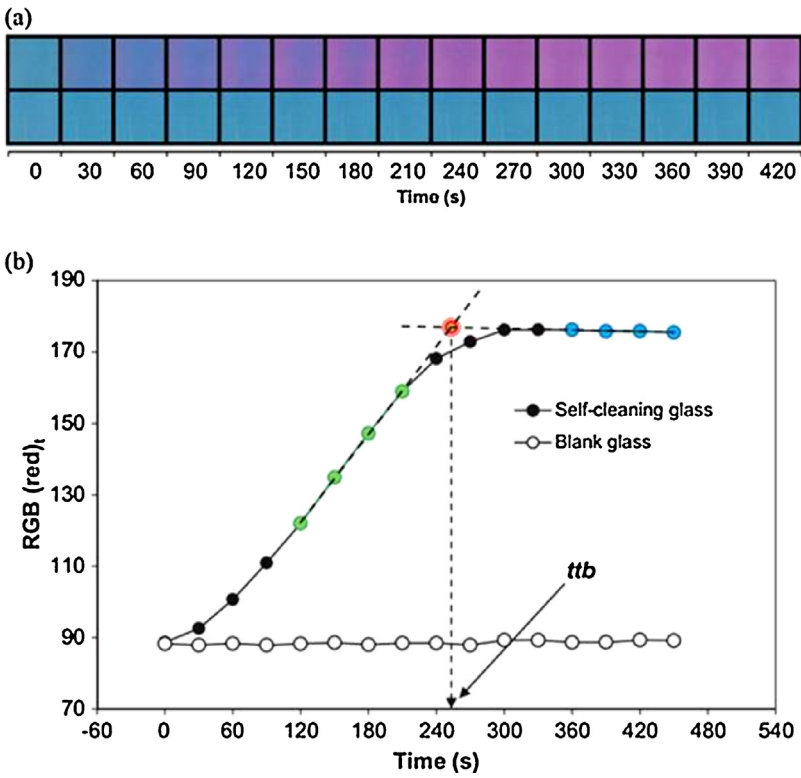

Fig. 39. Self-cleaning test using photocatalytic activity indicator ink (a) test results recorded at 30 s irradiation intervals for self-cleaning glass (top) and, plain glass (bottom). (b) A plot of variation of the RGB (red) with irradiation time, extracted from the images. (For interpretation of the references to color in this figure legend, the reader is referred to the web version of this article.)
(J. Photochem. Photobiol. A 272 (2013) 18–20. Reproduced with permission from Elsevier).

The round robin test on various surfaces showed that their average repeatability and reproducibility are around 11% and 21%, respectively. These test protocols have significant potential to grow in the area of rapid quality control for the photocatalytic industries [276].

11. Commercial applications of photocatalytic self cleaning surfaces

The photoinduced hydrophilic conversion of TiO_2 surface has been exploited commercially to develop anti-fogging, self-cleaning

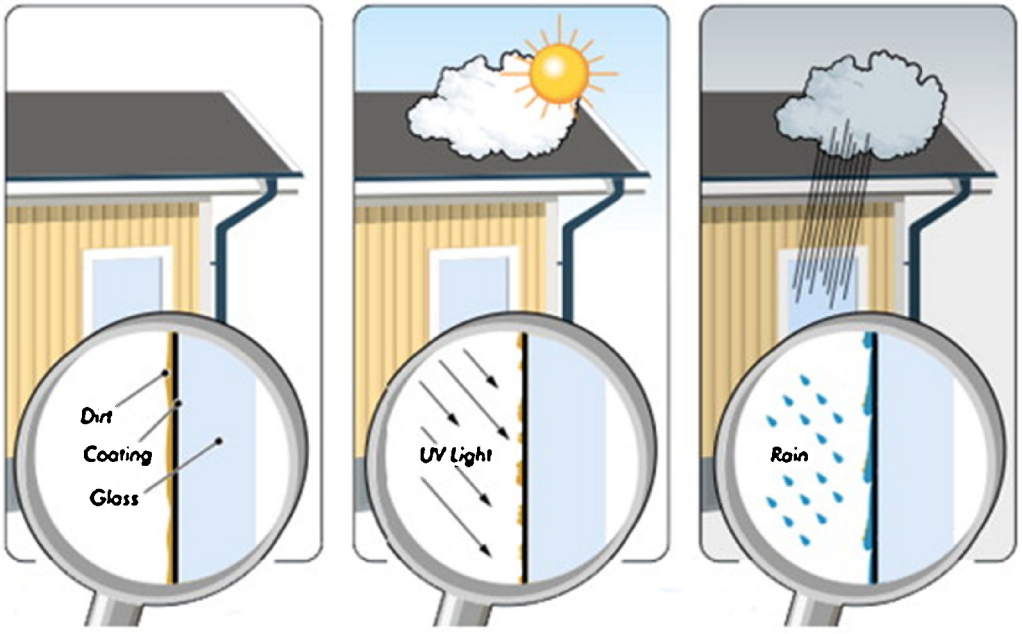

Fig. 40. Schematic illustration of the working mechanism of self-cleaning glasses (from left to right), which require: accumulation of pollutants on glass, activation of the photocatalytic coating by UV light, photocatalytic degradation of the organic pollutants and finally washing the decomposed materials by rain water.
(Reproduced from Sol. Energy Mater. Sol. Cells 109 (2013) 126–141 with permission from Elsevier).

Table 3
Uses of self-cleaning materials.

Substrate	Application	Reference
Glass	Mirrors for vehicles and indoor uses, windows, tunnel, road lights and vehicles	[4–8], [192]
Tile	Kitchen, bathroom, building roof, and walls	[9,10]
Textile/fiber/cotton	Hospital garments, medical devices, house hold appliances, interior furnishing and protective clothing	[1–3]
Plastic/polycarbonate	Automotive industry and buildings	[3,195]

surfaces for various applications such as fabrics, paints, glass, tiles and cement. A brief summary of use of self-cleaning materials is presented in Table 3.

Modification of tiles and glass windows using transparent TiO_2 photocatalysts thin films has been used to construct building materials with photocatalytic self-cleaning properties [280–284]. The self-cleaning action can be achieved by activating the photocatalysis process utilizing solar irradiation as illustrated in Fig. 40. Activ™ developed by Pilkington glass represents the first example of self-cleaning glass, consisting of a 15 nm thick nanocrystalline TiO_2 film deposited on a glass surface [285]. Activ™ represents one of the most successful self-cleaning products and is currently used in various commercial and private buildings world-wide. The suitability of Activ™ as a reference for semiconductor film photocatalysis has been investigated by Mills et al. [9]. The photocatalytic activity of Activ™ was measured in terms of its ability to degrade stearic acid. The suitability of Activ™ as a photocatalytic reference material results from its high mechanical endurance and reproducible photocatalytic activity. Additionally, low visible reflectance (7%), favorable absorption of solar radiation, and transmittance properties of Activ™ are also useful for the self-cleaning applications. In recent years, several other self-cleaning glasses such as Radiance Ti™, Sunclean™, and Bioclean™ are also coming into commercial applications.

The Japanese company TOTO Ltd., introduced a photoinduced superhydrophilicity based technology, Hydrotech™, which uses sunlight to break down pollutants that can be washed away with rain/water. Hydrotech™ has been successfully applied in building materials, coatings and paints made by TOTO Ltd., for indoor and outdoor applications. The photocatalytic products are manufactured by spraying a liquid suspension of TiO_2 on the surface. The surfaces are subsequently sintered at 600–800 °C to strongly attach the TiO_2 layer on the surfaces [286]. Commercial applications of photocatalytic TiO_2-coated materials in the fabrication of self-cleaning glazing products require high processing temperatures; hence, high-temperature stability of photocatalytically active anatase TiO_2 is highly desirable. Non-metallic doping has been reported to increase the thermal stability of anatase phase [287,288], however, this can also promote electron–hole recombination and reduced photocatalytic activity. Recently, visible-light-active, oxygen-rich TiO_2 has been developed in which anatase phase is stable up to 900 °C [289]. High thermal stability of anatase–TiO_2 can be useful for developing self-cleaning building materials.

Recently, it was shown that an ethenol suspension of perfluorooctyltriethoxysilane ($C_{14}H_{19}F_{13}O_3Si$) coated anatase TiO_2 nanoparticles produced a paint that can be coated or extruded onto both hard and soft materials to create a self-cleaning surface. These superhydrophobic coatings can be applied on clothes, paper, glass, and steel for numerous self-cleaning applications. As it is described in Fig. 41, water droplets bounce off from the surface without wetting the material [290].

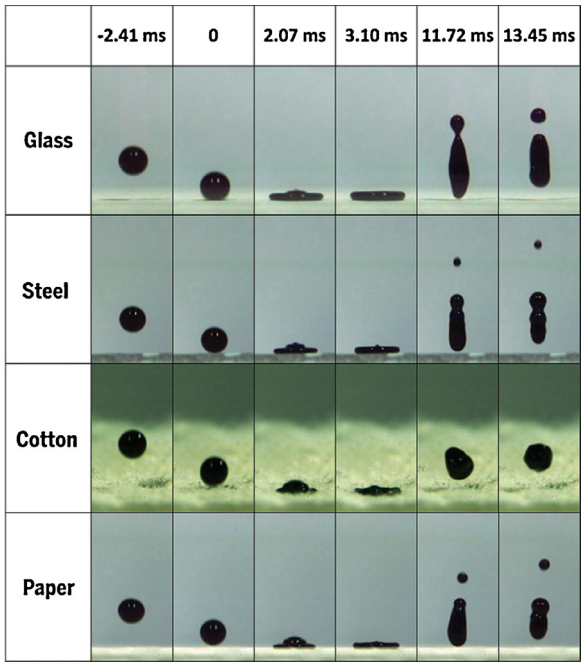

Fig. 41. Time-lapse images of water-drops bouncing on the self-cleaning glass, steel, cotton, and paper surfaces.
(Reproduced with permission from Science 347 (2015) 1132–1135).

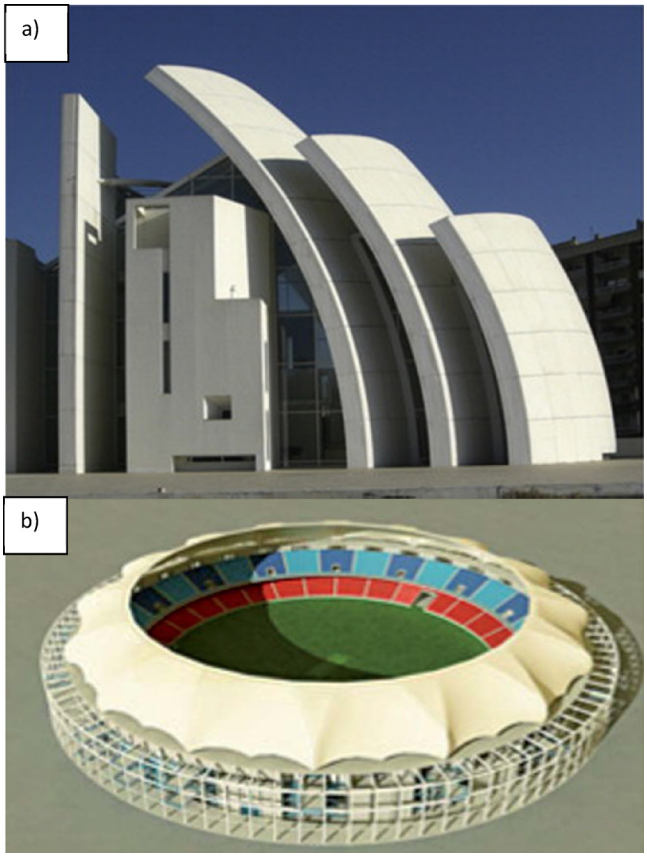

Fig. 42. Self-cleaning cement coated on (A) *Dives in Misericordia* Church in Rome (Reprinted Appl. Catal. B 170–171 (2015) 90–123 with permission from Elsevier Science). (B) Roof of Dubai Sports City's Cricket Stadium. (Reproduced from Energy Environ. Sci. 5 (2012) 7491–7507 with permission from Royal Society of Chemistry).

Fig. 43. Automotive mirror, left: uncoated, right: coated with TiO_2.
(Reproduced from Energy Environ. Sci. 5 (2012) 7491–7507 with permission from Royal Society of Chemistry).

Self-cleaning glass coated with TiO_2 nanoparticles has been applied on the surface of National Opera Hall, China [291]. TiO_2 nanoparticles containing white cement has also been used in *Dives in Misericordia* Church in Rome [292] and Roof of Dubai Sports City's Cricket Stadium (Fig. 42). The Italian multinational company, Italcementi is very active in the research and development of self-cleaning cements and has developed a range of photocatalytic cements and are commercially available in the form of TX Aria™, TX Active™, and TX Arca™ [293]. It has been reported that covering 15% of urban surfaces of the city of Milan with concrete containing TX Active® would reduce the pollution up to 50% [293]. TioCem™, supplied by Heidelberg Cement Technology Center, GmbH, is another popular self-cleaning photocatalytic cement product available in the market to reduce air pollution [294,295].

Eco-friendly, self-cleaning windows and roof tiles are widely used in Japan. Self-cleaning coatings with antifogging properties have been used in automotive industry to develop clean and glare free windows, automotive mirrors (Fig. 43), headlights, and mirrors [296]. Water droplets tend to form a continuous film on a superhydrophilic surface, which in turn eliminates scattering of light resulting from the presence of condensed water droplets and thus provides clear and unhindered view. In order to obtain visible light active self-cleaning building materials, TiO_2 thin films were developed using Ni^{2+} and Fe^{3+} dopants [297]. Addition of dopant metal ions into TiO_2 lattice creates intrinsic defects such as oxygen vacancies or Ti interstitial depending on the valence state of the dopant, which accounts for the visible light absorption. Visible light active glazed ceramic tiles were fabricated by coating the surface with Degussa P25–TiO_2 nanoparticles modified with TEOS [298]. The modified tiles exhibited higher photocatalytic activity and improved hydrophilicity under visible light irradiation. The improved photocatalytic activity and hydrophilicity of the TEOS modified TiO_2 nanoparticles results from the smaller particle size, larger surface area and increased surface roughness.

Photoinduced antimicrobial action of TiO_2 has huge potential in construction of building materials for both indoor and outdoor applications [299,300]. Antimicrobial activity of TiO_2 is extremely important for applications in the medical field as well as in food industries to prevent microbial contamination. Several companies including TOTO, Karpery and Biocera, have manufactured ceramics with a deposited thin film of semiconductor photocatalysts functioning as an antimicrobial agent [301]. The resulting products display photoinduced antimicrobial and deodorizing properties.

In recent time, several reviews have been published on functionalization of textile and wool with TiO_2 nanoparticles and their self-cleaning properties [302,303]; hence a brief summary of the recent developments is discussed in the current review. Photocatalytic and self-cleaning textile fibers have been designed based on cotton, polyester, polyamide, cellulose fibers coated with TiO_2 NPs [304–307]. Functionalization of textile fibers with TiO_2 is usually achieved using carboxylic acid as the anchoring group, which can coordinate to the Ti atom and can also bind to TiO_2 through H-bonding with lattice oxygen or surface hydroxyl group [302]. Addition of nanocrystalline TiO_2 also contributes to the UV protection factor of the fabric, which was found to be preserved after several cycles of home-washing [308,309]. The TiO_2 coating was found to improve the mechanical properties of cotton fibers [310] and the coated fibers demonstrated high stain removal and antibacterial properties [308,309]. Photocatalytic and self-cleaning cotton fabrics were designed by treating the cotton fibers with TiO_2 nanoparticles and multi-wall carbon nanotubes (MWCNTs) using succinic acid as a crosslinking agent [311]. The simultaneous coating with TiO_2 and MWCNTs significantly improved the photocatalytic activity of the cotton fiber under both UV and

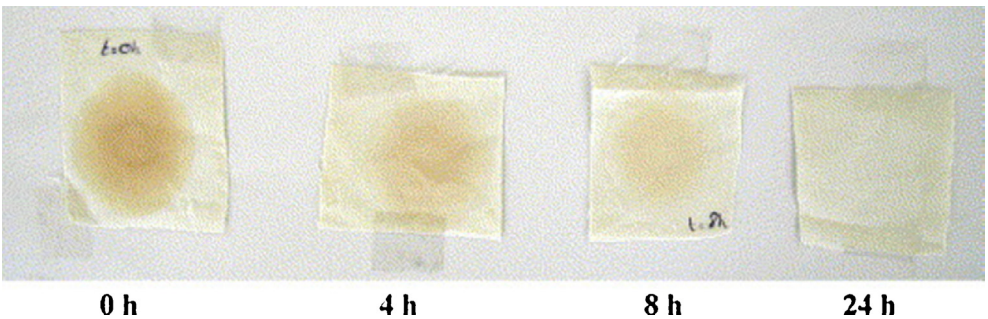

Fig. 44. Removal of wine stains from cotton textiles coated with TiO_2–SiO_2 after irradiating for 0, 4, 8 and 24 h.
(Reprinted from J. Mol. Catal. A 244 (2006) 160–167 permission from Elsevier Science).

sunlight, which has been assigned to the enhanced light absorption by the TiO_2–MWCNT composites and reduced rate of electron–hole recombination. The coating with TiO_2–MWCNT also improved the abrasion resistance and UV blocking capability of the cotton fibers. Development of the self-cleaning textiles coated with hydrophilic TiO_2 surfaces has also been reported by Bozzi et al. [312,313]. Radio frequency plasma and UV-C irradiation have been employed to introduce oxygenated polar functional groups. These functional groups facilitated the effective adhesion of metal oxides on the textile/fabric surface. The self-cleaning activity (Fig. 44) of the TiO_2–SiO_2-coated fabrics was analyzed by the decolorization of red wine stains [313]. Pakdel et al. also developed a similar strategy and it was observed that textiles coated with TiO_2/SiO_2 (30:70) showed the optimum efficiency in stain removal [202]. After a detailed web search, no manufacturers could be identified for the commercial supply of photocatalytic fabrics.

Visible light active self-cleaning cottons have been designed by coating cotton fibers with TiO_2-noble metal composites [204,314,315]. Wool fabrics coated with TiO_2–Ag nanocomposites using citric acid as a cross linking agent demonstrated improved photocatalytic efficiency for the degradation of methylene blue and saffron stain removal [316]. The combined treatment of polyester fabric with TiO_2 nanoparticles and colloidal Ag nanoparticles also showed improved UV protective properties and higher antimicrobial and self-cleaning action [317]. Polyester fabrics coated with AgI/AgCl/TiO_2 nanocomposites exhibited high efficiency for the photochemical destruction of methylene blue and antimicrobial properties against *E. coli* [318]. The superior self-cleaning activity resulting from the combination of superhydrophobic surface with photocatalytic activity of TiO_2 was recently demonstrated by TiO_2/TCPP functionalized cotton fabrics coated with trimethoxy(octadecyl) silane (OTMS) [319]. The functionalized cotton fabrics displayed a superhydrophobic surface induced by the presence of TiO_2 and (OTMS) with a WCA of 156° and caused degradation of methylene blue upon visible light illumination.

Keratin base fibrous materials are used in a wide range of applications including textiles, tires, insulation due to high durability, insulating ability and biodegradability. Photocatalytic and self-cleaning keratin wool fibers were developed by depositing nanocrystalline anatase TiO_2 [320,321].

CristalACTiV™ is a commercial paint based on semiconductor photocatalysis technology and was developed as a solution to remove NOx. These materials showed the ability to eliminate up to 0.5 g/m^2/day of NOx [322]. StoClimasan-Color™ (active interior paint) incorporated a semiconductor photocatalyst which can constantly degrade organic pollutants including carbon monoxide under the influence of light [323]. In an investigation to analyze the by-products formed during the photocatalytic reaction Auvinen et al. indicated that, if the photocatalytic mineralization is not fully completed, the end products are not always water and carbon dioxide. They have examined six different paint products to understand the by-products produced by photocatalytic paints during the decomposition of formaldehyde, and a mixture of volatile organic compound (VOC) containing five different indoor air pollutants [324]. This investigation showed that a number of by-products including acetone and acetaldehyde were formed during the photocatalytic reaction. It can therefore be concluded that the incomplete photocatalytic decomposition of indoor pollutants could result in a number of side products, which could be more harmful than the pollutants themselves [324].

The huge potential of TiO_2 based photocatalytic and self-cleaning materials, as discussed above, can be realized through rational designing of photocatalyst to utilize solar and indoor irradiation.

12. Conclusions

The article aims to give an overview on photocatalytic self-cleaning materials derived from TiO_2 with tunable wettability properties. These materials constitute an important area of research in materials chemistry that is experiencing vast growth in recent years. These photocatalytic self-cleaning materials can be used in many applications including antibacterial, antifogging, antireflective coatings and can provide a solution to the growing problem of environmental pollution. Various models were postulated to understand the mechanism for photoinduced hydrophilicity. The widely accepted mechanism relies on the formation of surface defects upon UV light illumination [7]. UV irradiation results in a structural change at the TiO_2 surface and as a result it induces an interfacial force along the solid–liquid boundary and subsequently the contact angle changes. It was also described that UV irradiation generates 'oxygen vacancies' and thereby Ti^{4+} ions will be converted to Ti^{3+}. These 'oxygen vacancies' will increase the affinity for water molecules.

In another theory, it was proposed that UV illumination results in the reconstruction of hydroxyl groups at the surface [64]. The extent of hydrophilic conversion is linked to the density of surface hydroxyl groups. In addition, the positive hole created by the UV irradiation can diffuse in to the surface of the photocatalyst and gets trapped at lattice oxygen. As a result, the binding energy between the Ti and lattice oxygen becomes fragile and water molecules can break this bond and form new hydroxyl bonds. In another study, it was proposed that the thermal energy formed as a result of the irradiation can cause desorption of the weakly attached molecules from the surface of TiO_2 [74]. It is therefore evident that no consensus has been reached so far in explaining the exact mechanism of photoinduced hydrophilicity and a combination of various mechanism is often required to account for the phenomenon.

Reversible photo-controlled materials with tunable wetting properties have recently attracted significant attention due to their technological application. Surface roughness, morphology, and the polarity of the surface are reported as the significant factors in controlling the reversible nature of the wetting. A number of methodologies such as doping with metals or non-metals, fabrication of semiconductor nano-composites, formation of hetero-junctions etc. were reported to improve the self-cleaning activity by the photocatalytic action. However, it has been noted that it is often difficult to compare the self-cleaning activity of various photocatalysts due to variation in the nature of irradiation, intensity of the light employed, time for irradiation etc. In general, any modifications which could increase the surface roughness by chemical treatments (e.g., doping or surface treatments) would be a promising strategy to increase the self-cleaning activity of the materials. Development of heterostructure of the photocatalysts with other materials to increase the charge separation appeared another effective approach to improve the self-cleaning efficiency. However, further investigations are required to understand structure activity relationships and excited state behavior of the photocatalysts, which will be crucial for designing novel TiO_2-based functional material with improved photoreactivity and wettability character. Moreover, current research mostly focuses on the development of photocatalytic superwetting materials for solid–liquid–vapor phase. Development of underwater superoleophobic materials is gaining attention due to their applications in waste water treatments and separation of oil-in-water emulsions. Further studies are required to understand the structure-wettability patterns of these groups of materials. Rational design of multifunctional TiO_2 materials by integrating biological inspired self-cleaning structure with tunable

wettability will be a promising strategy to address the current energy and environmental problems.

Acknowledgements

The authors wish to acknowledge financial support under the U. S.–Ireland R&D Partnership programme from the Science Foundation Ireland (SFI-grant number 10/US/I1822 (T)) and U. S. National Science Foundation-CBET (Award 1033317). D.D. Dionysiou also acknowledges support from the University of Cincinnati through a UNESCO co-Chair Professor position on "Water Access and Sustainability".

References

[1] K. Liu, M. Cao, A. Fujishima, L. Jiang, Chem. Rev. 114 (2014) 10044–10094.
[2] K. Qi, W.A. Daoud, J.H. Xin, C.L. Mak, W. Tang, W.P. Cheung, J. Mater. Chem. 16 (2006) 4567–4574.
[3] W.S. Tung, W.A. Daoud, J. Mater. Chem. 21 (2011) 7858–7869.
[4] H. Yaghoubi, N. Taghavinia, E.K. Alamdari, Surf. Coat. Technol. 204 (2010) 1562–1568.
[5] Y. Takata, S. Hidaka, J.M. Cao, T. Nakamura, H. Yamamoto, M. Masuda, T. Ito, Energy 30 (2005) 209–220.
[6] T. Watanabe, A. Nakajima, R. Wang, M. Minabe, S. Koizumi, A. Fujishima, K. Hashimoto, Thin Solid Films 351 (1999) 260–263.
[7] R. Wang, K. Hashimoto, A. Fujishima, M. Chikuni, E. Kojima, A. Kitamura, M. Shimohigoshi, T. Watanabe, Nature 388 (1997) 431–432.
[8] I.P. Parkin, R.G. Palgrave, J. Mater. Chem. 15 (2005) 1689–1695.
[9] A. Mills, A. Lepre, N. Elliott, S. Bhopal, I.P. Parkin, S.A. O'Neill, J. Photochem. Photobiol. A 160 (2003) 213–224.
[10] T.-H. Xie, J. Lin, J. Phys. Chem. C 111 (2007) 9968–9974.
[11] F. Bondioli, R. Taurino, A.M. Ferrari, J. Colloid Interface Sci. 334 (2009) 195–201.
[12] R.W. Andrews, A. Pollard, J.M. Pearce, Sol. Energy Mater. Sol. Cells 113 (2013) 71–78.
[13] R.M. Fillion, A.R. Riahi, A. Edrisy, Renew. Sustain. Energy Rev. 32 (2014) 797–809.
[14] L. Oberli, D. Caruso, C. Hall, M. Fabretto, P.J. Murphy, D. Evans, Adv. Colloid Interface Sci. 210 (2014) 47–57.
[15] W. Li, A. Amirfazli, Adv. Colloid Interface Sci. 132 (2007) 51–68.
[16] W. Barthlott, C. Neinhuis, Planta 202 (1997) 1–8.
[17] L. Feng, S. Li, Y. Li, H. Li, L. Zhang, J. Zhai, Y. Song, B. Liu, L. Jiang, D. Zhu, Adv. Mater. 14 (2002) 1857–1860.
[18] G.D. Bixler, B. Bhushan, Soft Matter 8 (2012) 11271–11284.
[19] M.E. Hay, J. Exp. Mar. Biol. Ecol. 200 (1996) 103–134.
[20] Y. Zhang, H. Wu, X. Yu, F. Chen, J. Wu, J. Bionic Eng. 9 (2012) 84–90.
[21] L. Zhang, R. Dillert, D. Bahnemann, M. Vormoor, Energy Environ. Sci. 5 (2012) 7491–7507.
[22] S. Nishimoto, B. Bhushan, RSC Adv. 3 (2013) 671–690.
[23] G.D. Bixler, B. Bhushan, Crit. Rev. Solid State Mater. Sci. 40 (2014) 1–37.
[24] N. Zhao, Z. Wang, C. Cai, H. Shen, F. Liang, D. Wang, C. Wang, T. Zhu, J. Guo, Y. Wang, X. Liu, C. Duan, H. Wang, Y. Mao, X. Jia, H. Dong, X. Zhang, J. Xu, Adv. Mater. 26 (2014) 6994–7017.
[25] G.D. Bixler, A. Theiss, B. Bhushan, S.C. Lee, J. Colloid Interface Sci. 419 (2014) 114–133.
[26] K. Liu, Y. Tian, L. Jiang, Prog. Mater. Sci. 58 (2013) 503–564.
[27] K. Liu, X. Yao, L. Jiang, Chem. Soc. Rev. 39 (2010) 3240–3255.
[28] A. Fujishima, X. Zhang, D.A. Tryk, Surf. Sci. Rep. 63 (2008) 515–582.
[29] K. Nakata, A. Fujishima, J. Photochem. Photobiol. C 13 (2012) 169–189.
[30] P. Ragesh, V. Anand Ganesh, S.V. Nair, A.S. Nair, J. Mater. Chem. A 2 (2014) 14773–14797.
[31] F.Ç. Cebeci, Z. Wu, L. Zhai, R.E. Cohen, M.F. Rubner, Langmuir 22 (2006) 2856–2862.
[32] E. Martines, K. Seunarine, H. Morgan, N. Gadegaard, C.D.W. Wilkinson, M.O. Riehle, Nano Lett. 5 (2005) 2097–2103.
[33] C. Fang, C. Hidrovo, F.-m. Wang, J. Eaton, K. Goodson, Int. J. Multiphase Flow 34 (2008) 690–705.
[34] L. Gao, T.J. McCarthy, Langmuir 22 (2006) 6234–6237.
[35] R.N. Wenzel, Ind. Eng. Chem. 28 (1936) 988–994.
[36] A.B.D. Cassie, S. Baxter, Trans. Faraday Soc. 40 (1944) 546–551.
[37] M. Miwa, A. Nakajima, A. Fujishima, K. Hashimoto, T. Watanabe, Langmuir 16 (2000) 5754–5760.
[38] A. Borras, A.R. González-Elipe, Langmuir 26 (2010) 15875–15882.
[39] E. Ueda, P.A. Levkin, Adv. Mater. 25 (2013) 1234–1247.
[40] D. Tian, Y. Song, L. Jiang, Chem. Soc. Rev. 42 (2013) 5184–5209.
[41] W. Song, J.F. Mano, Soft Matter 9 (2013) 2985–2999.
[42] X.-T. Zhang, O. Sato, A. Fujishima, Langmuir 20 (2004) 6065–6067.
[43] J.S. Li, E. Ueda, A. Nallapaneni, L.X. Li, P.A. Levkin, Langmuir 28 (2012) 8286–8291.
[44] K. Tadanaga, J. Morinaga, A. Matsuda, T. Minami, Chem. Mater. 12 (2000) 590–592.
[45] X. Zhang, M. Jin, Z. Liu, S. Nishimoto, H. Saito, T. Murakami, A. Fujishima, Langmuir 22 (2006) 9477–9479.
[46] Y. Lai, C. Lin, H. Wang, J. Huang, H. Zhuang, L. Sun, Electrochem. Commun. 10 (2008) 387–391.
[47] Q. Liang, Y. Chen, Y. Fan, Y. Hu, Y. Wu, Z. Zhao, Q. Meng, Appl. Surf. Sci. 258 (2012) 2266–2269.
[48] K. Nakata, S. Nishimoto, A. Kubo, D. Tryk, T. Ochiai, T. Murakami, A. Fujishima, Chem. – Asian J. 4 (2009) 984–988.
[49] Y. Lai, L. Lin, F. Pan, J. Huang, R. Song, Y. Huang, C. Lin, H. Fuchs, L. Chi, Small 9 (2013) 2945–2953.
[50] M. Pelaez, N.T. Nolan, S.C. Pillai, M.K. Seery, P. Falaras, A.G. Kontos, P.S.M. Dunlop, J.W.J. Hamilton, J.A. Byrne, K. O'Shea, M.H. Entezari, D.D. Dionysiou, Appl. Catal. B 125 (2012) 331–349.
[51] M.D. Hernandez-Alonso, F. Fresno, S. Suarez, J.M. Coronado, Energy Environ. Sci. 2 (2009) 1231–1257.
[52] Y. Zheng, J. Liu, J. Liang, M. Jaroniec, S.Z. Qiao, Energy Environ. Sci. 5 (2012) 6717–6731.
[53] H. Kisch, Angew. Chem. Int. Ed. 52 (2013) 812–847.
[54] Y. Inoue, Energy Environ. Sci. 2 (2009) 364–386.
[55] D.A. Keane, K.G. McGuigan, P.F. Ibanez, M.I. Polo-Lopez, J.A. Byrne, P.S.M. Dunlop, K. O'Shea, D.D. Dionysiou, S.C. Pillai, Catal. Sci. Technol. 4 (2014) 1211–1226.
[56] M.B. Fisher, D.A. Keane, P. Fernández-Ibáñez, J. Colreavy, S.J. Hinder, K.G. McGuigan, S.C. Pillai, Appl. Catal. B 130–131 (2013) 8–13.
[57] S. Banerjee, S.C. Pillai, P. Falaras, K.E. O'shea, J.A. Byrne, D.D. Dionysiou, J. Phys. Chem. Lett. 5 (2014) 2543–2554.
[58] Y. Qu, X. Duan, Chem. Soc. Rev. 42 (2013) 2568–2580.
[59] J.B. Joo, Q. Zhang, M. Dahl, I. Lee, J. Goebl, F. Zaera, Y. Yin, Energy Environ. Sci. 5 (2012) 6321–6327.
[60] G. Liu, L.-C. Yin, J. Wang, P. Niu, C. Zhen, Y. Xie, H.-M. Cheng, Energy Environ. Sci. 5 (2012) 9603–9610.
[61] Z. Zhao, H. Tan, H. Zhao, D. Li, M. Zheng, P. Du, G. Zhang, D. Qu, Z. Sun, H. Fan, Chem. Commun. 49 (2013) 8958–8960.
[62] T. Shibata, N. Sakai, K. Fukuda, Y. Ebina, T. Sasaki, Phys. Chem. Chem. Phys. 9 (2007) 2413–2420.
[63] V.A. Ganesh, A.S. Nair, H.K. Raut, T.M. Walsh, S. Ramakrishna, RSC Adv. 2 (2012) 2067–2072.
[64] N. Sakai, A. Fujishima, T. Watanabe, K. Hashimoto, J. Phys. Chem. B 107 (2003) 1028–1035.
[65] N. Sakai, A. Fujishima, T. Watanabe, K. Hashimoto, J. Phys. Chem. B 105 (2001) 3023–3026.
[66] T. Zubkov, D. Stahl, T.L. Thompson, D. Panayotov, O. Diwald, J.T. Yates, J. Phys. Chem. B 109 (2005) 15454–15462.
[67] R. Wang, K. Hashimoto, A. Fujishima, M. Chikuni, E. Kojima, A. Kitamura, M. Shimohigoshi, T. Watanabe, Adv. Mater. 10 (1998) 135–138.
[68] A. Nakajima, S.-i. Koizumi, T. Watanabe, K. Hashimoto, J. Photochem. Photobiol. A 146 (2001) 129–132.
[69] R. Wang, N. Sakai, A. Fujishima, T. Watanabe, K. Hashimoto, J. Phys. Chem. B 103 (1999) 2188–2194.
[70] A. Nakajima, S.-i. Koizumi, T. Watanabe, K. Hashimoto, Langmuir 16 (2000) 7048–7050.
[71] T. Shibata, H. Irie, K. Hashimoto, Chem. Commun. 25 (2009) 3735–3737.
[72] N. Sakai, R. Wang, A. Fujishima, T. Watanabe, K. Hashimoto, Langmuir 14 (1998) 5918–5920.
[73] M. Kamei, T. Mitsuhashi, Surf. Sci. 463 (2000) L609–L612.
[74] M. Takeuchi, K. Sakamoto, G. Martra, S. Coluccia, M. Anpo, J. Phys. Chem. B 109 (2005) 15422–15428.
[75] X. Yan, R. Abe, T. Ohno, M. Toyofuku, B. Ohtani, Thin Solid Films 516 (2008) 5872–5876.
[76] K. Guan, Surf. Coat. Technol. 191 (2005) 155–160.
[77] M. Miyauchi, A. Nakajima, T. Watanabe, K. Hashimoto, Chem. Mater. 14 (2002) 2812–2816.
[78] A.V. Emeline, A.V. Rudakova, M. Sakai, T. Murakami, A. Fujishima, J. Phys. Chem. C 117 (2013) 12086–12092.
[79] H.Y. Lee, Y.H. Park, K.H. Ko, Langmuir 16 (2000) 7289–7293.
[80] J.-J. Wang, D.-S. Wang, J. Wang, W.-L. Zhao, C.-W. Wang, Surf. Coat. Technol. 205 (2011) 3596–3599.
[81] J. Yu, X. Zhao, Q. Zhao, G. Wang, Mater. Chem. Phys. 68 (2001) 253–259.
[82] A. Murakami, T. Yamaguchi, S.-i. Hirano, K. Kikuta, Thin Solid Films 516 (2008) 3888–3892.
[83] J.L. Gole, J.D. Stout, C. Burda, Y. Lou, X. Chen, J. Phys. Chem. B 108 (2003) 1230–1240.
[84] M. Pelaez, B. Baruwati, R.S. Varma, R. Luque, D.D. Dionysiou, Chem. Commun. 49 (2013) 10118–10120.
[85] N.T. Nolan, D.W. Synnott, M.K. Seery, S.J. Hinder, A. Van Wassenhoven, S.C. Pillai, J. Hazard. Mater. 211 (2012) 88–94.
[86] X. Li, P. Liu, Y. Mao, M. Xing, J. Zhang, Appl. Catal. B 164 (2015) 352–359.
[87] S.U.M. Khan, M. Al-Shahry, W.B. Ingler, Science 297 (2002) 2243–2245.
[88] S. Sakthivel, H. Kisch, Angew. Chem. Int. Ed. 42 (2003) 4908–4911.
[89] S.K. Mohapatra, M. Misra, V.K. Mahajan, K.S. Raja, J. Phys. Chem. C 111 (2007) 8677–8685.
[90] H. Irie, Y. Watanabe, K. Hashimoto, Chem. Lett. 32 (2003) 772–773.
[91] Y. Huang, W. Ho, S. Lee, L. Zhang, G. Li, J.C. Yu, Langmuir 24 (2008) 3510–3516.

[92] Y. Zhang, Z. Zhao, J. Chen, L. Cheng, J. Chang, W. Sheng, C. Hu, S. Cao, Appl. Catal. B 166 (2015) 644.
[93] C. Lettmann, K. Hildenbrand, H. Kisch, W. Macyk, W.F. Maier, Appl. Catal. B 32 (2001) 215–227.
[94] T. Umebayashi, T. Yamaki, S. Tanaka, K. Asai, Chem. Lett. 32 (2003) 330–331.
[95] T. Ohno, M. Akiyoshi, T. Umebayashi, K. Asai, T. Mitsui, M. Matsumura, Appl. Catal. A 265 (2004) 115–121.
[96] R. Asahi, T. Morikawa, T. Ohwaki, K. Aoki, Y. Taga, Science 293 (2001) 269–271.
[97] N. Serpone, J. Phys. Chem. B 110 (2006) 24287–24293.
[98] C. Di Valentin, E. Finazzi, G. Pacchioni, A. Selloni, S. Livraghi, M.C. Paganini, E. Giamello, Chem. Phys. 339 (2007) 44–56.
[99] C. Di Valentin, G. Pacchioni, Catal. Today 206 (2013) 12–18.
[100] C. Di Valentin, G. Pacchioni, A. Selloni, S. Livraghi, E. Giamello, J. Phys. Chem. B 109 (2005) 11414–11419.
[101] F. Napoli, M. Chiesa, S. Livraghi, E. Giamello, S. Agnoli, G. Granozzi, G. Pacchioni, C. Di Valentin, Chem. Phys. Lett. 477 (2009) 135–138.
[102] H. Irie, S. Washizuka, N. Yoshino, K. Hashimoto, Chem. Commun. 11 (2003) 1298–1299.
[103] J. Premkumar, Chem. Mater. 16 (2004) 3980–3981.
[104] C.W. Dunnill, Z. Ansari, A. Kafizas, S. Perni, D.J. Morgan, M. Wilson, I.P. Parkin, J. Mater. Chem. 21 (2011) 11854–11861.
[105] H. Irie, S. Washizuka, K. Hashimoto, Thin Solid Films 510 (2006) 21–25.
[106] J. Tang, H. Quan, J. Ye, Chem. Mater. 19 (2006) 116–122.
[107] A.M. Czoska, S. Livraghi, M. Chiesa, E. Giamello, S. Agnoli, G. Granozzi, E. Finazzi, C.D. Valentin, G. Pacchioni, J. Phys. Chem. C 112 (2008) 8951–8956.
[108] J.-H. Xu, J. Li, W.-L. Dai, Y. Cao, H. Li, K. Fan, Appl. Catal. B 79 (2008) 72–80.
[109] G. Liu, C. Han, M. Pelaez, D. Zhu, S. Liao, V. Likodimos, A.G. Kontos, P. Falaras, D.D. Dionysiou, J. Mol. Catal. A: Chem. 372 (2013) 58–65.
[110] P. Periyat, D.E. McCormack, S.J. Hinder, S.C. Pillai, J. Phys. Chem. C 113 (2009) 3246–3253.
[111] A.V. Katsanaki, A.G. Kontos, T. Maggos, M. Pelaez, V. Likodimos, E.A. Pavlatou, D.D. Dionysiou, P. Falaras, Appl. Catal. B 140 (2013) 619–625.
[112] M. Pelaez, P. Falaras, A.G. Kontos, A.A. de la Cruz, K. O'Shea, P.S.M. Dunlop, J.A. Byrne, D.D. Dionysiou, Appl. Catal. B 121 (2012) 30–39.
[113] J.W.J. Hamilton, J.A. Byrne, P.S.M. Dunlop, D.D. Dionysiou, M. Pelaez, K. O'Shea, D. Synnott, S.C. Pillai, J. Phys. Chem. C 118 (2014) 12206–12215.
[114] Y.W. Sakai, K. Obata, K. Hashimoto, H. Irie, Vacuum 83 (2008) 683–687.
[115] A.G. Kontos, M. Pelaez, V. Likodimos, N. Vaenas, D.D. Dionysiou, P. Falaras, Photochem. Photobiol. Sci. 10 (2011) 350–354.
[116] Q.-C. Xu, D.V. Wellia, M.A. Sk, K.H. Lim, J.S.C. Loo, D.W. Liao, R. Amal, T.T.Y. Tan, J. Photochem. Photobiol. A 210 (2010) 181–187.
[117] Q. Li, J.K. Shang, Environ. Sci. Technol. 44 (2010) 3493–3499.
[118] A. Di Paola, E. García-López, S. Ikeda, G. Marcı, B. Ohtani, L. Palmisano, Catal. Today 75 (2002) 87–93.
[119] K.-W. Weng, Y.-P. Huang, Surf. Coat. Technol. 231 (2013) 201–204.
[120] M. Farbod, S. Rezaian, Thin Solid Films 520 (2012) 1954–1958.
[121] A. Eshaghi, A. Eshaghi, Mater. Res. Bull. 46 (2011) 2342–2345.
[122] S. Kitano, N. Murakami, T. Ohno, Y. Mitani, Y. Nosaka, H. Asakura, K. Teramura, T. Tanaka, H. Tada, K. Hashimoto, H. Kominami, J. Phys. Chem. C 117 (2013) 11008–11016.
[123] J. Xu, Y. Ao, D. Fu, C. Yuan, J. Colloid Interface Sci. 328 (2008) 447–451.
[124] L.G. Devi, S.G. Kumar, Appl. Surf. Sci. 261 (2012) 137–146.
[125] J. Reszczynska, T. Grzyb, J.W. Sobczak, W. Lisowski, M. Gazda, B. Ohtani, A. Zaleska, Appl. Catal. B 163 (2015) 40–49.
[126] M.K. Seery, R. George, P. Floris, S.C. Pillai, J. Photochem. Photobiol. A 189 (2007) 258–263.
[127] I.M. Arabatzis, T. Stergiopoulos, M.C. Bernard, D. Labou, S.G. Neophytides, P. Falaras, Appl. Catal. B 42 (2003) 187–201.
[128] N.T. Nolan, M.K. Seery, S.J. Hinder, L.F. Healy, S.C. Pillai, J. Phys. Chem. C 114 (2010) 13026–13034.
[129] S. Linic, P. Christopher, D.B. Ingram, Nat. Mater. 10 (2011) 911–921.
[130] K. Awazu, M. Fujimaki, C. Rockstuhl, J. Tominaga, H. Murakami, Y. Ohki, N. Yoshida, T. Watanabe, J. Am. Chem. Soc. 130 (2008) 1676–1680.
[131] X. Zhang, H. Yang, A. Tang, J. Phys. Chem. B 112 (2008) 16271–16279.
[132] S. Yang, L.E. Halliburton, A. Manivannan, P.H. Bunton, D.B. Baker, M. Klemm, S. Horn, A. Fujishima, Appl. Phys. Lett. 94 (2009) 162114.
[133] M.R. Bayati, R. Molaei, F. Golestani-Fard, Colloids Surf. A 373 (2011) 51–60.
[134] L. Zang, W. Macyk, C. Lange, W.F. Maier, C. Antonius, D. Meissner, H. Kisch, Chem. – Eur. J. 6 (2000) 379–384.
[135] L. Jing, B. Xin, F. Yuan, L. Xue, B. Wang, H. Fu, J. Phys. Chem. B 110 (2006) 17860–17865.
[136] Y. Qu, S. Song, L. Jing, Y. Luan, H. Fu, Thin Solid Films 518 (2010) 3177–3181.
[137] M. Yang, C. Hume, S. Lee, Y.-H. Son, J.-K. Lee, J. Phys. Chem. C 114 (2010) 15292–15297.
[138] S.S. Thind, G. Wu, A. Chen, Appl. Catal. B 111–112 (2012) 38–45.
[139] J. Liu, R. Han, Y. Zhao, H. Wang, W. Lu, T. Yu, Y. Zhang, J. Phys. Chem. C 115 (2011) 4507–4515.
[140] Y.-F. Li, D. Xu, J.I. Oh, W. Shen, X. Li, Y. Yu, ACS Catal. 2 (2012) 391–398.
[141] X. Wu, S. Yin, Q. Dong, C. Guo, T. Kimura, J.-i. Matsushita, T. Sato, J. Phys. Chem. C 117 (2013) 8345–8352.
[142] Y. Niu, M. Xing, J. Zhang, B. Tian, Catal. Today 201 (2013) 159–166.
[143] E. Wang, T. He, L. Zhao, Y. Chen, Y. Cao, J. Mater. Chem. 21 (2011) 144–150.
[144] H. Liu, Y. Wu, J. Zhang, ACS Appl. Mater. Interfaces 3 (2011) 1757–1764.
[145] N. Feng, Q. Wang, A. Zheng, Z. Zhang, J. Fan, S.-B. Liu, J.-P. Amoureux, F. Deng, J. Am. Chem. Soc. 135 (2013) 1607–1616.
[146] D.S. Tsoukleris, A.I. Kontos, P. Aloupogiannis, P. Falaras, Catal. Today 124 (2007) 110–117.
[147] P. Falaras, Sol. Energy Mater. Sol. Cells 53 (1998) 163–175.
[148] J. Zhao, C. Chen, W. Ma, Top. Catal. 35 (2005) 269–278.
[149] M. Zhang, C. Chen, W. Ma, J. Zhao, Angew. Chem. Int. Ed. 47 (2008) 9730–9733.
[150] X. Li, L. Liu, S.-Z. Kang, J. Mu, G. Li, Appl. Surf. Sci. 257 (2011) 5950–5956.
[151] S. Afzal, W.A. Daoud, S.J. Langford, ACS Appl. Mater. Interfaces 5 (2013) 4753–4759.
[152] S.-H. Wu, J.-L. Wu, S.-Y. Jia, Q.-W. Chang, H.-T. Ren, Y. Liu, Appl. Surf. Sci. 287 (2013) 389–396.
[153] D. Kuang, S. Ito, B. Wenger, C. Klein, J.-E. Moser, R. Humphry-Baker, S.M. Zakeeruddin, M. Grätzel, J. Am. Chem. Soc. 128 (2006) 4146–4154.
[154] A. Hagfeldt, M. Grätzel, Acc. Chem. Res. 33 (2000) 269–277.
[155] R. Argazzi, G. Larramona, C. Contado, C.A. Bignozzi, J. Photochem. Photobiol. A 164 (2004) 15–21.
[156] A. Islam, H. Sugihara, K. Hara, L.P. Singh, R. Katoh, M. Yanagida, Y. Takahashi, S. Murata, H. Arakawa, New J. Chem. 24 (2000) 343–345.
[157] B. Gholamkhass, H. Mametsuka, K. Koike, T. Tanabe, M. Furue, O. Ishitani, Inorg. Chem. 44 (2005) 2326–2336.
[158] S. Afzal, W.A. Daoud, S.J. Langford, Appl. Surf. Sci. 275 (2013) 36–42.
[159] B.-K. An, W. Hu, P.L. Burn, P. Meredith, J. Phys. Chem. C 114 (2010) 17964–17974.
[160] F.-X. Xiao, ACS Appl. Mater. Interfaces 4 (2012) 7055–7063.
[161] B. Liu, A. Khare, E.S. Aydil, ACS Appl. Mater. Interfaces 3 (2011) 4444–4450.
[162] V. Etacheri, G. Michlits, M.K. Seery, S.J. Hinder, S.C. Pillai, ACS Appl. Mater. Interfaces 5 (2013) 1663–1672.
[163] V. Etacheri, M.K. Seery, S.J. Hinder, S.C. Pillai, Chem. Mater. 22 (2010) 3843–3853.
[164] V. Etacheri, M.K. Seery, S.J. Hinder, S.C. Pillai, Inorg. Chem. 51 (2012) 7164–7173.
[165] M. Miyauchi, A. Nakajima, T. Watanabe, K. Hashimoto, Chem. Mater. 14 (2002) 4714–4720.
[166] M. Miyauchi, A. Nakajima, K. Hashimoto, T. Watanabe, Adv. Mater. 12 (2000) 1923–1927.
[167] A. Srinivasan, M. Miyauchi, J. Phys. Chem. C 116 (2012) 15421–15426.
[168] A.O.T. Patrocinio, L.F. Paula, R.M. Paniago, J. Freitag, D.W. Bahnemann, ACS Appl. Mater. Interfaces 6 (2014) 16859–16866.
[169] G. Tian, Y. Chen, R. Zhai, J. Zhou, W. Zhou, R. Wang, K. Pan, C. Tian, H. Fu, J. Mater. Chem. A 1 (2013) 6961–6968.
[170] T.H. Jun, K.-S. Lee, H.S. Song, Thin Solid Films 520 (2012) 2609–2612.
[171] R. Wang, H. Tan, Z. Zhao, G. Zhang, L. Song, W. Dong, Z. Sun, J. Mat. Chem. A 2 (2014) 7313–7318.
[172] R. Fateh, R. Dillert, D. Bahnemann, ACS Appl. Mater. Interfaces 6 (2014) 2270–2278.
[173] Y. Abdi, M. Khalilian, E. Arzi, J. Phys. D: Appl. Phys. 44 (2011) 255405.
[174] D. Wang, D. Choi, J. Li, Z. Yang, Z. Nie, R. Kou, D. Hu, C. Wang, L.V. Saraf, J. Zhang, I.A. Aksay, J. Liu, ACS Nano 3 (2009) 907–914.
[175] A. Cao, Z. Liu, S. Chu, M. Wu, Z. Ye, Z. Cai, Y. Chang, S. Wang, Q. Gong, Y. Liu, Adv. Mater. 22 (2010) 103–106.
[176] Y.H. Ng, A. Iwase, A. Kudo, R. Amal, J. Phys. Chem. Lett. 1 (2010) 2607–2612.
[177] S. Anandan, T. Narasinga Rao, M. Sathish, D. Rangappa, I. Honma, M. Miyauchi, ACS Appl. Mater. Interfaces 5 (2012) 207–212.
[178] L. Karimi, M.E. Yazdanshenas, R. Khajavi, A. Rashidi, M. Mirjalili, Cellulose 21 (2014) 3813–3827.
[179] J. Zhu, Y. Cao, J. He, J. Colloid Interface Sci. 420 (2014) 119–126.
[180] P. Nostell, A. Roos, B. Karlsson, Thin Solid Films 351 (1999) 170–175.
[181] Y.-J. Lee, D.S. Ruby, D.W. Peters, B.B. McKenzie, J.W.P. Hsu, Nano Lett. 8 (2008) 1501–1505.
[182] B.S. Richards, Sol. Energy Mater. Sol. Cells 79 (2003) 369–390.
[183] Z. Liu, X. Zhang, T. Murakami, A. Fujishima, Sol. Energy Mater. Sol. Cells 92 (2008) 1434–1438.
[184] M. Faustini, L. Nicole, C. Boissière, P. Innocenzi, C. Sanchez, D. Grosso, Chem. Mater. 22 (2010) 4406–4413.
[185] X.-T. Zhang, O. Sato, M. Taguchi, Y. Einaga, T. Murakami, A. Fujishima, Chem. Mater. 17 (2005) 696–700.
[186] L. Yao, J. He, Prog. Mater. Sci. 61 (2014) 94–143.
[187] J. Cai, J. Ye, S. Chen, X. Zhao, D. Zhang, S. Chen, Y. Ma, S. Jin, L. Qi, Energy Environ. Sci. 5 (2012) 7575–7581.
[188] M. Houmard, G. Berthomé, J.C. Joud, M. Langlet, Surf. Sci. 605 (2011) 456–462.
[189] M. Houmard, D. Riassetto, F. Roussel, A. Bourgeois, G. Berthomé, J.C. Joud, M. Langlet, Surf. Sci. 602 (2008) 3364–3374.
[190] Y.Y. Liu, L.Q. Qian, C. Guo, X. Jia, J.W. Wang, W.H. Tang, J. Alloys Compd. 479 (2009) 532–535.
[191] Y.J. Xu, J.X. Liao, Q.W. Cai, X.X. Yang, Sol. Energy Mater. Sol. Cells 113 (2013) 7–12.
[192] A. Tricoli, M. Righettoni, S.E. Pratsinis, Langmuir 25 (2009) 12578–12584.
[193] K. Guan, B. Lu, Y. Yin, Surf. Coat. Technol. 173 (2003) 219–223.
[194] X. Zhang, F. Zhang, K.-Y. Chan, Appl. Catal. A 284 (2005) 193–198.
[195] C. Kapridaki, L. Pinho, M.J. Mosquera, P. Maravelaki-Kalaitzaki, Appl. Catal. B 156 (2014) 416–427.
[196] S.-Y. Lien, A. Nautiyal, J.-H. Jhu, J.-K. Hsu, S.J. Lee, Asian J. Chem. 25 (2013) 6071–6074.
[197] T. Huang, W. Huang, C. Zhou, Y. Situ, H. Huang, Surf. Coat. Technol. 213 (2012) 126–132.

[198] B. Erdural, U. Bolukbasi, G. Karakas, J. Photochem. Photobiol. A 283 (2014) 29–37.
[199] A. Eshaghi, A. Eshaghi, Appl. Surf. Sci. 258 (2012) 2464–2467.
[200] M. Mokhtarimehr, M. Pakshir, A. Eshaghi, M.H. Shariat, Thin Solid Films 532 (2013) 123–126.
[201] J. Wang, C. Lu, J. Xiong, Appl. Surf. Sci. 298 (2014) 19–25.
[202] E. Pakdel, W.A. Daoud, X. Wang, Appl. Surf. Sci. 275 (2013) 397–402.
[203] E. Pakdel, W.A. Daoud, J. Colloid Interface Sci. 401 (2013) 1–7.
[204] R. Wang, X. Wang, J.H. Xin, ACS Appl. Mater. Interfaces 2 (2009) 82–85.
[205] X. Li, J. He, ACS Appl. Mater. Interfaces 5 (2013) 5282–5290.
[206] K. Nakata, M. Sakai, T. Ochiai, T. Murakami, K. Takagi, A. Fujishima, Langmuir 27 (2011) 3275–3278.
[207] K. Nakata, C. Terashima, A. Fujishima, Chem. Lett. 43 (2014) 1511–1513.
[208] <https://http://www.asme.org/engineering-topics/articles/energy/self-cleaning-solar-panels-maximize-efficiency>.
[209] J. Zhu, C.-M. Hsu, Z. Yu, S. Fan, Y. Cui, Nano Lett. 10 (2010) 1979–1984.
[210] S. Guldin, P. Kohn, M. Stefik, J. Song, G. Divitini, F. Ecarla, C. Ducati, U. Wiesner, U. Steiner, Nano Lett. 13 (2013) 5329–5335.
[211] Q. Mu, Y. Li, H. Wang, Q. Zhang, J. Colloid Interface Sci. 365 (2012) 308–313.
[212] Q.-c. Xu, D.V. Wellia, M.A. Sk, K.H. Lim, J.S.C. Loo, D.W. Liao, R. Amal, T.T.Y. Tan, J. Photochem. Photobiol. A 210 (2010) 181–187.
[213] H.M. Yadav, S.V. Otari, R.A. Bohara, S.S. Mali, S.H. Pawar, S.D. Delekar, J. Photochem. Photobiol. A 294 (2014) 130–136.
[214] G. Fu, P.S. Vary, C.-T. Lin, J. Phys. Chem. B 109 (2005) 8889–8898.
[215] Y. Kikuchi, K. Sunada, T. Iyoda, K. Hashimoto, A. Fujishima, J. Photochem. Photobiol. A 106 (1997) 51–56.
[216] L. Sun, Y. Qin, Q. Cao, B. Hu, Z. Huang, L. Ye, X. Tang, Chem. Commun. 47 (2011) 12628–12630.
[217] X. Qiu, M. Miyauchi, K. Sunada, M. Minoshima, M. Liu, Y. Lu, D. Li, Y. Shimodaira, Y. Hosogi, Y. Kuroda, K. Hashimoto, ACS Nano 6 (2011) 1609–1618.
[218] D. Mitoraj, A. Janczyk, M. Strus, H. Kisch, G. Stochel, P.B. Heczko, W. Macyk, Photochem. Photobiol. Sci. 6 (2007) 642–648.
[219] H. Li, Q. Cui, B. Feng, J. Wang, X. Lu, J. Weng, Appl. Surf. Sci. 284 (2013) 179–183.
[220] X. Chen, K. Cai, J. Fang, M. Lai, J. Li, Y. Hou, Z. Luo, Y. Hu, L. Tang, Surf. Coat. Technol. 216 (2013) 158–165.
[221] J. Podporska-Carroll, E. Panaitescu, B. Quilty, L. Wang, L. Menon, S.C. Pillai, Appl. Catal. B 176–177 (2015) 70–75, http://dx.doi.org/10.1016/j.apcatb.2015.03.029.
[222] C. Hu, J. Guo, J. Qu, X. Hu, Langmuir 23 (2007) 4982–4987.
[223] D. Wu, M. Long, Surf. Coat. Technol. 206 (2011) 1175–1179.
[224] Y. Xie, Y. Jin, Y. Zhou, Y. Wang, Appl. Surf. Sci. 313 (2014) 549–557.
[225] S.C. Xu, Y.X. Zhang, Y.Y. Luo, S. Wang, H.L. Ding, J.M. Xu, G.H. Li, Analyst 138 (2013) 4519–4525.
[226] K. Sunada, Y. Kikuchi, K. Hashimoto, A. Fujishima, Environ. Sci. Technol. 32 (1998) 726–728.
[227] Z.-X. Lu, L. Zhou, Z.-L. Zhang, W.-L. Shi, Z.-X. Xie, H.-Y. Xie, D.-W. Pang, P. Shen, Langmuir 19 (2003) 8765–8768.
[228] J.A. Rengifo-Herrera, K. Pierzchała, A. Sienkiewicz, L. Forró, J. Kiwi, C. Pulgarin, Appl. Catal. B 88 (2009) 398–406.
[229] J.A. Rengifo-Herrera, C. Pulgarin, Sol. Energy 84 (2010) 37–43.
[230] M. Macias-Montero, A. Borras, Z. Saghi, P. Romero-Gomez, J.R. Sanchez-Valencia, J.C. Gonzalez, A. Barranco, P. Midgley, J. Cotrino, A.R. Gonzalez-Elipe, J. Mater. Chem. 22 (2012) 1341–1346.
[231] T. Watanabe, N. Yoshida, Chem. Rec. 8 (2008) 279–290.
[232] N. Yoshida, M. Takeuchi, T. Okura, H. Monma, M. Wakamura, H. Ohsaki, T. Watanabe, Thin Solid Films 502 (2006) 108–111.
[233] P. Ragesh, S.V. Nair, A.S. Nair, RSC Adv. 4 (2014) 38498–38504.
[234] C.R. Crick, S. Ismail, J. Pratten, I.P. Parkin, Thin Solid Films 519 (2011) 3722–3727.
[235] S. Wooh, J.H. Koh, S. Lee, H. Yoon, K. Char, Adv. Funct. Mater. 24 (2014) 5550–5556.
[236] C.R. Crick, I.P. Parkin, Chem. Eur. J. 16 (2010) 3568–3588.
[237] A. Nakajima, K. Hashimoto, T. Watanabe, K. Takai, G. Yamauchi, A. Fujishima, Langmuir 16 (2000) 7044–7047.
[238] M. Wakamura, K. Hashimoto, T. Watanabe, Langmuir 19 (2003) 3428–3431.
[239] T. Kamegawa, Y. Shimizu, H. Yamashita, Adv. Mater. 24 (2012) 3697–3700.
[240] C.R. Crick, J.C. Bear, A. Kafizas, I.P. Parkin, Adv. Mater. 24 (2012) 3505–3508.
[241] X. Zhang, Y. Guo, Z. Zhang, P. Zhang, Appl. Surf. Sci. 284 (2013) 319–323.
[242] Q.F. Xu, Y. Liu, F.-J. Lin, B. Mondal, A.M. Lyons, ACS Appl. Mater. Interfaces 5 (2013) 8915–8924.
[243] I. Kartini, S. Santosa, E. Febriyanti, O. Nugroho, H. Yu, L. Wang, J. Nanopart. Res. 16 (2014) 1–14.
[244] A. Uyama, S. Yamazoe, S. Shigematsu, M. Morimoto, S. Yokojima, H. Mayama, Y. Kojima, S. Nakamura, K. Uchida, Langmuir 27 (2011) 6395–6400.
[245] P. Wan, Y. Jiang, Y. Wang, Z. Wang, X. Zhang, Chem. Commun. 44 (2008) 5710–5712.
[246] K. Ichimura, S.-K. Oh, M. Nakagawa, Science 288 (2000) 1624–1626.
[247] T. Onda, S. Shibuichi, N. Satoh, K. Tsujii, Langmuir 12 (1996) 2125–2127.
[248] W. Li, T. Guo, T. Meng, Y. Huang, X. Li, W. Yan, S. Wang, X. Li, Appl. Surf. Sci. 283 (2013) 12–18.
[249] U. Lehmann, S. Hadjidj, V.K. Parashar, C. Vandevyver, A. Rida, M.A.M. Gijs, Sens. Actuators B 117 (2006) 457–463.
[250] D.A. LaVan, T. McGuire, R. Langer, Nat. Biotechnol. 21 (2003) 1184–1191.
[251] K. Koch, B. Bhushan, W. Barthlott, Prog. Mater. Sci. 54 (2009) 137–178.
[252] M. Järn, Q. Xu, M. Lindén, Langmuir 26 (2010) 11330–11336.
[253] B. Yan, J. Tao, C. Pang, Z. Zheng, Z. Shen, C.H.A. Huan, T. Yu, Langmuir 24 (2008) 10569–10571.
[254] A. Mills, C. Hill, P.K.J. Robertson, J. Photochem. Photobiol. A 237 (2012) 7–23.
[255] L. Zhang, Y. Zhong, D. Cha, P. Wang, Sci. Rep. 3 (2013) 1–5.
[256] Y. Sawai, S. Nishimoto, Y. Kameshima, E. Fujii, M. Miyake, Langmuir 29 (2013) 6784–6789.
[257] H. Wang, Z. Guo, Appl. Phys. Lett. 104 (2014) 183703.
[258] S.J. Gao, Z. Shi, W.B. Zhang, F. Zhang, J. Jin, ACS Nano 8 (2014) 6344–6352.
[259] P. Gao, Z. Liu, D.D. Sun, W.J. Ng, J. Mater. Chem. A 2 (2014) 14082–14088.
[260] W. Zhu, X. Feng, L. Feng, L. Jiang, Chem. Commun. 26 (2006) 2753–2755.
[261] R. Andre, F. Natalio, M.N. Tahir, R. Berger, W. Tremel, Nanoscale 5 (2013) 3447–3456.
[262] J. Pan, X. Song, J. Zhang, H. Shen, Q. Xiong, J. Phys. Chem. C 115 (2011) 22225–22231.
[263] R.-D. Sun, A. Nakajima, A. Fujishima, T. Watanabe, K. Hashimoto, J. Phys. Chem. B 105 (2001) 1984–1990.
[264] Y. Zang, J. Yin, X. He, C. Yue, Z. Wu, J. Li, J. Kang, J. Mater. Chem. A 2 (2014) 7747–7753.
[265] Z. Guo, X. Chen, J. Li, J.-H. Liu, X.-J. Huang, Langmuir 27 (2011) 6193–6200.
[266] S. Balachandran, N. Prakash, K. Thirumalai, M. Muruganandham, M. Sillanpää, M. Swaminathan, Ind. Eng. Chem. Res. 53 (2014) 8346–8356.
[267] T. Kako, J. Ye, Langmuir 23 (2006) 1924–1927.
[268] T. Shibata, G. Takanashi, T. Nakamura, K. Fukuda, Y. Ebina, T. Sasaki, Energy Environ. Sci. 4 (2011) 535–542.
[269] in: ISO 27448: 2009 Fine ceramics (advanced ceramics, advanced technical ceramics) – Test method for self-cleaning performance of semiconducting photocatalytic materials – Measurement of water contact angle.
[270] in: ISO 10678: 2010 Fine ceramics (advanced ceramics, advanced technical ceramics) – Determination of photocatalytic activity of surfaces in an aqueous medium by degradation of methylene blue.
[271] A. Houas, H. Lachheb, M. Ksibi, E. Elaloui, C. Guillard, J.-M. Herrmann, Appl. Catal. B 31 (2001) 145–157.
[272] J. Krýsa, P. Novotná, Š. Kment, A. Mills, J. Photochem. Photobiol. A 222 (2011) 81–86.
[273] in: ISO 27447: 2009, 'Fine ceramics, advanced technical ceramics – Test method for antibacterial activity of semiconducting photocatalytic materials .
[274] J. Krýsa, E. Musilová, J. Zita, J. Hazard. Mater. 195 (2011) 100–106.
[275] A. Mills, J. Hepburn, D. Hazafy, C. O'Rourke, J. Krysa, M. Baudys, M. Zlamal, H. Bartkova, C.E. Hill, K.R. Winn, M.E. Simonsen, E.G. Søgaard, S.C. Pillai, N.S. Leyland, R. Fagan, F. Neumann, C. Lampe, T. Graumann, J. Photochem. Photobiol. A 272 (2013) 18–20.
[276] A. Mills, J. Hepburn, D. Hazafy, C. O'Rourke, N. Wells, J. Krysa, M. Baudys, M. Zlamal, H. Bartkova, C.E. Hill, K.R. Winn, M.E. Simonsen, E.G. Søgaard, S. Banerjee, R. Fagan, S.C. Pillai, J. Photochem. Photobiol. A 290 (2014) 63–71.
[277] A. Mills, N. Wells, C. O'Rourke, Catal. Today 230 (2014) 245–249.
[278] A. Mills, N. Wells, Chem. Soc. Rev. (2015), http://dx.doi.org/10.1039/C4CS00279B.
[279] A. Mills, J. Wang, S.-K. Lee, M. Simonsen, Chem. Commun. 21 (2005) 2721–2723.
[280] H.-Y. Chun, S.-S. Park, S.-H. You, G.-H. Kang, W.-T. Bae, K.-W. Kim, J.-E. Park, A. Ozturk, D.-W. Shin, J. Ceram. Process. Res. 10 (2009) 219–223.
[281] V.S. Smitha, K.A. Manjumol, K.V. Baiju, S. Ghosh, P. Perumal, K.G.K. Warrier, J. Sol–Gel Sci. Technol. 54 (2010) 203–211.
[282] M. Radeka, S. Markov, E. Lončar, O. Rudić, S. Vučetić, J. Ranogajec, J. Eur. Ceram. Soc. 34 (2014) 127–136.
[283] S. Ke, X. Cheng, Q. Wang, Y. Wang, Z. Pan, Ceram. Int. 40 (2014) 8891–8895.
[284] K. Midtdal, B.P. Jelle, Sol. Energy Mater. Sol. Cells 109 (2013) 126–141.
[285] <http://www.activglass.com/index.eng.htm>, (accessed 18.03.15).
[286] M. Shimohigoshi, Y. Saeki, Research and applications of photocatalyst tiles, in: P. Baglioni, L. Casssar (Eds.), International RILEM Symposium on Photocatalysis, Environment and Construction Materials – TDP 2007, RILEM Publications SARL, 2007, pp. 291–297.
[287] P. Periyat, S.C. Pillai, D.E. McCormack, J. Colreavy, S.J. Hinder, J. Phys. Chem. C 112 (2008) 7644–7652.
[288] M. Yan, F. Chen, J. Zhang, M. Anpo, J. Phys. Chem. B 109 (2005) 8673–8678.
[289] V. Etacheri, M.K. Seery, S.J. Hinder, S.C. Pillai, Adv. Funct. Mater. 21 (2011) 3744–3752.
[290] Y. Lu, S. Sathasivam, J. Song, C.R. Crick, C.J. Carmalt, I.P. Parkin, Science 347 (2015) 1132–1135.
[291] C. Bai, Science 309 (2005) 61–63.
[292] L. Cassar, MRS Bull. 29 (2004) 328–331.
[293] <http://www.italcementigroup.com/ENG/Research+and+Innovation/Innovative+Products/TX+Active/>, (accessed 28.02.15).
[294] <http://www.heidelbergcement.com/NR/rdonlyres/28528B72-3125-4370-B657-616609415500/0/TioCem_Broschuere_englisch.pdf>, (accessed 28.02.15).
[295] D. Spasiano, R. Marotta, S. Malato, P. Fernandez-Ibañez, I. Di Somma, Appl. Catal. B 170–171 (2015) 90–123.
[296] J.O. Carneiro, V. Teixeira, A. Portinha, A. Magalhães, P. Coutinho, C.J. Tavares, R. Newton, Mater. Sci. Eng. B 138 (2007) 144–150.
[297] K. Murugan, R. Subasri, T.N. Rao, A.S. Gandhi, B.S. Murty, Prog. Org. Coat. 76 (2013) 1756–1760.
[298] P. Zhang, J. Tian, R. Xu, G. Ma, Appl. Surf. Sci. 266 (2013) 141–147.
[299] J. Chen, C.-s. Poon, Build. Environ. 44 (2009) 1899–1906.

[300] P. Amézaga-Madrid, G.V. Nevárez-Moorillón, E. Orrantia-Borunda, M. Miki-Yoshida, FEMS Microbiol. Lett. 211 (2002) 183–188.
[301] A. Mills, S.-K. Lee, J. Photochem. Photobiol. A 152 (2002) 233–247.
[302] M. Radetić, J. Photochem. Photobiol. C 16 (2013) 62–76.
[303] M. Montazer, E. Pakdel, J. Photochem. Photobiol. C 12 (2011) 293–303.
[304] O.L. Galkina, A. Sycheva, A. Blagodatskiy, G. Kaptay, V.L. Katanaev, G.A. Seisenbaeva, V.G. Kessler, A.V. Agafonov, Surf. Coat. Technol. 253 (2014) 171–179.
[305] P.A.A.P. Marques, T. Trindade, C.P. Neto, Compos. Sci. Technol. 66 (2006) 1038–1044.
[306] D. Pasqui, R. Barbucci, J. Photochem. Photobiol. A 274 (2014) 1–6.
[307] M.J. Uddin, F. Cesano, F. Bonino, S. Bordiga, G. Spoto, D. Scarano, A. Zecchina, J. Photochem. Photobiol. A 189 (2007) 286–294.
[308] W. Daoud, J. Xin, J. Sol–Gel Sci. Technol. 29 (2004) 25–29.
[309] W.A. Daoud, J.H. Xin, Y.-H. Zhang, Surf. Sci. 599 (2005) 69–75.
[310] Qi Kaihong, X. Wang, J.H. Xin, Text. Res. J. 81 (2011) 101–110.
[311] L. Karimi, S. Zohoori, A. Amini, New Carbon Mater. 29 (2014) 380–385.
[312] A. Bozzi, T. Yuranova, J. Kiwi, J. Photochem. Photobiol. A 172 (2005) 27–34.
[313] T. Yuranova, R. Mosteo, J. Bandara, D. Laub, J. Kiwi, J. Mol. Catal. A: Chem. 244 (2006) 160–167.
[314] D. Wu, M. Long, ACS Appl. Mater. Interfaces 3 (2011) 4770–4774.
[315] M.J. Uddin, F. Cesano, D. Scarano, F. Bonino, G. Agostini, G. Spoto, S. Bordiga, A. Zecchina, J. Photochem. Photobiol. A 199 (2008) 64–72.
[316] M. Montazer, A. Behzadnia, M.B. Moghadam, J. Appl. Polym. Sci. 125 (2012) E356–E363.
[317] D. Mihailović, Z. Šaponjić, V. Vodnik, B. Potkonjak, P. Jovančić, J.M. Nedeljković, M. Radetić, Polym. Adv. Technol. 22 (2011) 2244–2249.
[318] M. Rehan, A. Hartwig, M. Ott, L. Gätjen, R. Wilken, Surf. Coat. Technol. 219 (2013) 50–58.
[319] S. Afzal, W.A. Daoud, S.J. Langford, J. Mater. Chem. A 2 (2014) 18005–18011.
[320] W.A. Daoud, S.K. Leung, W.S. Tung, J.H. Xin, K. Cheuk, K. Qi, Chem. Mater. 20 (2008) 1242–1244.
[321] W.S. Tung, W.A. Daoud, Acta Biomater. 5 (2009) 50–56.
[322] <http://www.cristalactiv.com/ourproducts/photocat_bro_voc.pdf>, (accessed 28.02.15).
[323] <http://www.climasan.com/33671_EN-Pictures-Brochure_6_Pages.pdf>, (accessed 28.02.15).
[324] J. Auvinen, L. Wirtanen, Atmos. Environ. 42 (2008) 4101–4112.

Dr. Swagata Banerjee completed her BSc (Chemistry Hons) from Presidency College (University of Calcutta) and MSc in Biophysics and Molecular Biology from the University of Calcutta, India. She obtained her PhD (Chemistry) from, Trinity College Dublin, where her project focused on the synthesis and photophysical studies of 1,8-naphthalimide derivatives and their interactions with DNA. She joined CREST, Dublin Institute of Technology, Ireland in 2013, where her research involved developing titania based functional materials and photocatalysis.

Prof. Dionysios (Dion) D. Dionysiou is currently a Professor of Environmental Engineering and Science, a Herman Schneider Professor of Engineering and Applied Science, and UNESCO Co-Chair Professor on "Water Access and Sustainability", at the University of Cincinnati. He teaches courses and performs research in the areas of drinking water quality and treatment, advanced oxidation technologies and nanotechnologies, and physical–chemical processes for water quality control. He is currently one of the editors of *Chemical Engineering Journal*, Editor of the *Journal of Advanced Oxidation Technologies*, Special Issue Editor of the *Journal of Environmental Engineering* (ASCE), and member of the Editorial Boards of several other journals. Dr. Dionysiou is the author or co-author of >200 refereed journal publications, >90 conference proceedings, >20 book chapter publications, >20 editorials, and >450 presentations. He is currently co-editing three books on water reuse, harmful algal blooms, and photocatalysis. Dr. Dionysiou's work received over 8000 citations with an H factor of 50.

Prof. Suresh C.Pillai obtained his PhD in the area of Nanotechnology from Trinity College Dublin and then performed a postdoctoral research at California Institute of Technology (Caltech), USA. Upon completion of this appointment he returned to Trinity College Dublin as a Research Fellow before joining CREST-DIT as a Senior Research Manager in April 2004. Suresh joined in IT Sligo as a Senior Lecturer in Environmental Nanotechnology in October 2013. He is an elected fellow of the UK's Royal Microscopical Society (FRMS) and the Institute of Materials, Minerals and Mining (FIMMM). Prof. Suresh was responsible for acquiring more than €3 million direct R&D funding. He has published several scientific articles in leading peer reviewed journals and has presented in more than forty international conferences. He has delivered over forty international invited talks including several key-note and plenary talks. He was also the recipient of the 'Hothouse Commercialization Award 2009' from the Minister of Science, Technology and Innovation and also the recipient of the 'Enterprise Ireland Research Commercialization Award 2009'. He has also been nominated for the 'One to Watch' award 2009 for commercializing R&D work (Enterprise Ireland). He has worked as the national delegate and technical expert for ISO standardization committee and European standardization (CEN) committee on photocatalytic materials.